Regulation of the *E. coli* phospholipid synthesis pathway

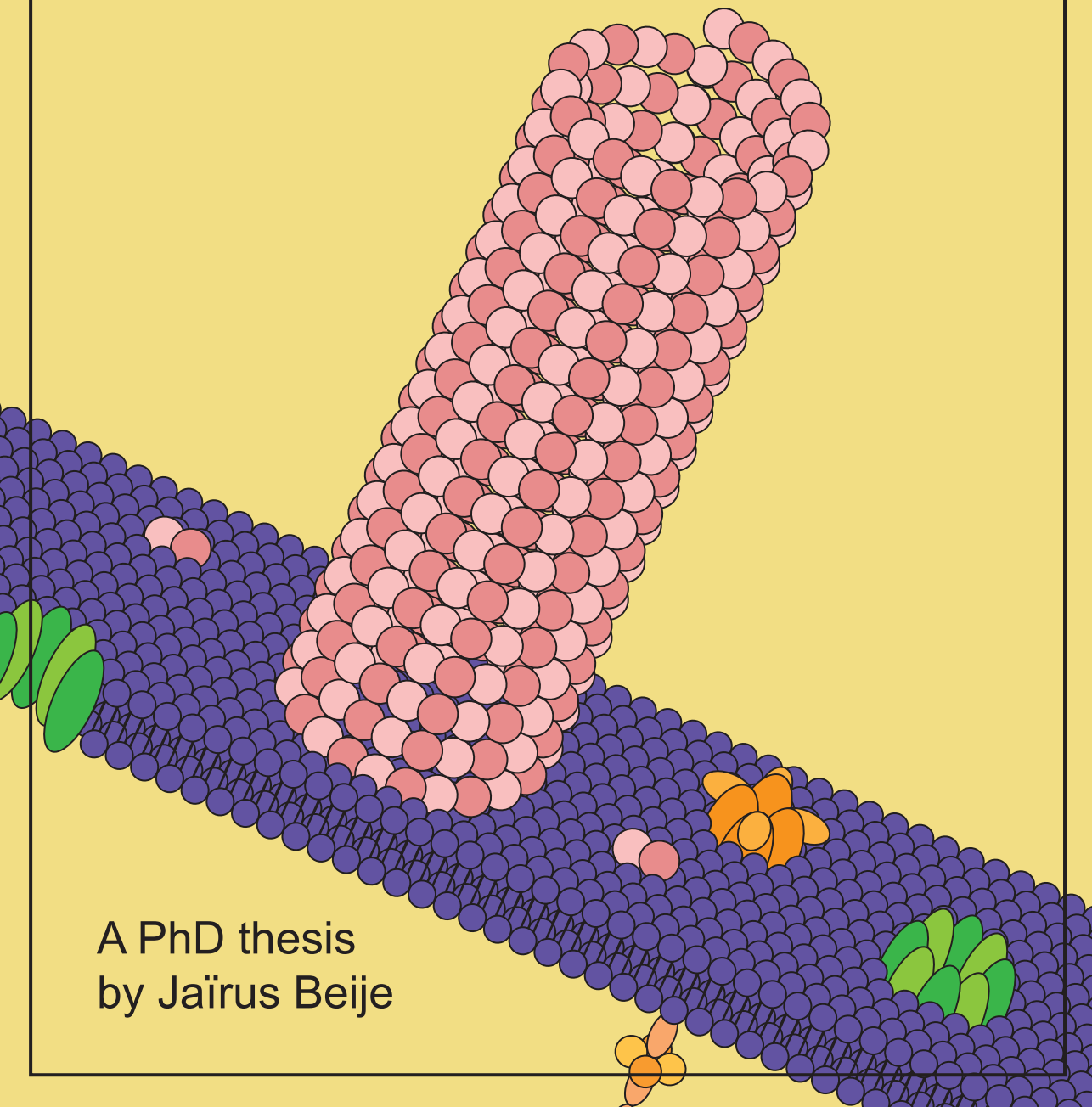

A PhD thesis
by Jaïrus Beije

Regulation of the *E. coli* phospholipid synthesis pathway

Regulation of the *E. coli* phospholipid synthesis pathway

Dissertation

for the purpose of obtaining the degree of doctor
at Delft University of Technology
by the authority of the Rector Magnificus, Prof.dr.ir. H. Bijl,
chair of the Board for Doctorates
to be defended publicly on
Friday 17th, April 2026 at 10:00 o'clock

Jaïrus Marinus BEIJE

This dissertation has been approved by the promotors.

Composition of the doctoral committee:

Rector Magnificus,	chairperson
Dr. G.E. Bokinsky,	Delft University of Technology, *promotor*
Prof.dr. C.J.A. Danelon,	Delft University of Technology / Toulouse Biotechnology Institute, France, *promotor*
Independent members:	
Prof. dr. G.H. Koenderink	Delft University of Technology
Prof. dr. F.J. Bruggeman	Vrije Universiteit Amsterdam
Prof. dr. D.J. Slotboom	Rijks Universiteit Groningen
Dr. M. Exterkate	Heinrich Heine Universität Düsseldorf, Germany
Prof.dr.ir. S.J.J. Brouns	Delft University of Technology (reserve member)

Keywords: Membrane, phospholipids, PlsB, filament, metabolism, *E.coli*, cell envelope, fluorescence microscopy

Printed by: *Gildeprint, Enschede*

Cover by: Digital illustration by J. M. Beije

ISBN 978-94-6384-944-9

An electronic copy of this dissertation is available at
https://repository.tudelft.nl/.

Luctor et emergo
I struggle and emerge

- Wapenspreuk van Zeeland

Contents

Summary

Inside and outside, intracellular and extracellular. This distinction is vital for cells and they expend vast amounts of energy to maintain the barriers that separate the in from the out. How this barrier, the cell envelope, is constructed varies wildly between organisms. We have long exploited differences between our own membrane and the bacterial cell envelope to develop targeted antibiotics. While this has resulted in a great deal of knowledge on bacterial, and especially *Escherichia coli*, cell envelope biosynthesis, many aspects of its regulation are still a mystery.

The phospholipid biosynthesis pathway is one the central pathways supplying crucial building blocks (phospholipids) to both the inner and outer membranes. In *E. coli*, much of this pathway has been thoroughly characterized and all the enzymes have been identified. Yet, despite decades of research, how this pathway is regulated remains disputed and unclear. Recent metabolomic research on the phospholipid and the preceding fatty acid biosynthesis pathways has now identified PlsB as the central point of regulation of both pathways. Furthermore, it was shown that its regulation is post-translational, and most likely through a negative feedback loop. PlsB is the first enzyme in the phospholipid pathway and catalyzes the committed step that sees the addition of acyl-ACP to glycerol-3-phosphate. It has long been reported that PlsB is able to self-assemble into a filament, something that in other enzymes has been shown can act as a regulatory mechanism. Combining these advances we now seek to determine if filament formation is indeed how PlsB is regulated and if, as we suspect, the abundance of the membrane, its end product, is what controls the rate of filamentation.

In **Chapter 1**, we give an overview of metabolic regulation, the many forms it can take, and how these relate to the regulation of cell envelope biosynthesis. First, we give a brief overview of transcriptional and post-translational regulation, before expanding on several different post-translational regulatory mechanisms, among which is filamentation. Using several examples, we show how these regulatory mechanisms can be used to regulate the cell envelope biosynthesis pathways. Finally, we present our hypothesis on how we believe filamentation plays a role in PlsB regulation and what we envision might be the signal that drives it.

In **Chapter 2**, we discuss our main research outcomes. When fluorescently labeled with msGFP2, we observe that PlsB forms punctuate foci at the cell poles. Only when unlabeled PlsB is overexpressed alongside fluorescently labeled PlsB, do we observe an elongated filament phenotype. Despite this, our results show that the fluorescent msGFP2 label does not appear to interfere with the function or regulation of PlsB, as we observe no changes in growth rates, phospholipid synthesis rates or cell morphology

as a result of labeling. Most exciting, when membrane abundance is reduced through depletion of acyl-ACP we report a complete dispersion of the foci. Furthermore, if the membrane abundance is increased by either restoring acyl-ACP pools or providing acyl-CoA, the foci rapidly reassemble.

In **Chapter 3**, we place our research into the broader field of bacterial cell envelope biosynthesis regulation. We give an overview of the current state of the field, highlighting regulatory mechanisms as described in literature. Furthermore, we use this information to show that cell envelope biosynthesis, in general, appears to be regulated by negative feedback loops. We do this by showing how previously described regulatory interactions are later shown to be either not physiologically relevant, or expressions of an overarching negative feedback loop. Finally, based on the evidence and the belief that these pathways are ultimately regulated through negative feedback, we express several hypotheses that we hope will be investigated by the field at large.

In **Chapter 4**, we detail our attempts at experimentally answering the remaining open questions, as well as the reasons we believe these attempts were largely unsuccessful. Primarily, we sought to address the mismatch between the expected elongated filament and the observed punctuate foci. Using several electron microscopy techniques we attempted to directly image the structure adopted by PlsB in these conditions. We also sought to gain more information on the higher order structure through the use of FRAP and native gels. These attempts did not succeed, likely due to a combination of the low number of PlsB filaments relative to the cell volume and experimental difficulty of purifying said filaments. To broaden our understanding of PlsB behavior, we attempted to show that dispersion of the foci is not unique to depletion of acyl-ACP. Unfortunately, our attempts at using genetic tools to create a strain inducibly depleted of glycerol-3-phosphate were unsuccessful. We sought to explore the effects of osmotic shocks *in vivo* on both regular cells and spheroplasts, as well as *in vitro* on vesicles. Furthermore, we explored the use of stop-codon readthrough to generate elongated filamentous foci at wild type expression levels, which while ostensibly successful did not yield the desired result. Finally, through rational design we attempted to make a non-filamentous mutant PlsB, but did not identify a successful mutant. While these methods did not achieve their intended goal, we do want to impress upon the reader the lessons learned and how we believe these questions could be answered in future research.

Overall, these results support our hypothesis that PlsB is regulated through filament formation controlled by membrane abundance. This information broadens our understanding of cell envelope biosynthesis and how these pathways are coordinated with cell growth. These results also raise interesting questions and opportunities, both on PlsB specifically and cell envelope biosynthesis regulation in general, that we can only hope will be thoroughly explored in the future.

Samenvatting

Binnen- en buitenkant, intracellulair en extracellulair. Dit onderscheid is van vitaal belang voor cellen en zij besteden daarom ook enorme hoeveelheden energie aan het in stand houden van de barrières die het binnenste van het buitenste scheiden. Hoe deze barrière, het cel omhulsel, wordt opgebouwd verschilt sterk tussen organismen. In de zorg maken we al langer gebruik van de verschillen tussen ons eigen membraan en het bacteriële cel omhulsel om antibiotica te ontwikkelen. Hoewel dit heeft geleid tot veel kennis over de biosynthese van het bacteriële cel omhulsel, en in het bijzonder dat van *Escherichia coli*, blijven veel aspecten van de regulatie ervan een raadsel.

Het fosfolipide-biosynthese pad is één van de centrale metabole paden die essentiële bouwstenen (fosfolipiden) aanleveren voor zowel het binnen- als het buitencelmembraan. In *E. coli* is een groot deel van dit pad grondig gekarakteriseerd en zijn alle betrokken enzymen geïdentificeerd. desalniettemin, ondanks decennia aan onderzoek blijft het onduidelijk en betwist hoe dit pad precies wordt gereguleerd. In recent metabolomisch onderzoek naar het fosfolipide biosynthese pad en het daaraan voorafgaande vetzuur biosynthese pad is PlsB geïdentificeerd als het centrale regulatiepunt van beide paden. Bovendien is aangetoond dat het hierbij om post-translationele regulatie gaat, hoogstwaarschijnlijk via een negatieve feedbacklus. PlsB is het eerste enzym in het fosfolipide biosynthese pad en katalyseert de ‘gecommitteerde stap’ waarbij acyl-ACP wordt toegevoegd aan glycerol-3-fosfaat. Het is al lange tijd bekent dat PlsB in staat is tot zelfordening tot een filament, iets wat bij andere enzymen kan fungeren als regulatiemechanisme. Door deze inzichten te combineren willen we nu bepalen of filamentvorming inderdaad de wijze van regulatie van PlsB is, en of zoals wij vermoeden de overmaat aan membraan (het eindproduct) de filament vorming reguleert.

In **Hoofdstuk 1** geven we een overzicht van metabolische regulatie, de vormen die het kan aannemen en hoe dit van toepassing is op de synthese van het cel omhulsel. We beginnen met een overzicht van transcriptionele en post-translationele regulatie. Vervolgens gaan we dieper in op post-translationele regulatiemechanismen, waaronder filamentatie. Hierna laten we aan de hand van voorbeelden zien hoe deze regulatie mechanisme gebruikt kunnen worden om verschillende biosynthese paden van het cel omhulsel te reguleren. Ten slotte presenteren we onze hypothese over de rol van filamentatie in de regulatie van PlsB en wat volgens ons het signaal is dat dit aanstuurt.

In **Hoofdstuk 2** bespreken we onze belangrijkste onderzoeksresultaten. Wanneer we met msGFP2 fluorescent gelabeld PlsB observeerden zien we puntvormige foci bij de celpolen. Enkel wanneer ongelabeld PlsB tot overexpressie wordt gebracht in combinatie met gelabeld PlsB nemen we een langgerekt filament weer. Desondanks tonen onze resultaten aan dat het fluorescentielabel msGFP2 niet lijkt te interfereren met de functie of

regulatie van PlsB, aangezien we geen veranderingen zien in groei, fosfolipidesynthese of cel morfologie als gevolg van labelen. De meest fascinerende resultaten zien we als de membraanvoorraad wordt verminderd door uitputting van acyl-ACP voorraden. Onder deze omstandigheden observeren we een volledige dispersie van de foci. Wanneer de membraanvoorraad wordt verhoogd door ofwel herstel van de acyl-ACP voorraad of het aanbieden van het alternatief acyl-CoA, hervormen de foci zich snel.

In **Hoofdstuk 3** plaatsen we ons onderzoek in het bredere veld van de regulatie van de biosynthese van het bacteriële cel omhulsel. We geven een overzicht van de huidige stand van zaken, waarbij we regulatiemechanismen uit de literatuur belichten. Daarnaast gebruiken we deze informatie om aan te tonen dat de biosynthese van het cel omhulsel in het algemeen gereguleerd lijkt te worden door negatieve feedbacklussen. Dit laten we zien door te beschrijven hoe eerder gepubliceerde regulatie interacties later ofwel niet fysiologisch relevant bleken, of manifestaties blijken van een alles-overkoepelende negatieve feedbacklus. Ten slotte formuleren we op basis van het bewijs en de overtuiging dat deze paden uiteindelijk door negatieve feedback worden gereguleerd verschillende hypothesen waarvan we hopen dat het veld deze verder zal onderzoeken.

In **Hoofdstuk 4** beschrijven we de methode waarmee wij experimenteel getracht hebben de overgebleven openstaande vragen te beantwoorden, en belichten daarbij ook de redenen waarom wij denken dat deze methode grotendeels niet geslaagd zijn. We wilden voornamelijk het verschil verklaren tussen het verwachte langgerekte filament en de waargenomen puntvormige foci. Met behulp van verschillende elektronenmicroscopietechnieken probeerden we de structuur te visualiseren die PlsB aanneemt. Ook probeerden we meer informatie te verkrijgen over de hogere-orde-structuur door middel van FRAP en native gels. Deze pogingen zijn helaas mislukt, waarschijnlijk door een combinatie van het lage aantal PlsB filamenten in vergelijking met het cel volume en problemen met het zuiveren van de filamenten. Om ons begrip van het gedrag van PlsB te verbreden, probeerden we aan te tonen dat de dispersie van de foci niet uniek is voor uitputting van de acyl-ACP voorraad door met genetische modificatie een stam te creëren waarbij induceerbaar de voorraad van glycerol-3-fosfaat uitgeput kan worden. We onderzochten de effecten van osmotische schokken *in vivo* op zowel reguliere cellen als spheroplasten, evenals *in vitro* op vesicles. Verder onderzochten we het gebruik van stopcodon-doorlees om langgerekte filament-vormige foci te genereren bij wildtype-expressieniveaus, een methode die ondanks success niet het beoogde resultaat haalden. Ten slotte probeerden we via rationeel ontwerp een niet-filamenteerende mutant van PlsB te maken. Hoewel deze methoden hun beoogde doel niet bereikten, willen we de lezer graag meegeven welke lessen we hebben geleerd en hoe deze vragen volgens ons in toekomstig onderzoek kunnen worden beantwoord.

Over het geheel genomen ondersteunen deze resultaten onze hypothese dat PlsB wordt gereguleerd via filamentvorming die wordt aangestuurd door de membraanvoorraad. Deze informatie verbreedt ons begrip van de biosynthese van het bacteriële cel omhulsel en hoe deze paden worden gecoördineerd met celgroei. Deze resultaten roepen ook interessante vragen en kansen op, zowel specifiek met betrekking tot PlsB als in het algemeen voor de regulatie van de biosynthese van het cel omhulsel. We kunnen enkel hopen dat deze vragen in de toekomst grondig zullen worden onderzocht.

1

Introduction

Sensing and transducing: the difficult task of regulating the *E. coli* cell envelope

J. M. Beije and G. E. Bokinsky

Life can be described as a series of controlled chemical reactions, and understanding their regulatory mechanisms is key to understanding cellular biochemistry. This thesis focuses on the regulation of the cell envelope biosynthesis pathways. In general, metabolic pathways require fast response times to ensure stable product concentrations, often achieved through post-translational regulatory mechanisms and negative feedback loops. These typically involve end-products inhibiting their own synthesis, with signals transduced via a variety of mechanisms such as allosteric inhibition, PTMs, or filamentation. However, for the cell envelope the end-products are insoluble and incorporated into large cell-spanning structures, complicating abundance or stress sensing. Nevertheless, there are known systems able to sense cell envelope stress and trigger cellular action through transcriptional or post-translational regulation. The regulatory mechanisms of most of cell envelope biosynthesis pathways remain unclear, but we hypothesize that E. coli regulates phospholipid synthesis through filamentation and inactivation of PlsB, the enzyme catalyzing the committed step.

1.1. Life as a series of controlled and coordinated chemical reactions

Life requires a constant supply of chemical compounds with the correct properties and in the correct ratios. Even the simplest of cells contain a plethora of compound classes such as sugars, lipids, and larger molecules like proteins and DNA. Each of these compounds needs to be taken up from the environment or synthesized by a metabolic pathway. In bacteria, the vast majority of the reactions in these metabolic pathways happen in the crowded and chaotic cytoplasm. For the cell to function, these processes cannot be random or dictated by the whims of the environment. It is vital that cells are able to exercise strong control over the chemical storm that rages within them, and this can only be achieved through regulation.

The need for regulation holds true for all biosynthetic pathways, and this includes those involved in the synthesis of the building blocks for the cell envelope. The *E. coli* cell envelope features three distinct layers (**Fig. 1.1**). The outer membrane is the first line of defense against external insults. This membrane is asymmetric, with the inner leaflet composed of phospholipids and the outer leaflet of lipopolysaccharide. Next, a cell wall composed of extensively cross-linked peptidoglycan is largely responsible for maintaining cell shape. Finally, the inner membrane is a symmetric phospholipid bilayer predominantly composed of phosphatidylethanolamine (PE) and phosphatidylglycerol (PG) (*1*, *2*). To maintain these structures, the biosynthesis pathways of all three components (phospholipids, lipopolysaccharides, and peptidoglycan), as well as the fatty acid synthesis pathway that supplies precursors to all three pathways, must be coordinated with each other and with cell growth.

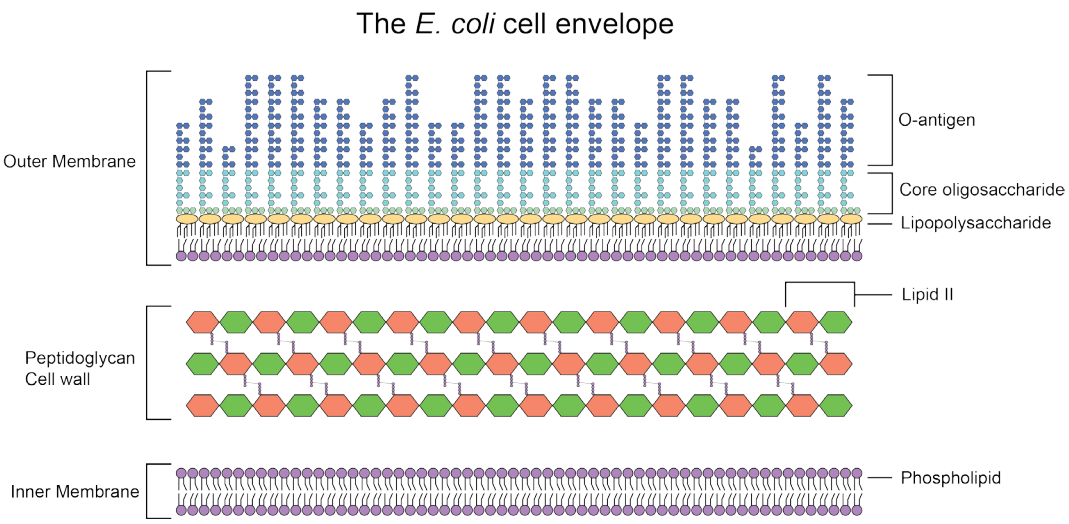

Figure 1.1: A schematic overview of the *E. coli* cell envelope. Shown are three structures that make up the cell envelope: the outer membrane, inner membrane, and cell wall. Each of the major components (phospholipids, peptidoglycan/Lipid II, and lipopolysaccharides) that make up these structures is labelled.

Decades of research have generated an extensive body of knowledge on these pathways. Not only have all the enzymes involved been identified and characterized, but many proposals have been put forward for mechanisms regulating (parts of) these pathways. This has resulted in a complex network of regulatory interactions, at times overlapping, that govern (subsections) of pathways and generally involve soluble intermediates or products as signal molecules. However, how the abundance of the final products, the two membranes and the cell wall, regulates the various biosynthesis pathways remains largely undiscovered or disputed.

Furthermore, for all but the fatty acid synthesis pathway, an additional complication arises because unlike most metabolic pathways, the end-products of these pathways are not small soluble molecules, but the large cell envelope structures themselves. In this chapter, and indeed the thesis at large, we describe the various forms of regulation cells have at their disposal, and explore how they might use these mechanisms to sense and regulate large scale structures such as the membrane. Ultimately, we believe addressing these questions will not only uncover how the individual pathways are regulated, but also how they are coordinated with each other and cell growth in general.

1.2. Post translational regulation is able to translate a variety of signals into various forms of metabolic control

As with any pathway, there are two main ways the cell envelope biosynthesis pathways can be regulated: transcriptional or post-translational regulation. Transcriptional regulation governs the transcription of DNA into RNA, which subsequently results in the translation of that RNA into proteins. By controlling the expression rate of any given protein, the cell can also control the maximum attainable activity for that protein (*3*). However, this form of regulation is not absolute and has been shown to lead to significant variability in the ratio between transcription and translation events, as well as not always correlating with changes in metabolic flux (*4*–*9*). Post-translational control can take a variety of forms, such as direct product inhibition, allosteric binding sites, and post-translational modifications (*10*). For many of the enzymes in *E. coli*, substrate concentrations around their K_m make these reactions quite sensitive to fluctuations in substrate concentrations, though this passive regulation comes at the cost of such enzymes operating at roughly 50% capacity (*10*, *11*). However, more active forms of regulation are required not only to prevent futile loops, but also to control flux through a branch point (*10*, *12*). Furthermore, control of the committed step in a pathway is often required to induce the changes in substrate concentrations needed for passive regulation to reduce flux in the whole pathway.

A universal and central motif: The feedback loop

Feedback loops are one of the central motifs found in regulatory networks in all kingdoms of life. At its core, a feedback loop is when components of a given pathway modulate the flux through that pathway (**Fig. 1.2A**). In practice, these loops can be very simple, an end product competitively inhibiting a first enzyme, or very complex, spanning a vast network of proteins for signal transduction and integration. Regardless of complexity, feedback loops come in two main variations: they can be either positive or negative.

A negative feedback loop is inhibitory, where accumulation of a metabolite or activation of a protein causes deactivation of an upstream protein, ultimately preventing further accumulation or activation of the metabolite or protein. In contrast, a positive regulatory interaction is defined as activation of a protein or accumulation of a metabolite leading to activation or accumulation of another protein or metabolite (*13*). Another way to describe them is to see positive feedback loops as amplifiers and negative feedback loops as stabilizers (*14*). Of the two types, positive feedback loops are generally less common, as most processes in life tend to prefer stability over amplification. As a result, most metabolic pathways are controlled by a negative feedback loop, or even multiple loops. Decades of research has been devoted to the identification and characterization of negative feedback loops. Given this breadth of work, it is not possible to give a comprehensive review within the scope of this chapter. Instead, we aim to provide the reader with a sufficient degree of familiarity.

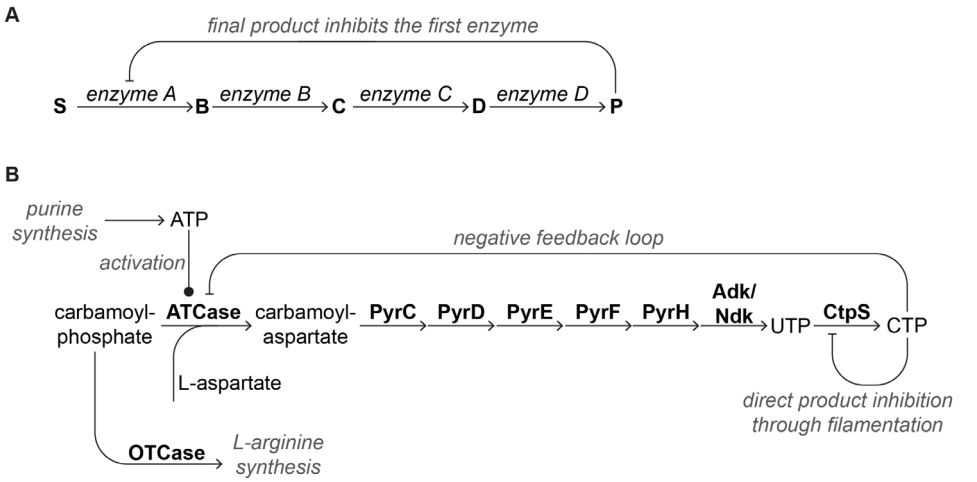

Figure 1.2: A generalized and specific example of negative feedback loops. **A.** A highly generalized example of a negative feedback loop where the committed step (conversion of substrate S to metabolite B by enzyme A) is inhibited by the final product P. **B.** The pyrimidine synthesis pathway showing the enzymes involved (in bold), as well as selected metabolites (in regular font). The committed step is the conversion of carbamoyl-phosphate to carbamoyl-aspartate, catalyzed by the ATCase complex. The activity of this enzyme is regulated by two feedback loops, one positive and one negative. The end product of the pyrimidine pathway, CTP, inhibits ATCase, while the end product of the purine pathway, ATP, activates ATCase. These two loops allow for balanced synthesis between the two pathways. Also shown is the feedback loop controlling CtpS, the final enzyme in the pathway. CtpS forms a filament in the presence of CTP, which inhibits its activity, and ensures balanced synthesis between UTP and CTP.

The principles of negative feedback loops are beautifully illustrated by ATCase and IlvA

The concept of feedback inhibition and negative feedback loops has, by this point, long been known. In the middle of the 1950s, the concept of feedback inhibition had been discovered and demonstrated by a series of papers culminating in a report by Umbarger et al. (*15*, *16*). In fact, it had already been discovered and reported more than a decade earlier in a publication by Dische. However, this 1940 report published in wartime France was, perhaps understandably, not widely circulated (*17*). These experiments by Umbarger et al. first showed the rapid halt in endogenous synthesis of metabolites upon the addition of exogenous metabolites. Second, using cell extracts, the direct inhibition of the first enzyme by the final product was shown for the isoleucine-valine pathway, as well as for ATCase (*15*, *16*).

Aspartate transcarbamoylase (ATCase) has long been a textbook example of feedback regulation (**Fig. 1.2B**). ATCase is the first enzyme in the pyrimidine synthesis pathway, which makes two nucleotides: CTP and UTP. This pathway must be balanced with the purine synthesis pathway, which makes the other two nucleotides: ATP and GTP. ATCase uses two substrates, aspartate and carbamoyl phosphate both of which are chemically very different from CTP, the end product of the pathway (*18*). Nevertheless, early experiments *in vitro* showed inhibition of ATCase with CMP, the monophosphate version of the regular end-product CTP (*19*, *20*). At the time, this raised questions: how could CMP (and likely CTP) inhibit ATCase while presumably being unable to bind the active site? Many years of research, beautifully retold in Gerhart (2014) (*18*), discovered that they did not occupy the same site (*18*, *21*). Around the same time, another team working on a different protein, threonine deaminase IlvA, coined the term we now use to describe this phenomenon: allostery (*22*, *23*).

Negative feedback loops are involved in almost every metabolic pathway and can present themselves in a variety of ways

ATCase and IlvA illustrate a relatively straightforward form of negative feedback inhibition, but certainly not the only one. There are a plethora of mechanisms by which signals and enzymes can be linked in a negative feedback loop. A relatively straightforward implementation of a negative feedback loop in transcriptional regulation is found in the arginine biosynthesis pathway. The expression of enzymes in this pathway, as well as those involved in arginine (and histidine) transport, are repressed by ArgR (*24–26*). ArgR forms a hexamer and in this form is able to bind L-arginine, forming a more stable and conformationally changed complex (*27*, *28*). This complex then binds palindromic 18-bp sites (called ARG boxes), thereby repressing expression of the biosynthetic pathway, as well as repressing its own expression (*25*, *29*). This feedback loop allows the concentration of L-arginine to control the expression of the biosynthetic pathway, something that is especially relevant in conditions where arginine can be sourced from the environment. The latter is further shown by evidence that ArgR induces the expression of arginine catabolism genes (*30*).

Post-translational regulation describes a diverse collection of regulatory mechanisms that modulate enzyme activity, often involving negative feedback loops. The active degradation of enzymes is a post-translational regulatory mechanism most conceptually similar to transcriptional control, as both forms of regulation seek to control enzyme activity by modulating total enzyme concentrations. Since proteolytic regulation is often carried out by ATP-dependent proteases, this form of regulation is inherently energetically expensive. Nevertheless, proteolytic regulation is used by cells, especially for those processes where dysregulation is fatal. Proteins are generally degraded by a specific protease, and this will often involve adaptor proteins and/or the binding of small molecules, often end-products, as part of a negative feedback loop (*31*).

Another mechanism of post-translational control is the chemical modification of existing proteins, allowing cells to regulate enzyme properties and activity. There are many different chemical groups that can be attached to proteins to change a variety of properties like charge and hydrophobicity, that in turn can cause structural and ultimately functional changes in the protein (*32*). These groups are most commonly added after translation and are thus called post-translational modifications (PTMs), though in some cases, such as N-terminal acetylation or glycosylation, they can be attached already during translation (*33*, *34*). It is estimated that roughly half of all proteins can be modified, and these modifications themselves can be quite varied. However, analysis of PTMs in bacteria remains challenging because the absolute number of modifications is relatively low (compared to eukaryotic cells), while the diversity of PTM types is much higher (*32*).

Metabolic enzymes can form filaments as part of their regulatory mechanisms

For the purpose of this thesis, a special form of post-translational regulation we want to highlight is the filamentation of metabolic enzymes. It has long been known that enzymes are able to form filamentous structures, having been observed *in vitro* using a wide variety of assays, such as electron microscopy (*35*). In recent years, the advent of widely available (confocal) fluorescent microscopy combined with genetic tools has vastly increased the ease of tagging enzymes of interest with fluorescent proteins. This has resulted in a sharp increase in interest not only in identifying filament-forming enzymes, but also in elucidating the role of filament formation (*35*). Filamentation has been shown to affect enzymatic activity in a myriad of ways: by both inhibiting and increasing enzymatic activity, to increase substrate specificity, and even improve coupling in two-step reactions. This diversity is also found in the signals, triggers, and mechanisms that govern filament formation. We will here give a brief overview of breadth of filament formation and its effects through a number of examples. For further reading and a more thorough overview, we recommend the excellent reviews by Park et al. (2019), Lynch et al. (2020), and Hvorecny et al. (2023) (*35*–*37*).

Both *E. coli* CtpS and *S. cerevisiae* Glk1 are good examples of how filamentation can be part of a near-classical negative feedback loops (for a schematic representation, **Fig. 1.3**). CtpS is the final enzyme in the CTP synthesis pathway, catalyzing the conversion of UTP to CTP. Glk1 is a glucokinase, part of the larger actin ATPase clan, that catalyzes the phosphorylation of sugars. *In vitro* studies of CtpS have shown that filament formation only occurs after binding its product, CTP. Similarly, an *in vitro* study found that Glk1 forms filaments in the presence of its substrates (ATP and glucose, mannose, or glucosamine) or its products (ADP and sugar-6-phosphate). In both cases, it was shown that filamentation inhibits enzyme activity. Analysis of the crystal structure of both CtpS and Glk1 revealed that filamentation inhibits the enzymes by sterically obstructing a conformational change required for activity. Therefore, like a classic negative feedback loop, the end products, CTP or sugar-6-phosphate, decrease their own synthesis rate by inhibiting CtpS or Glk1, though with the twist of doing so through filament formation (*38*, *39*).

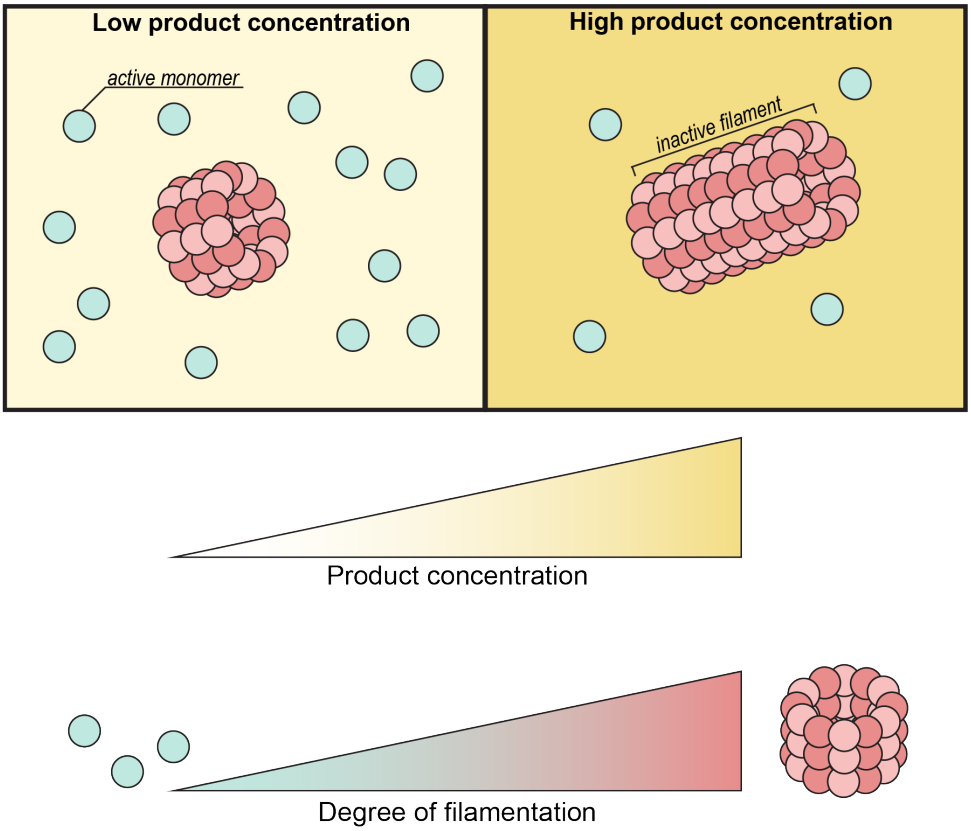

Figure 1.3: A schematic drawing showing a negative feedback loop implemented through filamentation. Enzymes regulated in this way exist in two states, active (teal) and inactive (red). The degree to which the enzymes assemble into filaments is controlled by the concentration of (end-)product, thereby establishing a feedback loop where the product inhibits the pathway.

Further structural analysis of these filament structures revealed amino acid residues likely responsible for forming the filaments. For CtpS, several residues were suggested and tested, and a glutamic acid (E155) was found to be crucial for stabilizing the filament interface. In Glk1, an N-terminal phenylalanine that inserted into a hydrophobic pocket was identified as crucial for filamentation. In both cases, mutants lacking these residues were unable to form filaments. Expressing these non-filamenting mutants allowed investigation into the *in vivo* importance of filament formation. In both cases, it was found that cells expressing mutant CtpS or Glk1 were unable to form filaments, and as a result suffered from growth and metabolism defects. These results clearly show the physiological relevance of filament formation and how filamentation can be integrated into negative feedback loops that sense small, soluble metabolites (*38*, *39*).

1.3. Linking the cell envelope, growth and metabolism – various strategies employed by the cell

Something that links all the examples showcased so far is the signal inducing the regulatory mechanism, be that filamentation or inhibition, is a soluble molecule. While for most metabolic pathways the end product is indeed soluble, this is not generally true of the cell envelope pathways. For example, while the end product of the phospholipid synthesis pathway is a small molecule, the various phospholipids are exclusively present in the two membranes. Therefore, if this pathway is ultimately regulated by the abundance of its end product, the signal is not the concentration of phospholipids, but rather their abundance, and thus the surface of the membrane, in relation to the cell volume. And this holds true for all the cell envelope biosynthesis pathways. While it is still unclear whether the abundance of Lipid II or the activity of peptidoglycan hydrolases is the regulated step in cell wall synthesis, both are ultimately dependent on the relative abundance of cell wall relative to cell volume. An important question then is how cells are able to measure such properties, and by which regulatory mechanisms this is translated to changes in metabolic flux.

Perturbations of the cell envelope can trigger transcriptional stress responses

One possible way for the cell to sense a problem with the cell envelope is to sense a symptom that arises from it. This is the approach taken by the σ^E stress response system, activation of which occurs upon disruptions or damage to the outer membrane (*40*). Under regular conditions, σ^E is bound to the anti-sigma factor RseA, thereby preventing it from interacting with RNA polymerases (*41*). However, if due to some external or internal insult (for example heat stress, the presence of ethanol, or overexpression of porins) there is unfolding or misfolding of outer membrane proteins, σ^E is released. This release occurs through a series of signal transduction events. First, the misfolded protein binds and activates DegS, which cleaves the periplasmic domain of RseA. This in turn activates protease YaeL, which cleaves the cytoplasmic domain of RseA, thereby releasing σ^E (*42–44*). Once freed, σ^E is able to bind RNA polymerase and activate transcription of chaperones, which then facilitate the refolding of un- and misfolded outer membrane proteins.

Outside this main pathway, there are also additional facets of σ^E regulation that have been proposed. Most notably is the role of the periplasmic RseB. This protein has been proposed to bind both RseA, increase the affinity of RseA for σ^E, as well as unfolded periplasmic protein (*45*). It has therefore been proposed that RseB might be a periplasmic sensor for unfolded protein. In the presence of unfolded protein, RseB unbinds RseA, thereby reducing RseA's affinity for σ^E, and in turn causing upregulated expression of chaperones. Furthermore, there is also evidence that RseB binding increases the stability of RseA (*46*). These two interactions are proposed to constitute a secondary, non-proteolytic, feedback loop to activate σ^E (*47*).

Another system is the Rcs system, which responds to changes in LPS charge and fluidity (*48*), peptidoglycan stress (*49*), or changes in the transport of lipoproteins to the outer membrane (*50*). The primary sensor and signaling protein of this system is RcsF, a lipidated protein stretching from the outer leaflet of the outer membrane to the periplasm. When activated by a stress condition, RcsF binds and sequesters IgaA, preventing the latter from inhibiting RcsC. RcsC is the first enzyme of a three-step signaling cascade featuring RcsD and ending in RcsB. The final enzyme, RcsB, acts as either a homodimer or together with other regulators to upregulate the expression of stress response genes, most notably RprA, which in turn promotes the expression of RpoS (*51*).

Post-translational response to cell envelope perturbations – Faster response but harder to measure

Compared to post-translational regulation, transcriptional systems such as those described here tend to be easier to both discover and study, as their effects are often bigger and more readily interpretable. The expression or repression of an entire biosynthetic pathway, as is the effect of ArgR, is more readily apparent and measurable than the degree of inhibition and even filamentation, such as seen in CtpS. Nevertheless, as metabolomic and genetic/microscope tools continue to improve, the often subtler effects of post-translational regulation will likely become more and more apparent in cell envelope regulation.

One interesting example of a post-translational mechanism sensing and responding to cell envelope stress are the filament-like invaginations found in yeast. Though perhaps not strictly filamentous, eisosomes nevertheless assemble into a polymeric structure (*52*). These structures are found in yeast (as well as certain algae), and are linear, half-piped shaped invaginations of the membrane composed of proteins. Pil1 and Lsp1 are the main proteins in eisosomes, and have been shown to form dimers with an inherent curvature able to bind the membrane directly (*53–55*). In cells, eisosomes are largely static and do not appear to move. However, it has been shown that during hypoosmotic shocks, eisosomes rapidly disassemble, releasing their bound phospholipids to rapidly increase the size of the membrane (*56–58*). Furthermore, when this happens, they also release signaling proteins that trigger stress pathways (*59*). While much is still unknown about eisosomes, such as how they assemble and disassemble, the response to hypoosmotic shocks does offer the tantalizing possibility of being able to sense the relative abundance of membrane and, partially through stress response, translate this information into action and metabolic activity (*60*).

These stress response systems showcase how post-translational mechanisms can be used to sense the status of the cell envelope and convert this signal into action. It therefore seems quite possible that similar systems exist to link the major cell envelope structures and their biosynthesis pathways. Indeed, for some pathways feedback loops have already been proposed, such as for the Lpt system. This system transports LPS

from the periplasm to the outer leaflet of the outer membrane, and appears to be regulated by the abundance of LPS in the outer leaflet. This and other systems are described in more detail in Chapter 3. One system we will describe here is PlsB, and our hypothesis for how it links membrane abundance and phospholipid synthesis.

A HYPOTHESIS – PLSB IS REGULATED BY FILAMENT FORMATION IN RESPONSE TO MEMBRANE ABUNDANCE

Prior research from our lab has shown that PlsB is the main point of regulation. Since PlsB does not appear to be controlled by either substrate or protein concentrations **(Fig. 1.4C)**, it is therefore controlled through post-translational means (*61*). PlsB, or glycerol-3-phosphate acyltransferase, is a peripheral membrane protein which catalyzes the acylation of glycerol-3-phosphate, the committed step in phospholipid synthesis (**Fig. 1.4A**). The study of PlsB has a long history (*62*–*66*), with one interesting property of PlsB being first reported by Wilkison et al (*67*). They reported that when overexpressed, PlsB forms long filaments spanning the length of the cell observable with electron microscopy (**Fig. 1.4B**). In follow-up papers, these filaments were purified and it was shown that filaments retained almost no activity, indicating PlsB was in a latent form. Reconstituting the PlsB in a membrane resulted in a recovery of almost all activity, making filament formation the only currently known method of reversibly inhibiting PlsB activity (*67*–*69*). Furthermore, they found PlsB filaments have an association with the membrane, and there are lipids present inside the hollow PlsB tubules (*69*).

We propose, like in the case of CtpS, PlsB forms a filament in response to its end product, the phospholipid membrane. The membrane is not the smooth, uniform layer often depicted in schematic drawings and can in fact vary considerably in height (*70*). Furthermore, there is also evidence that cells maintain membrane reservoirs to maintain homeostatic membrane tension (*71*). One potential shape that such a reservoir or excess membrane might take is as a (small) lipid filament (*72*). We hypothesize that membrane excess, serving as a signal of sufficient phospholipid abundance, induces PlsB filamentation. (**Fig. 1.4D**). The resulting inactivation of (part of the) PlsB pool would then reduce the synthesis rate of new phospholipids, bringing the cell into balance.

Much is unknown of the structure of the membrane, and what a moderate excess of phospholipids might look like. At larger excesses, it is known that blebbing can start to occur, but what happens before that point, what geometry the excess membrane adopts, is still largely unknown. One possibility shown by *in vitro* experiments is that the excess membrane might assemble into filamentous extrusions. This was shown both using vesicles and on a flexible supported bilayer (*72*, *73*). It is an intriguing possibility that these membrane extrusions might also occur *in vivo*. Such structures could potentially serve as a way to measure the relative abundance of phospholipids, similar to eisosomes, and a place for PlsB filaments to assemble (**Fig. 1.4E**)

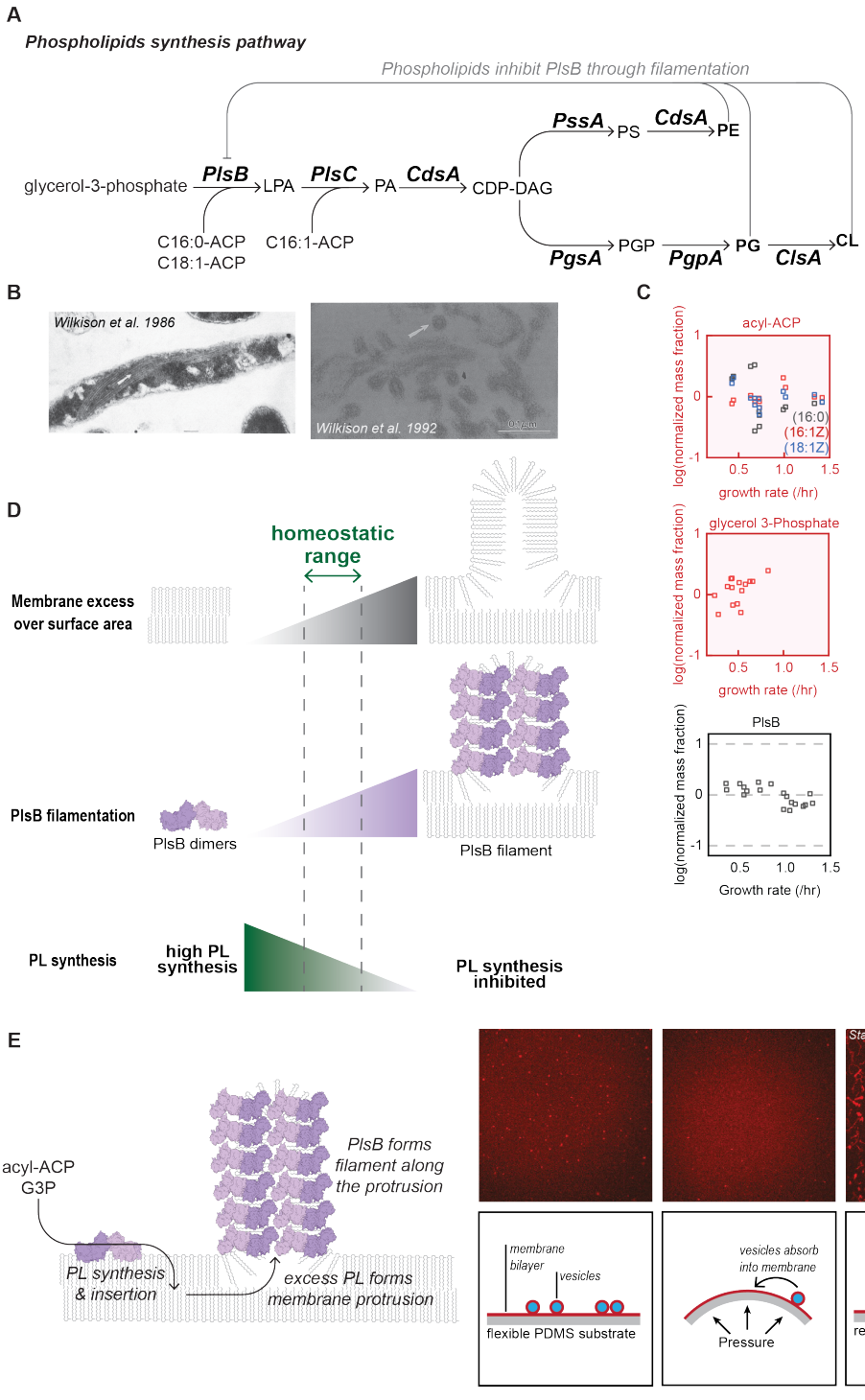
A
Phospholipids synthesis pathway
Phospholipids inhibit PlsB through filamentation
glycerol-3-phosphate
PlsB
LPA
PlsC
PA
CdsA
CDP-DAG
PssA
PS
CdsA
PE
C16:0-ACP
C18:1-ACP
C16:1-ACP
PgsA
PGP
PgpA
PG
ClsA
CL
B
Wilkison et al. 1986
Wilkison et al. 1992
C
acyl-ACP
log(normalized mass fraction)
(16:0)
(16:1Z)
(18:1Z)
growth rate (/hr)
glycerol 3-Phosphate
PlsB
Growth rate (/hr)
D
homeostatic range
Membrane excess over surface area
PlsB filamentation
PlsB dimers
PlsB filament
PL synthesis
high PL synthesis
PL synthesis inhibited
E
acyl-ACP
G3P
PL synthesis & insertion
PlsB forms filament along the protrusion
excess PL forms membrane protrusion
Staykova et al. 2011
50 μm
membrane bilayer
vesicles
flexible PDMS substrate
vesicles absorb into membrane
Pressure
membrane tubules
relaxed PDMS substrate

Figure 1.4: **A.** The phospholipid synthesis pathway. Noted are all the enzymes involved (bold-italic) and the metabolites (regular). The grey inhibition arrow depicts our hypothesis that the total membrane abundance inhibits PlsB. **B.** Images adapted from Wilkison et al. 1986 (left) and 1992 (right) (*67*, *68*). The left image shows a negative stain section of an *E. coli* cell with elongated filaments of PlsB (indicated by an arrow). The right image shows purified PlsB filaments, the arrow indicates the cross section of a filament. **C.** Log2 normalized metabolic data on PlsB (and PlsC) substrates show their concentrations vary little with growth rate. Data on acyl-ACP is adapted from Noga et al. 2020 (*61*) (62), data on glycerol-3-phosphate is adapted from Rados et al. 2022 (*74*). Proteomic data shows the abundance of PlsB varies little and even slightly decreases with increasing growth rates, data adapted from Mori et al. 2021 (*75*). **D.** A schematic overview of our hypothesis, where membrane excess promotes PlsB filamentation, which in turn decreases the effective total PlsB activity. **E.** A speculative schematic model of how PlsB filamentation might occur. On the right are top view microscopy images and side view schematic drawings showing from left to right: Left, a flat bilayer membrane on a flexible PDMS substrate with small vesicles adsorbed onto the surface. Middle, using pressure, the PDMS layer can be pushed into a convex shape, causing an increase in surface area and absorption of the vesicles. Right, relaxing the PDMS layer causes shrinkage of the surface area, excess lipids are extruded as membrane tubules. Images adapted from Staykova et al. 2011 (*72*).

1.4. Thesis Outline

In the following chapters we argue that phospholipid synthesis is regulated through PlsB filamentation. Furthermore, we will show evidence that PlsB filamentation is a response to the relative membrane abundance. Taken together, we aim to show that PlsB filamentation is not only plausible, but also a sufficient mechanism for *E. coli* to regulate membrane synthesis.

In **Chapter 2**, we present the main experimental evidence for our hypothesis. *In vivo* microscopy data shows that PlsB forms clear foci, which can rapidly and reversibly disassemble depending on the level of membrane abundance. Furthermore, we discuss our efforts to design a non-filamentous mutant of PlsB.

In **Chapter 3**, we present the broader argument that the *E. coli* cell envelope biosynthesis pathways are allosterically controlled. We support this argument using a variety of published data and findings. These include, among others, *in vitro* activity assays, *in vivo* microscopy, proteomics, and metabolomics data, and genetic studies. We combine these data to both support our argument, as well as highlight opportunities and challenges for the field.

In **Chapter 4**, we discuss our experimental attempts at answering remaining open questions regarding the structure and mechanism of assembly of the PlsB filaments. We approached these problems using a variety of light microscopy, electron microscopy, and genetic techniques. In this chapter we discuss what questions we sought to address, what we believe caused these approaches to be unsuccessful, and finally, what experiments we would recommend to continue this line of inquiry.

Finally, in **Chapter 5**, we summarize the findings of the preceding chapters. We also highlight several open questions we believe are both interesting and important to address for the general field. Furthermore, for each question we suggest a method to (initiate) investigations.

Bibliography

(*1*) Bayer, M. H. and Bayer, M. E. (1985). Phosphoglycerides and Phospholipase C in Membrane Fractions of *Escherichia coli*. *Journal of Bacteriology 162*, 50–54.

(*2*) Ballesta, J. P. G. and Schaechter, M. (1972). Dependence of the Rate of Synthesis of Phosphatidylethanolamine and Phosphatidylglycerol on the Rate of Growth of *Escherichia coli*. *Journal of Bacteriology 110*, 452–453.

(*3*) Balleza, E., López-Bojorquez, L. N., Martínez-Antonio, A., Resendis-Antonio, O., Lozada-Chávez, I., Balderas-Martínez, Y. I., Encarnación, S. and Collado-Vides, J. (2009). Regulation by transcription factors in bacteria: Beyond description. *FEMS Microbiology Reviews 33*, 133–151.

(*4*) Elowitz, M. B., Levine, A. J., Siggla, E. D. and Swain, P. S. (2002). Stochastic gene expression in a single cell. *Science 297*, 1180–1183.

(*5*) Stewart-Ornstein, J., Weissman, J. S. and El-Samad, H. (2012). Cellular Noise Regulons Underlie Fluctuations in *Saccharomyces cerevisiae*. *Molecular Cell 45*, 483–493.

(*6*) Li, G. W. and Xie, X. S. (2011). Central dogma at the single-molecule level in living cells. *Nature 475*, 308–315.

(*7*) Bar-Even, A., Paulsson, J., Maheshri, N., Carmi, M., O'Shea, E., Pilpel, Y. and Barkai, N. (2006). Noise in protein expression scales with natural protein abundance. *Nature Genetics 38*, 636–644.

(*8*) Kochanowski, K., Sauer, U. and Chubukov, V. (2013). Somewhat in control: the role of transcription in regulating microbial metabolic fluxes. *Current Opinion in Biotechnology 24*, 987–993.

(*9*) Chubukov, V., Uhr, M., Chat, L. L., Kleijn, R. J., Jules, M., Link, H., Aymerich, S., Stelling, J. and Sauer, U. (2013). Transcriptional regulation is insufficient to explain substrate-induced flux changes in *Bacillus subtilis*. *Molecular Systems Biology 9*, 709.

(*10*) Kochanowski, K., Sauer, U. and Noor, E. (2015). Posttranslational regulation of microbial metabolism. *Current Opinion in Microbiology 27*, 10–17.

(*11*) Taymaz-Nikerel, H., Mey, M. D., Baart, G., Maertens, J., Heijnen, J. J. and van Gulik, W. (2013). Changes in substrate availability in *Escherichia coli* lead to rapid metabolite, flux and growth-rate responses. *Metabolic Engineering 16*, 115–129.

(*12*) Hart, Y. and Alon, U. (2013). The Utility of Paradoxical Components in Biological Circuits. *Molecular Cell 49*, 213–221.

(*13*) Mitrophanov, A. Y. and Groisman, E. A. (2008). Positive feedback in cellular control systems. *BioEssays 30*, 542–555.

(*14*) Thomas, R. and d'Ari, R., *Biological Feedback*; CRC Press, Inc: 1990, pp 316–317.

(*15*) Umbarger, H. E. (1956). Evidence for a negative feedback mechanism in the biosynthesis of isoleucine. *Science 123*, 848–848.

(*16*) Umbarger, H. E. and Brown, B. (1958). Isoleucine and Valine Metabolism in *Escherichia coli* VII. a negative feedback mechanism controlling isoleucine biosynthesis. *The Journal of Biological Chemistry 233*, 415–420.

(*17*) Dische, Z. (1976). The discovery of feedback inhibition. *Trends in Biochemical Sciences 1*, N269–N270.

(*18*) Gerhart, J. (2014). From feedback inhibition to allostery: The enduring example of aspartate transcarbamoylase. *FEBS Journal 281*, 612–620.

(*19*) Yates, R. A. and Pardee, A. B. (1956). Control of pyrimidine biosynthesis in E coli by a feedback mechanism. *The Journal of Biological Chemistry 221*, 757–770.

(*20*) Yates, R. A. and Pardee, A. B. (1956). Pyrimidine biosynthesis in E coli. *The Journal of Biological Chemistry 221*, 743–756.

(*21*) Gerhart, J. C. and Pardee, A. B. (1963). The Effect of the Feedback Inhibitor, CTP, on Subunit Interactions in Aspartate Transcarbamylase. *Cold Spring Harbor Laboratory Press 2*, 491–496.

(*22*) Changeux, J.-P. In *Cold Spring Harbor symposia on quantitative biology*, Cold Spring Harbor Laboratory Press.: 1961; Vol. 26, pp 313–318.

(*23*) Monod, J. and Jacob, F. In *In Cold Spring Harbor symposia on quantitative biology*, Cold Spring Harbor Laboratory Press.: 1961; Vol. 26, pp 389–401.

(*24*) Gorini, L., Gundersen, W. and Burger, M. In *Cold Spring Harbor symposia on quantitative biology*, Cold Spring Harbor Laboratory Press: 1961; Vol. 26, pp 173–182.

(*25*) Caldara, M., Charlier, D. and Cunin, R. (2006). The arginine regulon of *Escherichia coli*: Whole-system transcriptome analysis discovers new genes and provides an integrated view of arginine regulation. *Microbiology 152*, 3343–3354.

(*26*) Maas, W. K. In *Cold Spring Harbor symposia on quantitative biology*, Cold Spring Harbor Laboratory Press: 1961; Vol. 26, pp 183–191.

(*27*) van Duyne, G. D., Ghosh, G., Maas, W. K. and Sigler, P. B. (1996). Structure of the oligomerization and L-arginine binding domain of the arginine repressor of *Escherichia coli*. *Journal of Molecular Biology 256*, 377–391.

(*28*) Jin, L., Xue, W. F., Fukayama, J. W., Yetter, J., Pickering, M. and Carey, J. (2005). Asymmetric allosteric activation of the symmetric ArgR hexamer. *Journal of Molecular Biology 346*, 43–56.

(*29*) Beny, G., Boyen, A., Charlier, D., Lissens, W., Feller, A. and Glansdorff, N. (1982). Promoter mapping and selection of operator mutants by using insertion of bacteriophage Mu in the argECBH divergent operon of *Escherichia coli* K-12. *Journal of Bacteriology 151*, 62–67.

(*30*) Kiupakis, A. K. and Reitzer, L. (2002). ArgR-independent induction and ArgR-dependent superinduction of the astCADBE operon in *Escherichia coli*. *Journal of Bacteriology 184*, 2940–2950.

(*31*) Gottesman, S. (2003). Proteolysis in Bacterial Regulatory Circuits. *Annual Review of Cell and Developmental Biology 19*, 565–587.

(*32*) Macek, B., Forchhammer, K., Hardouin, J., Weber-Ban, E., Grangeasse, C. and Mijakovic, I. (2019). Protein post-translational modifications in bacteria. *Nature Reviews Microbiology 17*, 651–664.

(*33*) Ree, R., Varland, S. and Arnesen, T. (2018). Spotlight on protein N-terminal acetylation. *Experimental and Molecular Medicine 50*, 1–13.

(*34*) Latousakis, D. and Juge, N. (2018). How sweet are our gut beneficial bacteria? A focus on protein glycosylation in Lactobacillus. *International Journal of Molecular Sciences 19*, 136–136.

(*35*) Park, C. K. and Horton, N. C. (2019). Structures, functions, and mechanisms of filament forming enzymes: a renaissance of enzyme filamentation. *Biophysical Reviews 11*, 927–994.

(*36*) Lynch, E. M., Kollman, J. M. and Webb, B. A. (2020). Filament formation by metabolic enzymes—A new twist on regulation. *Current Opinion in Cell Biology 66*, 28–33.

(*37*) Hvorecny, K. L. and Kollman, J. M. (2023). Greater than the sum of parts: Mechanisms of metabolic regulation by enzyme filaments. *Current Opinion in Structural Biology 79*, 102530.

(*38*) Barry, R. M., Bitbol, A. F., Lorestani, A., Charles, E. J., Habrian, C. H., Hansen, J. M., Li, H. J., Baldwin, E. P., Wingreen, N. S., Kollman, J. M. and Gitai, Z. (2014). Large-scale filament formation inhibits the activity of CTP synthetase. *eLife 3*, e03638.

(*39*) Stoddard, P. R., Lynch, E. M., Farrell, D. P., Dosey, A. M., Dimaio, F., Williams, T. A., Kollman, J. M., Murray, A. W. and Garner, E. C. (2020). Polymerization in the actin ATPase clan regulates hexokinase activity in yeast. *Science 367*, 1039–1042.

(*40*) Raivio, T. L. and Silhavy, T. J. (2001). Periplasmic stress and ECF sigma factors. *Annual Review of Microbiology 55*, 591–624.

(*41*) Campbell, E. A., Tupy, J. L., Gruber, T. M., Wang, S., Sharp, M. M., Gross, C. A. and Darst, S. A. (2003). Crystal structure of *Escherichia coli* σE with the cytoplasmic domain of its anti-σ RseA. *Molecular Cell 11*, 1067–1078.

(*42*) Alba, B. M., Zhong, H. J., Pelayo, J. C. and Gross, C. A. (2001). degS (hhoB) is an essential *Escherichia coli* gene whose indispensable function is to provide σE activity. *Molecular Microbiology 40*, 1323–1333.

(*43*) Alba, B. M., Leeds, J. A., Onufryk, C., Lu, C. Z. and Gross, C. A. (2002). DegS and YaeL participate sequentially in the cleavage of RseA to activate the σE-dependent extracytoplasmic stress response. *Genes and Development 16*, 2156–2168.

(*44*) Kanehara, K., Ito, K. and Akiyama, Y. (2002). YaeL (EcfE) activates the σE pathway of stress response through a site-2 cleavage of anti-σE, RseA. *Genes and Development 16*, 2147–2155.

(*45*) Collinet, B., Yuzawa, H., Chen, T., Herrera, C. and Missiakas, D. (2000). RseB binding to the periplasmic domain of RseA modulates the RseA:σ(E) interaction in the cytoplasm and the availability of σ(E)·RNA polymerase. *The journal of biological chemistry 275*, 33898–33904.

(*46*) Ades, S. E., Connolly, L. E., Alba, B. M. and Gross, C. A. (1999). The *Escherichia coli* σ(E)-dependent extracytoplasmic stress response is controlled by the regulated proteolysis of an anti-σ factor. *Genes and Development 13*, 2449–2461.

(*47*) Ades, S. E. (2004). Control of the alternative sigma factor σE in *Escherichia coli*. *Current Opinion in Microbiology 7*, 157–162.

(*48*) Konovalova, A., Mitchell, A. M. and Silhavy, T. J. (2016). A lipoprotein/b-barrel complex monitors lipopolysaccharide integrity transducing information across the outer membrane. *eLife 5*, e15276.

(*49*) Laubacher, M. E. and Ades, S. E. (2008). The Rcs phosphorelay is a cell envelope stress response activated by peptidoglycan stress and contributes to intrinsic antibiotic resistance. *Journal of Bacteriology 190*, 2065–2074.

(*50*) Shiba, Y., Miyagawa, H., Nagahama, H., Matsumoto, K., Kondo, D., Matsuoka, S., Matsumoto, K. and Hara, H. (2012). Exploring the relationship between lipoprotein mislocalization and activation of the Rcs signal transduction system in *Escherichia coli*. *Microbiology 158*, 1238–1248.

(*51*) Mitchell, A. M. and Silhavy, T. J. (2019). Envelope stress responses: balancing damage repair and toxicity. *Nature Reviews Microbiology 17*, 417–428.

(*52*) Moor, H. and Mühlethaler, K. (1963). Fine structure in frozen-etched yeast cells. *The Journal of Cell Biology 17*, 609–628.

(*53*) Moreira, K. E., Walther, T. C., Aguilar, P. S. and Walter, P. (2009). Pil1 Controls Eisosome Biogenesis. *Molecular Biology of the Cell 20*, 809–818.

(*54*) Lacy, M. M., Baddeley, D. and Berro, J. (2017). Single-molecule imaging of the BAR-domain protein Pil1p reveals filament-end dynamics. *Molecular Biology of the Cell 28*, 2251–2259.

(*55*) Kabeche, R., Baldissard, S., Hammond, J., Howard, L. and Moseley, J. B. (2011). The filament-forming protein Pil1 assembles linear eisosomes in fission yeast. *Molecular Biology of the Cell 22*, 4059–4067.

(*56*) Kabeche, R., Howard, L. and Moseley, J. B. (2015). Eisosomes provide membrane reservoirs for rapid expansion of the yeast plasma membrane. *Journal of Cell Science 128*, 4057–4062.

(*57*) Karotki, L., Huiskonen, J. T., Stefan, C. J., Ziółkowska, N. E., Roth, R., Surma, M. A., Krogan, N. J., Emr, S. D., Heuser, J., Grünewald, K. and Walther, T. C. (2011). Eisosome proteins assemble into a membrane scaffold. *Journal of Cell Biology 195*, 889–902.

(*58*) Fröhlich, F., Christiano, R., Olson, D. K., Alcazar-Roman, A., DeCamilli, P. and Walther, T. C. (2014). A role for eisosomes in maintenance of plasma membrane phosphoinositide levels. *Molecular Biology of the Cell 25*, 2797–2806.

(*59*) Strádalová, V., Stahlschmidt, W., Grossmann, G., Blažíková, M., Rachel, R., Tanner, W. and Malinsky, J. (2009). Furrow-like invaginations of the yeast plasma membrane correspond to membrane compartment of Can1. *Journal of Cell Science 122*, 2887–2894.

(*60*) Moseley, J. B. (2018). Eisosomes - quick guide. *Current Biology 28*, R376–R378.

(*61*) Noga, M. J., Büke, F., van den Broek, N. J. F., Imholz, N. C. E., Scherer, N., Yang, F. and Bokinsky, G. (2020). Posttranslational Control of PlsB Is Sufficient To Coordinate Membrane Synthesis with Growth in *Escherichia coli*. *mBio 11*, e02703–19.

(*62*) Ray, T. K., Cronan, J. E., Mavis, R. D. and Vagelos, P. R. (1970). The Specific Acylation of Glycerol 3-Phosphate to Monoacylglycerol 3-Phosphate in *Escherichia coli* - Evidence for a single enzyme conferring this specificity. *The journal of biological chemistry 245*, 6442–6448.

(*63*) Cooper, C. L., Jackowski, S. and Rock, C. O. (1987). Fatty Acid Metabolism in sn-Glycerol-3-Phosphate Acyltransferase (plsB) Mutants. *Journal of bacteriology 169*, 605–611.

(*64*) Lightner, V. A., Larson, T. J., Tailleur, P., Kantor, G. D., Raetz, C. R. H., Bell, R. M. and Modrich, P. (1980). Membrane phospholipid synthesis in *Escherichia coli*. Cloning of a structural gene (plsB) of the sn-glycerol-3-phosphate acyl-transferase. *The journal of biological chemistry 255*, 9413–9420.

(*65*) van den Bosch, H. and Vagelos, P. R. (1970). Fatty acyl-CoA and fatty acyl-acyl carrier protein as acyl donors in the synthesis of lysophosphidate and phosphatidate in *Escherichia coli*. *Biochimica et Biophysica Acta (BBA)-Lipids and Lipid Metabolism 218*, 233–248.

(*66*) Lightner, V. A., Bell, R. M. and Modrich, P. (1983). The DNA Sequences Encoding plsB and dgk Loci of *Escherichia coli*. *The journal of biological chemistry 258*, 10856–10861.

(*67*) Wilkison, W. O., Walsh, J. P., Corless, J. M. and Bell, R. M. (1986). Crystalline Arrays of the *Escherichia coli* sn-Glycerol-3-phosphate Acyltransferase, an Integral Membrane Protein. *The Journal of Biological Chemistry 261*, 9951–9958.

(*68*) Wilkison, W. O., Bell, R. M., Taylor, K. A. and Costello, J. M. (1992). Structural Characterization of Ordered Arrays of sn-Glycerol-3-Phosphate Acyltransferase from *Escherichia coli*. *Journal of Bacteriology 174*, 6608–6616.

(*69*) Wilkison, W. O. and Bell, R. M. (1997). sn-Glycerol-3-phosphate acyltransferase from *Escherichia coli*. *Biochimica et Biophysica Acta (BBA)-Lipids and Lipid Metabolism 1348*, 3–9.

(*70*) Lithgow, T., Stubenrauch, C. J. and Stumpf, M. P. (2023). Surveying membrane landscapes: a new look at the bacterial cell surface. *Nature Reviews Microbiology 21*, 502–518.

(*71*) Sens, P. and Turner, M. S. (2006). Budded membrane microdomains as tension regulators. *Physical Review E - Statistical, Nonlinear, and Soft Matter Physics 73*, 031918.

(*72*) Staykova, M., Holmes, D. P., Read, C. and Stone, H. A. (2011). Mechanics of surface area regulation in cells examined with confined lipid membranes. *Proceedings of the National Academy of Sciences 108*, 9084–9088.

(*73*) Litschel, T., Ramm, B., Maas, R., Heymann, M. and Schwille, P. (2018). Beating vesicles: encapsulated protein oscillations cause dynamic membrane deformations. *Angewandte Chemie 130*, 16522–16527.

(*74*) Radoš, D., Donati, S., Lempp, M., Rapp, J. and Link, H. (2022). Homeostasis of the biosynthetic *E. coli* metabolome. *iScience 25*, e104503.

(*75*) Mori, M., Zhang, Z., Banaei-Esfahani, A., Lalanne, J.-B., Okano, H., Collins, B. C., Schmidt, A., Schubert, O. T., Lee, D.-S., Li, G.-W., Aebersold, R., Hwa, T. and Ludwig, C. (2021). From coarse to fine: the absolute *Escherichia coli* proteome under diverse growth conditions. *Molecular Systems Biology 17*, MSB20209536.

2

Chapter 2

Localization of the phospholipid synthesis enzyme PlsB responds to membrane abundance: evidence for a PlsB filamentation-mediated negative feedback loop

J. M. Beije, D. Fierlier, M. Guurink, A.J. Stapert, A. Zoumaro-Djayoon, and G. E. Bokinsky

A version of this chapter has been made publically available as a pre-print on BioRxiv. *bioRxiv (2025): 2025-11* **DOI:** https://doi.org/10.1101/2025.11.03.685888

Cell viability demands tight coordination between growth and the synthesis of new membrane. The first enzyme in the Escherichia coli phospholipid synthesis pathway, PlsB, has been identified as the main point of regulation, but the mechanism of regulation has remained undetermined. Overexpressed PlsB assembles into filaments that are enzymatically inactive, suggesting that filamentation may play a role in regulating PlsB activity and coordinating membrane synthesis with growth. Here, we test this hypothesis by labelling PlsB with a fluorescent tag and observing its behavior using live-cell microscopy. During growth PlsB localizes as discrete foci, consistent with a fraction of PlsB assembling into inactive filaments. Reducing the membrane content of the cell by inhibiting fatty acid synthesis or expression of a cytoplasmic thioesterase causes PlsB to disperse into the cytoplasm. Restoring membrane synthesis causes the foci to reform after a delay. These results are consistent with a model in which PlsB reversibly assembles into filaments in response to phospholipid abundance, effectively establishing a negative feedback loop that coordinates membrane synthesis with growth.

2.1. Introduction

The membrane is perhaps the most fundamental component of living cells. A cell without an intact membrane rapidly loses viability; however a cell that cannot expand its volume cannot grow. Thus, cell growth and viability requires the membrane to expand at a rate that is coordinated with growth. This property is essential for all cells and yet is not understood in any organism.

The membrane synthesis pathway of the model prokaryote *Escherichia coli* is perhaps the best-characterized to date (*1*). *E. coli* is a Gram-negative species whose inner membrane is composed of phospholipids while the outer membrane is an asymmetric bilayer featuring a phospholipid inner leaflet and a lipopolysaccharide outer leaflet. The synthesis of membrane phospholipids is initiated by the enzyme PlsB, which transfers fatty acids from acyl thioesters to glycerol-3-phosphate (G3P), a reaction that generates lysophosphatidic acid (LPA) **(Fig. 2.1A)**. LPA is further acylated by PlsC to generate phosphatidic acid (PA), the universal precursor to all glycerophospholipids (*2*), while subsequent reactions add either anionic or zwitterionic headgroups to the G3P backbone, yielding major phospholipid species phosphatidylglycerol (PG) and phosphatidylethanolamine (PE). While LPA is also generated via the PlsX/PlsY enzymes, this pathway is not essential in *E. coli*, indicating that most LPA is synthesized by PlsB (*3*). Synthesized phospholipids partition into the inner membrane and are subsequently transferred to the inner leaflet of the outer membrane by several redundant pathways (*4*).

As the first enzyme of the phospholipid synthesis pathway, the reaction catalyzed by PlsB is considered to determine the overall flux into membrane phospholipids, and thus the reaction that must be synchronized with growth rate. Evidence indicates that PlsB flux and thus total phospholipid abundance is not determined by the abundance of PlsB substrates (G3P and fatty acyl thioesters) (*5*–*7*) or even PlsB concentration, which does not vary with growth rate (*8*). Furthermore, PlsB overexpression does not affect

phospholipid abundance (*9*, *10*). Thus, PlsB activity must be regulated by an allosteric mechanism that activates and deactivates PlsB enzymes according to a signal that effectively coordinates membrane synthesis with growth. But how does cell growth allosterically regulate PlsB?

Extensive biochemical studies of PlsB (*11–15*) have determined that PlsB is a peripheral membrane protein that requires association with a phospholipid membrane for activity. Nevertheless, the existence of any allosteric mechanism that might control activity has remained elusive. Intriguingly, an early study that overexpressed PlsB discovered that PlsB assembles into well-ordered protein filaments (*10*). PlsB filaments consist of a repeating unit (likely PlsB dimers) helically arranged around a phospholipid core (*16*). While filamentous PlsB is enzymatically inactive, solubilization of PlsB filaments with mild detergent restores activity. Whether filamentation coordinates PlsB activity with cell growth has remained unexplored. Lately, protein filamentation has been discovered to play an important role in the regulation of metabolic enzymes (*17*, *18*). High-throughput imaging screens and biochemical experiments have found that many metabolic enzymes reversibly assemble into filaments (*19*, *20*). In many cases, filamentation of metabolic enzymes is triggered by the accumulation of a product metabolite (*21*, *22*). In cases where product-triggered filamentation inactivates the enzyme, filamentation is a form of allosteric regulation that enables negative feedback control over metabolic flux in response to product demand. Maintaining some amount of enzyme in an inactive form (described as “excess capacity” or “enzyme storage”) ensures that biosynthetic activity can be rapidly increased when needed (*23*).

How might filamentation play a role in regulating the activity of PlsB? By analogy to other enzymes, assembly of PlsB into enzymatically-inactive filaments might be triggered by accumulation of excess product – in this case, membrane phospholipids. The fraction of PlsB sequestered into inactive filaments might vary in proportion with the abundance of phospholipids within the inner membrane: more abundant phospholipids would tend to increase the fraction of PlsB within a filament, decreasing overall PlsB activity, while decreased phospholipid content would liberate PlsB from filaments and increase the active fraction. This mechanism would establish a direct link between membrane phospholipid abundance and PlsB activity that acts as a classic negative feedback loop.

Several lines of indirect evidence are consistent with this model. As already stated, PlsB assembles into well-ordered filaments that are enzymatically inactive. Second, multiple studies indicate that *E. coli* grows with a reservoir of excess phospholipids: *E. coli* protoplasts can be osmotically expanded to some degree without lysis (*24*, *25*), and *E. coli* continues to grow for a short time after phospholipid synthesis is inhibited (*26*). Third, the maximum activity of PlsB available during steady-state growth far exceeds the levels needed to provide *E. coli* with phospholipids (i.e. PlsB is present in excess) (*8*). Finally, when phospholipid synthesis inhibition is relieved, the rate of phospholipid synthesis is transiently faster than the rate observed during steady-state growth, consistent with a brief period of uninhibited phospholipid synthesis in cells lacking a phospholipid reservoir (*27*).

However, direct evidence for the PlsB filamentation hypothesis is lacking. PlsB filaments have never been observed in wild-type cells. This is likely due to the comparatively low abundance of PlsB in native cells (estimated as 1000/cell). As protein filaments typically assemble in a cooperative manner (i.e. the energetic barrier for nucleating a new filament is higher than for extending an existing filament (*21*)), each cell might have at most a few filaments (1-2 per cell). From these assumptions and estimates of PlsB filament geometry from low-resolution structures (*16*), any PlsB filament consisting of 500 PlsB proteins would be small (180 nm) and thus very difficult to observe in situ. In this chapter, we use fluorescent tagging to determine PlsB localization in wild-type cells. Our observations are consistent with our PlsB filamentation hypothesis: specifically, accumulation of membrane phospholipids triggers PlsB filamentation and inactivation, enabling negative feedback regulation of phospholipid synthesis and coordinating phospholipid synthesis with growth.

2.2. PlsB localizes as punctate foci.

The ability of proteins to assemble into filaments *in vivo* has been identified in several studies by examining libraries of strains expressing fluorescently-tagged proteins (*19*, *20*). To enable PlsB localization, we fused a monomeric GFP variant (msGFP2) to the C-terminus of PlsB via a flexible linker of 7 amino acids (*28*). As protein fusions may perturb localization and activity of proteins (*29*), we first investigated whether our fusions influenced PlsB activity. As PlsB is an essential enzyme, any detrimental effects of protein fusion on PlsB activity are expected to be reflected in the growth rate. Furthermore, localization artefacts may also arise because of overexpression of protein over native levels. To ensure that PlsB-msGFP2 is expressed at native levels and that any localization observed is not a consequence of overexpression, we integrated the *plsB-msGFP2* gene into the chromosome of the wild-type *E. coli* NCM3722 (a prototrophic K-12 strain) at the *plsB* locus, replacing unlabelled PlsB while retaining transcriptional control by the *plsB* promoter. *E. coli plsB-msGFP2* grew normally in all tested media **(Fig. 2.1B)**. To determine whether our fusion construct perturbs function, we quantified both membrane phospholipids and phospholipid intermediates using liquid chromatography coupled with mass spectroscopy (LCMS). The phospholipid composition (determined by phospholipids/OD) and levels of phospholipid synthesis intermediates of *plsB-msGFP2* cultures was identical to the wild-type strain in multiple conditions **(Fig. 2.1C)**. To determine whether PlsB-msGFP2 is expressed at wild-type levels, we quantified PlsB-msGFP2 using LCMS-based targeted proteomics. The abundance of PlsB peptides in *plsB-msGFP2* closely matched those measured in the wild-type strain, confirming that PlsB-msGFP2 is expressed at native levels **(Fig. 2.1D)**.

To confirm that msGFP2 labelling does not disrupt regulatory mechanisms that prevent overexpressed PlsB from increasing phospholipid content, we compared phospholipid abundance in *plsB-msGFP2* overexpressing PlsB-msGFP2 with NCM3722 overexpressing unmodified PlsB. Phospholipid abundance did not substantially change in both cases, indicating that tagging does not release control over phospholipid content **(Fig. 2.1E)**.

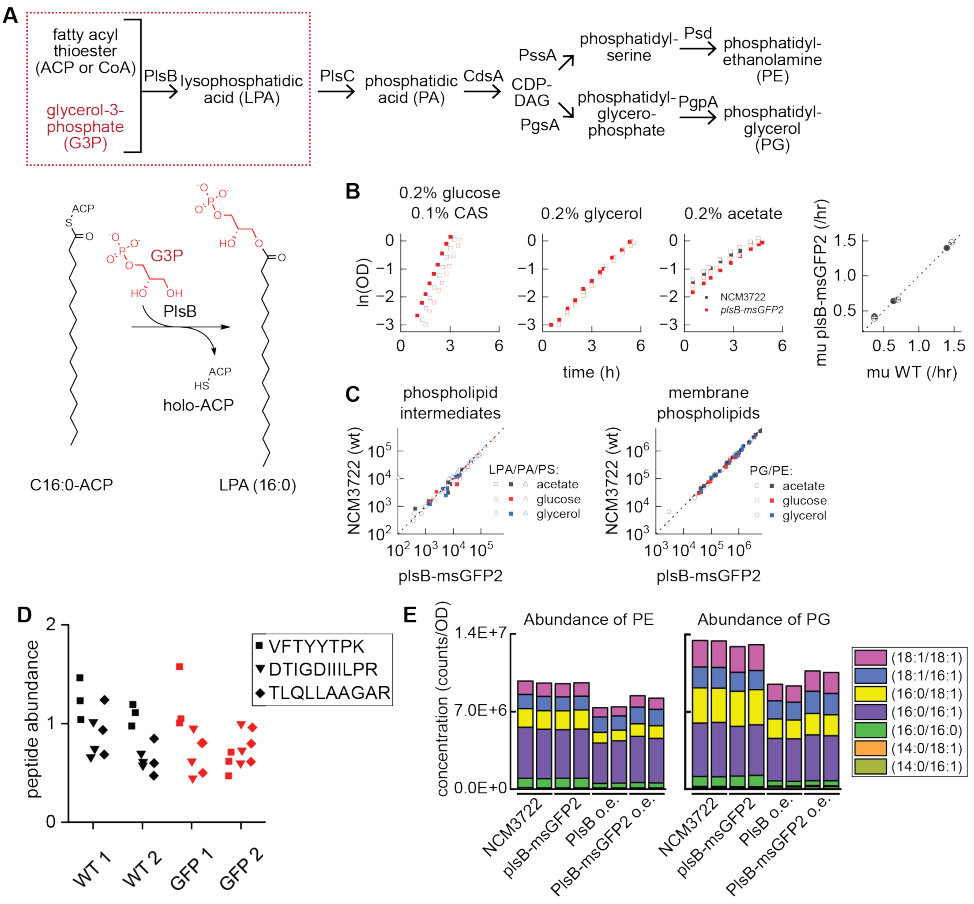

Figure 2.1: A msGFP2 fusion with PlsB retains activity. **A.** The role of PlsB in the *E. coli* phospholipid synthesis pathway. **B.** Growth curves of *E. coli* NCM3722 (wild-type) and NCM3722 *plsB-msGFP2* (expressed from the *plsB* operon) obtained in three defined media. Two biological replicates of each strain in each condition are shown. Growth rates obtained from linear fits to log-transformed data. **C.** Abundance of phospholipid synthesis intermediates (LPA, PA, and PS) and membrane phospholipids (PG and PE) are unaffected by expression of PlsB-msGFP2. Data obtained from one biological replicate in each condition. **D.** Peptide quantification by LCMS indicate that PlsB and PlsB-msGFP2 are expressed at roughly equal levels. **E.** Phospholipid quantification by LCMS indicate that labelling PlsB with msGFP2, overexpressing PlsB-msGFP2, or overexpressing PlsB, do not cause increased abundance of major phospholipid species PE and PG.

To determine how PlsB localizes during steady-state growth, we transferred *plsB-msGFP2* cells from defined rich medium (MOPS / 0.2% glucose / 0.1% CAS amino acids) to an agar pad supplemented with the same medium and imaged using live-cell epifluorescence microscopy. Fluorescent foci were found within 90% of the population, with diffuse fluorescence appearing within the cytoplasm **(Fig. 2.2A & B)**. Most PlsB foci localized at the cell poles **(Fig. 2.2C)**. PlsB foci were present in cells in all growth medium tested, indicating foci are not an artefact of a specific condition. Interesting to note is that when grown on MOPS glycerol, both images and intensity profiles appear to indicate a smaller difference between foci and cytoplasmic fluorescent intensity. To determine whether foci localization is an artefact caused by the msGFP2 fluorescent tag, we also imaged PlsB localization using a PlsB-HaloTag fusion. PlsB-HaloTag also localized as punctate foci **(Fig. 2.2D)**. Finally, we exchanged msGFP2 with the HA epitope and imaged PlsB using immunofluorescence. PlsB-HA was expressed from a plasmid in wild-type NCM3722 that was subsequently fixed and imaged with anti-HA antibodies. Overexpressed PlsB-HA (in wild-type NCM3722) also localized as punctate foci **(Fig. 2.2E)**. Thus, PlsB foci are not an artefact of specific tags or overexpression.

2.3. PlsB foci brightness and number increase in parallel with PlsB expression.

The observation that fluorescently-tagged proteins localize as foci may be consistent with the assembly of proteins into specific oligomers such as filaments or other assemblies such as chemotaxis receptor arrays (*30*). In many cases, the degree of oligomerization is dependent upon the total concentration of protein monomers within the cell, with increased protein concentrations correlating with increased oligomerization. In contrast, if the number or size of foci do not correlate with protein expression, any foci detected are less likely to indicate a protein oligomer. For instance, the primary phospholipid synthesis enzyme in Bacillus subtilis, PlsX, was found to localize as foci in some conditions, but foci formation did not increase in parallel with PlsX expression (*31*). To determine whether the PlsB foci represent protein oligomers, we expressed the PlsB-msGFP fusion from a plasmid-borne inducible promoter in our *plsB-msGFP2* strain. Inducing expression of PlsB-msGFP2 increased the number of fluorescent foci detected as well as the foci brightness **(Fig. 2.2F)**, consistent with PlsB foci indicating formation of an oligomeric complex. Thus, the effects of increased PlsB-msGFP2 expression on the properties of the foci observed are also consistent with assembly of multimeric complexes.

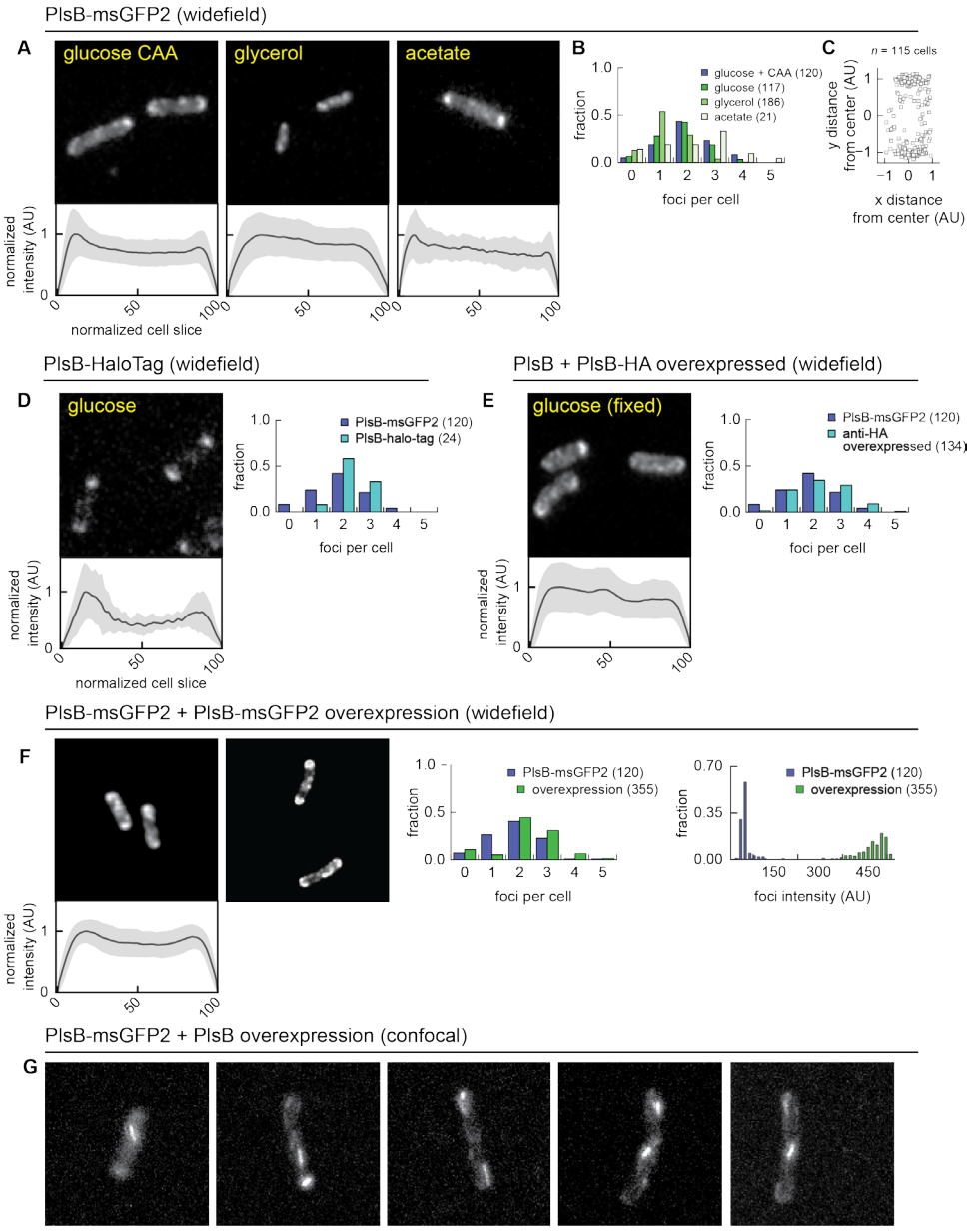
PlsB-msGFP2 (widefield)
A
glucose CAA
glycerol
acetate
normalized intensity (AU)
normalized cell slice
B
glucose + CAA (120)
glucose (117)
glycerol (186)
acetate (21)
fraction
foci per cell
C
n = 115 cells
y distance from center (AU)
x distance from center (AU)
PlsB-HaloTag (widefield)
D
glucose
PlsB-msGFP2 (120)
PlsB-halo-tag (24)
PlsB + PlsB-HA overexpressed (widefield)
E
glucose (fixed)
PlsB-msGFP2 (120)
anti-HA overexpressed (134)
PlsB-msGFP2 + PlsB-msGFP2 overexpression (widefield)
F
PlsB-msGFP2 (120)
overexpression (355)
foci intensity (AU)
PlsB-msGFP2 + PlsB overexpression (confocal)
G

Figure 2.2

Figure 2.2: PlsB localizes as foci during steady-state growth. **A.** Live-cell fluorescent microscopy images of *E. coli* NCM3722 *plsB-msGFP2* on agar pads supplemented with defined medium. Averaged and normalized intensity profiles show on average higher fluorescence at the cell poles, consistent with foci. **B.** PlsB foci form at similar frequencies across conditions and usually localize at cell poles **(C.)**. **D.** PlsB foci are also observed with different protein fusions, and in fixed cells **(E.)**. **F.** Plasmid-based overexpression of PlsB-msGFP2 does not affect the number of PlsB foci detected per cell but increases the brightness of the foci. **G.** Overexpression of unlabelled PlsB in *plsB-msGFP2* background allows resolution of fluorescence patterns that more closely resemble filaments rather than foci.

2.4. C-TERMINAL TAGGING PERTURBS FORMATION OF ORDERLY FILAMENTS.

The foci observed following overexpression of PlsB-msGFP2 did not appear as elongated filaments as expected from previous studies **(Fig. 2.2F)**. To determine whether the GFP fusion affects the formation of filaments, we overexpressed unlabeled PlsB in the *plsB-msGFP2* strain and imaged our cells using confocal microscopy. In contrast to the foci detected within cells overexpressing PlsB-msGFP2 alone, we observed clear fluorescent filaments **(Fig. 2.2G)**. This implies that the presence of a bulky C-terminal tag may adversely affect either the assembly of PlsB into an orderly filamentous array or the parallel packing of multiple PlsB filaments. However, immunofluorescence imaging of overexpressed PlsB-HA also appear as foci. Thus, modification of PlsB on the C-terminus may affect the assembly of filaments.

2.5. INHIBITION OF FATTY ACID SYNTHESIS DELOCALIZES PLSB.

Despite the effect of C-terminal tagging on the formation of orderly PlsB filaments, the consistent foci-forming behaviour of PlsB is consistent with assembly into some oligomeric structure. However, the functional relevance of the foci is unclear. Fluorescent tagging often introduces artefacts that do not reflect the native location of untagged proteins (*32*, *33*). One approach for testing connections between foci formation and enzyme function is to determine whether foci formation is responsive to metabolic perturbations linked with the function of the enzyme (*22*). Specifically, if the PlsB foci we observe reflect oligomerization in response to phospholipid membrane abundance, perturbations to membrane abundance or phospholipid metabolism are expected to affect localization. Conversely, if the PlsB foci instead are the consequence of a labelling artefact (e.g. fusion-induced aggregation), the PlsB foci are expected to be unresponsive to perturbations in membrane metabolism. As direct inhibition of phospholipid metabolism is difficult to achieve, we instead tested whether PlsB localization is relevant to its physiological function by inhibiting fatty acid synthesis.

Triclosan is a fatty acid synthesis inhibitor that acts on the 2E-enoyl-acyl-ACP reductase FabI. Triclosan was added to cells growing in liquid culture, which were subsequently transferred to an agar pad also containing growth medium and triclosan for live-cell imaging. Triclosan greatly reduced the number of PlsB foci and delocalized fluorescence throughout the cytoplasm **(Fig. 2.3A)**. A similar result was obtained using the fatty acid synthesis inhibitor cerulenin, which inactivates the β-keto-acyl-ACP synthases FabB and FabF. To determine whether PlsB foci respond to milder perturbations of fatty acid synthesis, we overexpressed the *E. coli* thioesterase TesA without its periplasmic trafficking signal. When localized to the cytoplasm, TesA hydrolyses long-chain fatty acid thioesters (including acyl-ACP PlsB substrates) (*34*) and reduces the abundance of membrane phospholipids (*35*) while allowing growth to continue. Overexpression of TesA in *plsB-msGFP2* dispersed PlsB-msGFP2 and reduced the foci count **(Fig. 2.3A)**. Thus, PlsB consistently delocalizes in response to perturbations in fatty acid and phospholipid synthesis.

To determine whether PlsB foci dispersal is caused by generic cell growth arrest rather than a specific consequence of fatty acid synthesis inhibition, we imaged *plsB-msGFP2* after adding protein translation inhibitors chloramphenicol and mupirocin. Cells treated with either translation inhibitor ceased to grow but retained PlsB foci **(Fig. 2.3B)**, indicating that PlsB delocalization is not a generic response to growth arrest but is a consequence of fatty acid synthesis inhibition.

The cytoplasmic localization of PlsB observed when phospholipid synthesis is inhibited is unexpected. While PlsB is a peripheral membrane protein and not integrated into the membrane, it is generally regarded as associating stably with the membrane. To further investigate PlsB localization with higher spatial resolution, we imaged triclosan-treated *plsB-msGFP2* using confocal microscopy. Consistent with observations from our wide-field images, PlsB-msGFP2 in triclosan-treated cells is also cytoplasmic and not membrane-associated **(Fig. 2.3C)**. We note that the phosphatidylserine synthesis enzyme PssA is also a peripheral membrane enzyme that reversibly associates with the membrane in response to electrostatic charge and substrate availability.

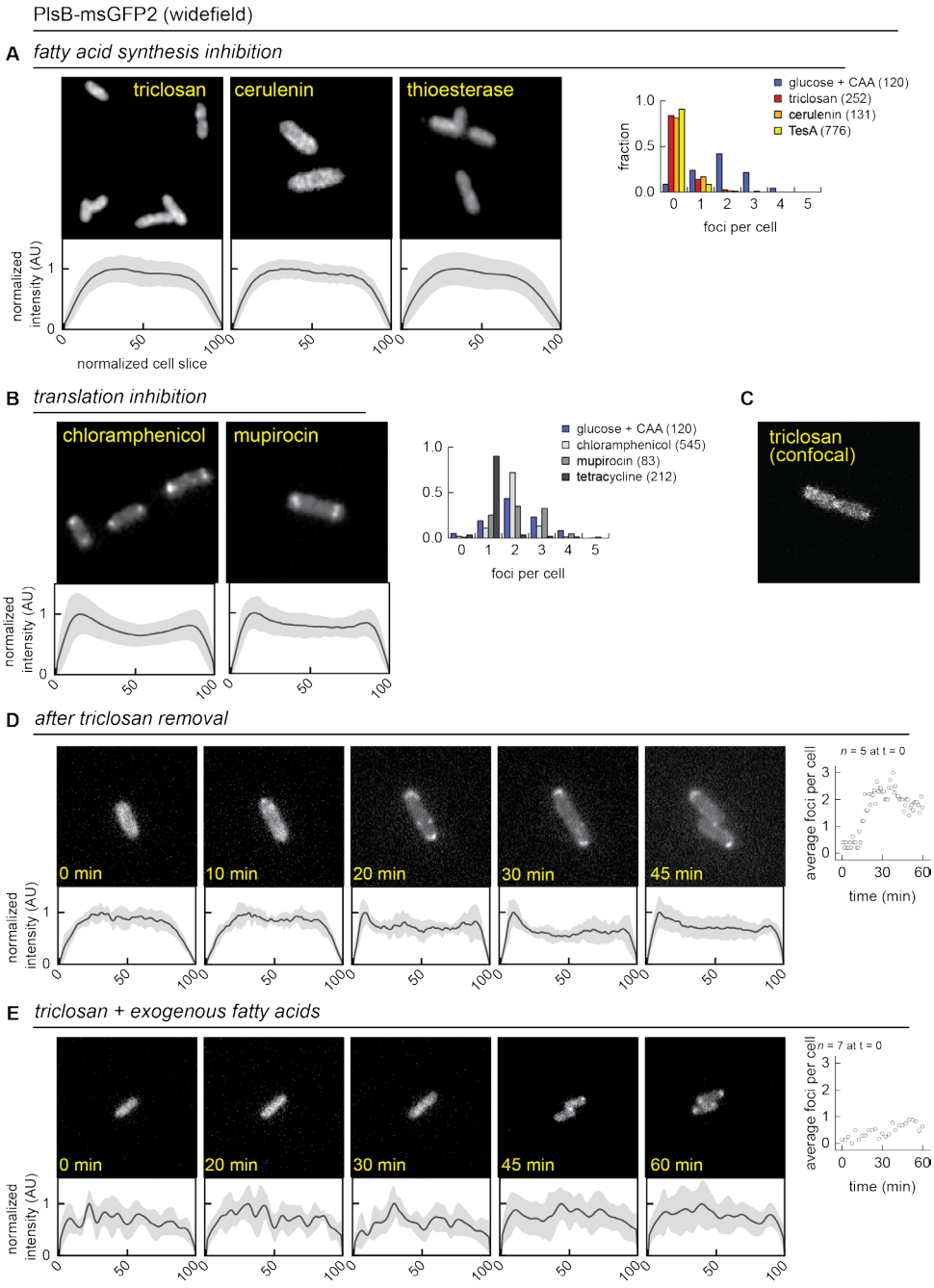
PlsB-msGFP2 (widefield)
A fatty acid synthesis inhibition
triclosan
cerulenin
thioesterase
normalized intensity (AU)
normalized cell slice
glucose + CAA (120)
triclosan (252)
cerulenin (131)
TesA (776)
fraction
foci per cell
B translation inhibition
chloramphenicol
mupirocin
glucose + CAA (120)
chloramphenicol (545)
mupirocin (83)
tetracycline (212)
C
triclosan (confocal)
D after triclosan removal
0 min
10 min
20 min
30 min
45 min
n = 5 at t = 0
average foci per cell
time (min)
E triclosan + exogenous fatty acids
0 min
20 min
30 min
45 min
60 min
n = 7 at t = 0

Figure 2.3

Figure 2.3: PlsB foci respond dynamically to phospholipid abundance. **A.** PlsB-msGFP2 delocalizes into the cytoplasm after membrane synthesis inhibition. Images of *plsB-msGFP2* cells grown in MOPS/0.2% glucose 0.1% CAS amino acids treated with triclosan, cerulenin, or expressing the thioesterase TesA and transferred to agar pads supplemented with identical medium and antibiotics. Intensity profiles do not show any fluorescence peak, indicating a uniformly dispersed signal. **B.** PlsB-msGFP2 foci do not substantially respond to translation inhibitors, indicating that delocalization is not a generic response to growth arrest. Intensity profiles show clear fluorscence peaks at the cell poles, consistend with foci. **C.** A confocal image of triclosan-treated *plsB-msGFP* suggests that PlsB-msGFP2 delocalizes into the cytoplasm and does not associate with the membrane. **D&E.** PlsB-msGFP2 foci reappear when membrane synthesis is restored by either removing triclosan **(D.)** or by adding free fatty acids palmitate and cis-vaccenate **(E.)**. Intensity profiles for triclosan recovery show the reappearance of foci, while those of free fatty acid addition do not.

2.6. PlsB foci reform after resumption of phospholipid synthesis.

We next tested whether resumption of fatty acid synthesis after inhibition with triclosan would cause PlsB foci to reform. Triclosan-treated cells in liquid culture were pelleted, resuspended in fresh medium, and plated on agar containing growth medium and imaged over time. Growth resumed immediately upon triclosan removal, while PlsB remained dispersed at the beginning of imaging. However, after 30 minutes of growth, foci reappeared, coincident with the time of the first division **(Fig. 2.3D)**. Foci reappearance is highly synchronized across the population. Thus, both formation and dispersion of PlsB is reversible and responsive to phospholipid metabolism.

To further investigate what causes PlsB foci formation after phospholipid synthesis resumes, we restarted phospholipid synthesis by feeding exogenous fatty acids while continuing to inhibit *de novo* fatty acid synthesis with triclosan. Exogenous fatty acids palmitate and cis-vaccenate are converted by the fatty acid-CoA ligase FadD to acyl-CoA, which are substrates for phospholipid synthesis by PlsB and PlsC. Triclosan-inhibited cells resumed growth at a much slower rate; nevertheless PlsB foci appeared after 40 minutes at a point that roughly coincided with cell division, although foci reappearance is less synchronized than when phospholipid synthesis is restarted by triclosan removal **(Fig. 2.3E)**. We speculate that the slower growth rate and delayed appearance of foci is due to the inability to synthesize lipopolysaccharides, which require lipid precursors that cannot be supplied or obtained from exogenous fatty acids. Thus, PlsB consistently localizes as foci when membrane synthesis is unperturbed during steady-state growth but disperses when phospholipid abundance is reduced.

2.7. Discussion

Evidence from studies prior to this work already strongly supports our hypothesis that PlsB activity (and thus phospholipid synthesis) is regulated by reversible PlsB filamentation: concentrations of PlsB in wild-type cells is far above levels required to provide sufficient phospholipids for steady-state growth (*1*, *8*, *36*); overexpressed PlsB forms well-ordered filaments that are enzymatically inactive (*10*, *16*), and many metabolic proteins assemble into enzymatically-inactive filaments in the presence of their products (*17*, *21*). The observations from live-cell imaging experiments presented here further support our hypothesis. First, we find that PlsB localizes as a combination of foci and distributed fluorescence, consistent with the formation of a non-diffusive, membrane-associated state. Further supporting our hypothesis is the observation that PlsB foci intensity varies in proportion with PlsB expression. This behaviour is consistent with increased PlsB oligomerization, and contrasts with results obtained from fluorescently labelled PlsX in B. subtilis cells, where foci formation showed no correlation with the expression levels of labelled PlsX (*31*). However, while fluorescent foci are consistent with our hypothesis, many other mechanisms (natural and artefactual) are also known to cause labelled proteins to appear as foci (*29*). Thus, our strongest evidence is that PlsB localization responds to phospholipid synthesis inhibition in a manner entirely consistent with our hypothesis. Specifically, PlsB foci disappear when membrane phospholipids are depleted (fatty acid synthesis inhibition and thioesterase expression) and reappear when phospholipid limitation is alleviated by restarting membrane synthesis.

While our live-cell microscopy data are entirely consistent with our hypothesis, some questions remain. First, the foci that we observe may not necessarily indicate the formation of PlsB filaments. For instance, the foci may simply reflect increased localization of PlsB monomers or dimers rather than an oligomeric structure. This may be due to a preference for binding in regions of anionic phospholipids or for the curved membrane at the cell poles. Issues also arise from our use of protein fusions to localize PlsB in live cells. C-terminal fusions appear to compromise filament formation. This may be caused by the C-terminal extensions disrupting contacts or tweaking the alignment of monomers and preventing helical packing observed in untagged PlsB. Alternatively, C-terminal tagging may disrupt the arrangement of multiple PlsB filaments into parallel bundles. Unfortunately, solutions such as appending tags to the N-terminus, or inserting a tag in an unstructured loop (an approach successfully used to study MreB localization (*37*)) are not straightforward to apply to PlsB: the N-terminus lies at the interface with the membrane, and the Alphafold-predicted structure of PlsB does not reveal any obvious unstructured loops that might allow the insertion of a bulky fluorescent label (although a smaller label may be tolerated). Interestingly, although formation of orderly filaments appears to be disrupted, C-terminal tagging does not dramatically affect PlsB function: growth rate and phospholipid abundance of *plsB-msGFP2* are unaffected. This may even be interpreted as an indication that PlsB and phospholipid homeostasis do not in fact rely upon PlsB filamentation. However, multiple studies that have established the role of filamentation in regulation of other metabolic enzymes found that disabling filamentation caused surprisingly subtle effects upon fitness: for instance, disrupting

glucokinase filamentation lowered fitness only during growth transitions, not during steady-state growth (38).

In **Chapter 4** we describe our efforts to further test our hypothesis using methods such as *in vitro* reconstitution and mutation.

2.8. Methods

Culture conditions

Cells were cultured on MOPS (3-(N-morpholino)propanesulfonic acid) minimal media. Three different variations were used, namely MOPS 0.2% Glucose 0.1% Cas Amino Acids (CAA), MOPS 0.2% Glycerol, and MOPS 0.2% Acetate. For strains containing additional plasmids with antibiotic resistance markers this media was further complemented with the appropriate antibiotics. Unless otherwise stated cells were cultured in small volumes (5 mL) in glass tubes. Cultures were incubated at 37°C while rotating at 400 rpm.

Plasmids and strains

For all experiments NCM3722, a K12 *E. coli* strain, was used as a base. Many experiments were performed with modified strain where chromosomal copy of PlsB was tagged with msGFP2, referred to as NCM3722 *plsB-msGFP2*. Either of these strains were further modified with plasmids, a full list is found in **Table 2.1**. For these strains the naming convention is the base strain followed by the plasmid (e.g. NCM3722 *plsB-msGFP2* + pBbE5K-PlsB). These plasmids are part of the BglBrick plasmid library containing a ColE1 origin of replication, a LacUV5 promotor (indicated by E5) and a resistance marker for either kanamycin or ampicilin (indicated by a K or A, respectively).

Table 2.1: strains used in this work

Strains	Antibiotics resistance marker	Inducer
NCM3722	NA	NA
NCM3722 *plsB-msGFP2*	NA	NA
NCM3722 *plsB-msGFP2* + pBbE5K-PlsB-msGFP2	Kanamycin	IPTG
NCM3722 + pBbE5K-PlsB	Kanamycin	IPTG
NCM3722 + pBbE5K-PlsB-msGFP2	Kanamycin	IPTG
NCM3722 + pBbE5K-PlsB-HA	Kanamycin	IPTG
MG1655 + pBbE5K-PlsB-Halo	Kanamycin	IPTG
NCM3722 + pBbE5A-TesA	Ampicilin	IPTG

Culture sampling and LCMS analysis

For the purpose of acquiring samples for LCMS (liquid chromatography-mass spectrometry) analysis, cultures were grown in large volumes (25 mL) in Erlenmeyer flasks. These flasks contained a magnetic stirrer and were placed into a warm water bath set to 37°C. At regular intervals 1 mL samples were taken to measure the OD600 (Optical density at 600 nm) of the culture. Once the exponential phase was reached (OD600 of 0.3 – 0.4), 1 mL samples were taken and added to 1.5 mL Eppendorf tubes. These tubes were kept on ice and to each 250 µL of 10% trichloroacetic acid (TCA) is added. For each condition two biological replicates were done, and for each biological replicate three samples (technical replicates) were taken. Samples are incubated on ice for 5 to 30 min, after which they are centrifuged for 10 min at 20,000 g and 4°C. The supernatant is discarded and the tube containing the pellet is stored at -80°C. This workflow stays the same, regardless of the final analysis.

For phospholipid analysis, a liquid-liquid extraction is performed. The samples are taken from the -80°C and 150 µL of methanol is added. Next, 250 µL of internal standard (C-13 labelling) is added to each sample, followed by 250 µL of methyl tert-butyl ether (MTBE). This mixture is vigorously mixed and subsequently sonicated for 10 minutes, this is repeated until there is a homogenous opaque solution. For the extraction, 125 µL of new extraction buffer is added and then the mixture is vigorously vortexed to form an emulsion. The samples are incubated for 10 minutes at room temperature and subsequently centrifuged for 10 minutes at 20,000 g. The upper phase (500 µL) is carefully transferred to a new tube, taking care not to disturb the interface. The sample is placed in a vacuum to allow full evaporation of the solvent. For injection into the LCMS, the dry sample is re-dissolved into 10 µL injection solvent (65:30:5 – 2-PrOH:ACN:H2O with 10mM acac) and 5 µL milli-Q. To ensure full dissolution this mixture is first vortexed and then sonicated for 10 minutes, then vortexed once again. Finally, the solution is centrifuged for 5 minutes at 20,000g. The samples are transferred to HPLC (high-performance liquid chromatography) vials with glass inserts and placed into the LCMS for analysis.

For the proteomics analysis, the first step is to add 100 µL of internal standard (N-15 labelled) to each sample. Afterwards, 400 µL of methanol and 100 µL of chloroform is added. The solution is mixed well and sonicated for 10 min in an ultrasonic bath. Next, 300 µL of milli-Q is added and the mixture is vigorously mixed to create a turbid emulsion. The emulsion is centrifuged for 10 minutes at 20,000 g. The upper phase is carefully removed, taking care not to disturb the protein pellet at the interface. Afterwards, 300 µL of methanol is added and the solution is vortexed. After centrifuging for 15 minutes at 20,000 g at 4°C, a pellet is formed at the bottom of the tube. The supernatant is removed and the pellet is washed once with 300 µL of methanol. The final bit of supernatant is allowed to evaporate off. Next, a digestion buffer is prepared (10 µL per sample) from 4 µL of 10% 2-OG in water, 5 µL of 50 mM Tris buffer with 2 mM CaCl2 (pH 8.1) and 1 µL of 50 mM TCEP. To each sample 10 µL of the digestion buffer as well as 3 µL of 50 mM iodoacetamide is added. This is briefly spun down and then left to incubate for 15 min in darkness. Next, 10 µL of 0.2 µg/mL trypsin stock is added

to each sample and they are left to incubate overnight at 37°C on a plate shaker. The next day, the samples are centrifuged for 10 minutes at 20,000 g and the supernatant is carefully transferred to a HPLC vial with glass insert for analysis.

Growth rate experiments

Growth rate experiments on bulk cultures were performed in 250 mL Erlenmeyer flasks. These were filled with 25 mL of the desired medium (see culture conditions). Flasks were inoculated with either an overnight culture or a colony from an agar plate, depending on the doubling time. The flasks also contained a magnetic stir bar and were placed on a magnetic plate stirrer inside a water bath heated to 37°C. Every 30 minutes a 1 mL sample is taken from the culture and the OD600 is determined. This is continued until the culture reaches stationary phase (OD600 above 1.00).

Microscopy

The cultures used for microscopy were prepared as described in the “culture conditions” section. To ensure the bacteria are able to grow and/or continue to be exposed to antibiotics during the imaging they were placed on agar pads. To make these pads, first a larger batch of agarose was prepared using 1.5 g low gelling point agarose dissolved in 50 mL milli-Q for a final concentration of 3%. This agar was then autoclaved to ensure sterility. Afterwards, the full volume was divided into 0.5 mL aliquots which were stored at -20°C. For each experiment, one of these aliquots was used and remelted at 80°C in a heating block. Once melted, 0.5 mL of a 2x medium (e.g. MOPS 0.2% glucose 0.1% CAA) is added as well as any inducer or antibiotic. The solution is mixed through vortexing and briefly (less than 5 min) placed back in the heating block to ensure it does not gel in the tube. Three 15 x 15 mm glass coverslips are place on a flat piece of parafilm and 0.3 mL of agar is pipetted on each of these. A second coverslip is then gently placed on top of the agar droplet, spreading it out to a (near) uniform shape. These are covered and left to gel, after they have solidified they are placed at 37°C to pre-heat.

The slides for microscopy were prepared in two different ways, depending on the microscope used. For widefield, a prepared and pre-heated agar pad is taken and one of the coverslips peeled off. A small amount of culture (1 – 2 µL) is then placed onto the agar pad, which is then placed agar side down onto a larger 22 x 50 mm coverslip. If used for a timelapse, the sides are sealed to prevent drying of the agar pad during the acquisition. For confocal microscopy there is a slight variation on the above protocol, instead of placing the agar onto a 22 x 50 mm coverslip, they are instead placed onto a microscopy dish with a lid and a small amount of wet tissue paper inside. This is done because the holder on the confocal microscope is not suitable for the coverslip slides and this way still ensures the sample does not dry out.

Widefield microscopy was done initially on an Inverted Olympus IX81 equipped with a Andor Luca R camera (EM-CCD, 104x1002 pixel chip size, 8x8µm pixel size, 14-bit dynamic range, 65% quantum efficiency at 600nm), CoolLED pE-4000 fluorescence excitation source, 100x 1.45 NA oil objective (0.13 mm WB), GFP filter cube (ET-EGFP, 470/40 excitation filter, T515lp dichroic filter cut-off, 525/50 emission filter, reference: C229863), phase ring and heating box. The microscope was heated to 37°C before the start of the experiment, at least 30 minutes in advance to ensure a stable temperature. At the start of acquisition the 10x or 20x objective was used to check alignment of the phase ring and make adjustments if needed. Positions were chosen keeping in mind a sufficient number of cells in the field of view and no or minimal non-cell debris. Images were taken in two channels, one in phase contrast (50 ms exposure) and one for GFP (1000 ms exposure, 490 nm, 40% intensity). Phase contrast imaged were taken through the GFP filter cube to save time switching blocks. Where relevant, Z-stacks were taken using a 0.2 µm interval between slices. For timelapses, multiple positions are marked and imaged at 2.5 minute intervals, generally for at least 4 hours but up to 8 hours.

Confocal microscopy is done on a Nikon Eclipse Ti microscope with a 488 nm laser (confocal-CW, 16 mW), a 100x SR Apo TIRF 1.49 NA oil objective (0.12 mm WB), a 482/35 fluorescence emission filter, a EM-CCD Andor iXon X3 DU897 detection device (512x512 pixel chip size, 16x16 µm pixel size, 14 bit dynamic range, >90% quantum efficiency at 600nm), and Tokai Hit sample incubator chamber. The sample is incubated at 37°C during imaging. Suitable locations are found by looking at the sample using the Resonant scanning. Once a position is found a high resolution image is taken using Galvano scanning.

Image analysis

To augment the qualitative analysis of microscopy images we developed an image analysis pipeline. The primary goal of this pipeline is to count the number of foci within each cell. This requires detection of individual cells and the subsequent detection of the foci within each cell. The first step is to create image stacks of both the phase contrast and fluorescent images separately. The phase contrast images are then loaded into Fiji. The MicrobeJ plugin is then used to segment the cells (*34*). The first segmentation is automatic, and this is then followed by manual refinement where necessary. Manual refinement is almost exclusively reserved for eliminating false positives or for separating touching cells. Cells touching the edge are discarded and for all remaining cells the coordinates of their contours are exported. Next, both these contours and the fluorescent images stack are loaded into a custom-made Matlab script. Here the contours are used to find each individual cell in the fluorescent images. All other pixels not defined as cell are considered background and the average background value is subtracted across the image. Next, each cell is analyzed individually. First the cytoplasmic background is estimated by taking the median intensity of cell. This value is then multiplied with a set factor (1.7) to create a threshold. All pixels higher than this threshold are located and further filtered on cluster size. Only clusters of more than 5 pixels are considered a foci. From this we can then collect the number of foci per cell, the number of pixels (i.e. size) and the total intensity of the foci. Next, the centroid of the

cell is found as well as the centroid of each foci in order to determine where in the cell they are located. Besides the exact location of each foci, they are also classified as polar or non-polar. For this determination, foci are considered to be located at the poles when located at the outer 10% of the cell length on either end. Finally, the cell length and width are measured by determining the long and short axis of the cell. All this data is then collected and exported for further analysis.

To generate intensity profiles, the images of individual cells with the background removed were first rotated so their long-axis is horizontal. Then, the intensities of each vertical slice were summed, giving the raw individual cell intensity profiles. To make these comparable, each cell length was then normalized to be 100 slice from pole to pole, interpolating the intensity for each slice. Next, for all the cells in a given condition the average intensity of each slice was found. Finally, these average values were then normalized to the highest value. For timelapse data, each timepoint was treated separately.

2.9. Acknowledgments

We thank Michal Shemesh for expertise and extensive assistance with microscopy, Jeremie Capoulade for performing pilot experiments, and Tanneke den Blaauwen for suggestions and assistance with cell fixation and immunofluorescence. We thank Ariane Briegel and Arjen Jakobi for encouragement and insightful suggestions, and the entire Bokinsky Lab for stimulating discussions and support.

2.10. Author Contributions

JB: designed and performed experiments, built image analysis pipeline, evaluated data. DF: collected samples for LCMS experiments. MG: constructed plsB-HaloTag strain and performed HaloTag imaging experiments. AS: performed initial experiments confirming TesA-driven PlsB delocalization. AZ-D: LCMS analysis. GB: supervised project, constructed plsB-msGFP2 strain, evaluated data. JB and GB wrote the manuscript. All authors approved the final manuscript.

Bibliography

(*1*) Dowhan, W. (2013). A retrospective: Use of *Escherichia coli* as a vehicle to study phospholipid synthesis and function. *Biochimica et Biophysica Acta - Molecular and Cell Biology of Lipids 1831*, 471–494.

(*2*) Yao, Z. and Carballido-López, R. (2014). Fluorescence imaging for bacterial cell biology: From localization to dynamics, from ensembles to single molecules. *Annual Review of Microbiology 68*, 459–476.

(*3*) Yoshimura, M., Oshima, T. and Ogasawara, N. (2007). Involvement of the YneS/YgiH and PlsX proteins in phospholipid biosynthesis in both *Bacillus subtilis* and *Escherichia coli*. *BMC Microbiology 7*, DOI: 10.1186/1471-2180-7-69.

(*4*) Ruiz, N., Davis, R. M. and Kumar, S. (2021). YhdP, TamB, and YdbH Are Redundant but Essential for Growth and Lipid Homeostasis of the Gram-Negative Outer Membrane. *mBio 12*, DOI: 10.1128/mBio.02714-21.

(*5*) Goelz, S. E. and Cronan, J. E. (1980). The Positional Distribution of Fatty Acids in *Escherichia coli* Phospholipids Is Not Regulated by sn-Glycerol 3-Phosphate Levels. *Journal of Bacteriology 144*, 462–464.

(*6*) Davis, M. S., Solbiati, J. and Cronan, J. E. (2000). Overproduction of acetyl-CoA carboxylase activity increases the rate of fatty acid biosynthesis in *Escherichia coli*. *Journal of Biological Chemistry 275*, 28593–28598.

(*7*) Heath, R. J., Jackowski, S. and Rock, C. O. (1994). Guanosine Tetraphosphate Inhibition of Fatty Acid and Phospholipid Synthesis in *Escherichia coli* Is Relieved by Overexpression of Glycerol-3-phosphate Acyltransferase (PlsB). *The Journal of Biological Chemistry 269*, 26584–26590.

(*8*) Noga, M. J., Büke, F., van den Broek, N. J. F., Imholz, N. C. E., Scherer, N., Yang, F. and Bokinsky, G. (2020). Posttranslational Control of PlsB Is Sufficient To Coordinate Membrane Synthesis with Growth in *Escherichia coli*. *mBio 11*, e02703–19.

(*9*) Snider, M. D. (1979). Control of membrane lipid synthesis in *Escherichia coli* during growth and during the stringent response. *Journal of Biological Chemistry 254*, 7197–7202.

(*10*) Wilkison, W. O., Walsh, J. P., Corless, J. M. and Bell, R. M. (1986). Crystalline Arrays of the *Escherichia coli* sn-Glycerol-3-phosphate Acyltransferase, an Integral Membrane Protein. *The Journal of Biological Chemistry 261*, 9951–9958.

(*11*) Rock, C. O., Goelz, S. E. and Cronan, J. E. (1981). Phospholipid synthesis in *Escherichia coli*. Characteristics of fatty acid transfer from acyl-acyl carrier protein to sn-glycerol 3-phosphate. *Journal of Biological Chemistry 256*, 736–742.

(*12*) Green, P. R., Merrill, A. H. and Bell, R. M. (1981). Membrane phospholipid synthesis in *Escherichia coli*. Purification, reconstitution, and characterization of sn-glycerol-3-phosphate acyltransferase. *The Journal of Biological Chemistry 256*, 11151–11159.

(*13*) Green, P. R. and Bell, R. M. (1984). Asymmetric reconstitution of homogenous *Escherichia coli* sn-glycerol-3-phosphate acyltransferase into phospholipid vesicles. *Journal of Biological Chemistry 259*, DOI: 10.1016/s0021-9258(17)42657-3.

(*14*) Scheideler, M. A. and Bell, R. M. (1989). Phospholipid dependence of homogeneous, reconstituted sn-glycerol-3-phosphate acetyltransferase of *Escherichia coli*. *Journal of Biological Chemistry 264*, DOI: 10.1016/s0021-9258(18)63880-3.

(*15*) Scheideler, M. A. and Bell, R. M. (1991). Characterization of Active and Latent Forms of the Membrane-associated sn-Glycerol-3-phosphate Acyltransferase of *Escherichia coli**. *The Journal of Biological Chemistry 266*, 14321–14327.

(*16*) Wilkison, W. O., Bell, R. M., Taylor, K. A. and Costello, J. M. (1992). Structural Characterization of Ordered Arrays of sn-Glycerol-3-Phosphate Acyltransferase from *Escherichia coli*. *Journal of Bacteriology 174*, 6608–6616.

(*17*) Park, C. K. and Horton, N. C. (2019). Structures, functions, and mechanisms of filament forming enzymes: a renaissance of enzyme filamentation. *Biophysical Reviews 11*, 927–994.

(*18*) Simonet, J. C., Burrell, A. L., Kollman, J. M. and Peterson, J. R. (2020). Freedom of assembly: Metabolic enzymes come together. *Molecular Biology of the Cell 31*, 1201–1205.

(*19*) Narayanaswamy, R., Levy, M., Tsechansky, M., Stovall, G. M., O'Connell, J. D., Mirrielees, J., Ellington, A. D. and Marcotte, E. M. (2009). Widespread reorganization of metabolic enzymes into reversible assemblies upon nutrient starvation. *Proceedings of the National Academy of Sciences of the United States of America 106*, DOI: 10.1073/pnas.0812771106.

(*20*) Noree, C., Begovich, K., Samilo, D., Broyer, R., Monfort, E. and Wilhelm, J. E. (2019). A quantitative screen for metabolic enzyme structures reveals patterns of assembly across the yeast metabolic network. *Molecular Biology of the Cell 30*, DOI: 10.1091/mbc.E19-04-0224.

(*21*) Barry, R. M., Bitbol, A. F., Lorestani, A., Charles, E. J., Habrian, C. H., Hansen, J. M., Li, H. J., Baldwin, E. P., Wingreen, N. S., Kollman, J. M. and Gitai, Z. (2014). Large-scale filament formation inhibits the activity of CTP synthetase. *eLife 3*, e03638.

(*22*) Stoddard, P. R., Lynch, E. M., Farrell, D. P., Dosey, A. M., Dimaio, F., Williams, T. A., Kollman, J. M., Murray, A. W. and Garner, E. C. (2020). Polymerization in the actin ATPase clan regulates hexokinase activity in yeast. *Science 367*, 1039–1042.

(*23*) Davidi, D. and Milo, R. (2017). Lessons on enzyme kinetics from quantitative proteomics. *Current Opinion in Biotechnology 46*, 81–89.

(*24*) Sun, Y., Sun, T. L. and Huang, H. W. (2014). Physical properties of *Escherichia coli* spheroplast membranes. *Biophysical Journal 107*, 2082–2090.

(*25*) Buda, R., Liu, Y., Yang, J., Hegde, S., Stevenson, K., Bai, F. and Pilizota, T. (2016). Dynamics of *Escherichia coli*'s passive response to a sudden decrease in external osmolarity. *Proceedings of the National Academy of Sciences of the United States of America 113*, E5838–E5846.

(*26*) Bell, R. M. (1974). Mutants of *Escherichia coli* Defective in Membrane Phospholipid Synthesis: Macromolecular Synthesis in an sn-Glycerol 3-Phosphate Acyltransferase Km Mutant. *Journal of Bacteriology 117*, 1065–1076.

(*27*) McIntyre, T. M., Chamberlain, B. K., Webster, R. E. and Bell, R. M. (1977). Mutants of *Escherichia coli* defective in membrane phospholipid synthesis. Effects of cessation and reinitiation of phospholipid synthesis on macromolecular synthesis and phospholipid turnover. *Journal of Biological Chemistry 252*, 4487–4493.

(*28*) Valbuena, F. M., Fitzgerald, I., Strack, R. L., Andruska, N., Smith, L. and Glick, B. S. (2020). A photostable monomeric superfolder green fluorescent protein. *Traffic 21*, 534–544.

(*29*) Margolin, W. (2012). The price of tags in protein localization studies. *Journal of Bacteriology 194*, 6369–6371.

(*30*) Thiem, S. and Sourjik, V. (2008). Stochastic assembly of chemoreceptor clusters in *Escherichia coli*. *Molecular Microbiology 68*, DOI: 10.1111/j.1365-2958.2008.06227.x.

(*31*) Sastre, D. E., Bisson-Filho, A., de Mendoza, D. and Gueiros-Filho, F. J. (2016). Revisiting the cell biology of the acyl-ACP: Phosphate transacylase PlsX suggests that the phospholipid synthesis and cell division machineries are not coupled in *Bacillus subtilis*. *Molecular Microbiology 100*, 621–634.

(*32*) Ghodke, H., Caldas, V. E., Punter, C. M., van Oijen, A. M. and Robinson, A. (2016). Single-Molecule Specific Mislocalization of Red Fluorescent Proteins in Live *Escherichia coli*. *Biophysical Journal 111*, DOI: 10.1016/j.bpj.2016.05.047.

(*33*) Swulius, M. T. and Jensen, G. J. (2012). The helical MreB cytoskeleton in *Escherichia coli* MC1000/pLE7 is an artifact of the N-terminal yellow fluorescent protein tag. *Journal of Bacteriology 194*, 6382–6386.

(*34*) Bonner, W. M. and Bloch, K. (1972). Purification and properties of fatty acyl thioesterase I from *Escherichia coli*. *The Journal of Biological Chemistry 247*, DOI: 10.1016/s0021-9258(19)45222-8.

(*35*) Cho, H. and Cronan, J. E. (1995). Defective export of a periplasmic enzyme disrupts regulation of fatty acid synthesis. *Journal of Biological Chemistry 270*, 4216–4219.

(*36*) Wilkison, W. O. and Bell, R. M. (1997). sn-Glycerol-3-phosphate acyltransferase from *Escherichia coli*. *Biochimica et Biophysica Acta (BBA)-Lipids and Lipid Metabolism 1348*, 3–9.

(*37*) Bendezú, F. O., Hale, C. A., Bernhardt, T. G. and Boer, P. A. D. (2009). RodZ (YfgA) is required for proper assembly of the MreB actin cytoskeleton and cell shape in *E. coli*. *EMBO Journal 28*, DOI: 10.1038/emboj.2008.264.

3

Chapter 3

Not that complicated: Allosteric control and post-translational negative feedback loops are sufficient to coordinate Gram-negative envelope assembly

J. M. Beije and G. E. Bokinsky

A version of this chapter has been submitted and is under revision as a opinion/hypothesis to *mBio*.

How Gram negative bacteria coordinate the assembly pathways that build their multilayered envelopes is a long-standing fundamental question. We compile proteomic and metabolomic data sets obtained from Escherichia coli to eliminate mechanisms that do not control envelope biogenesis. The growth rate insensitivities of pathway enzymes and transport complex proteins indicate that transcription does not control envelope biogenesis. Similarly, the growth rate insensitivities of envelope precursor concentrations indicate that precursor and metabolite levels also do not control envelope biogenesis. We propose instead that envelope biogenesis is coordinated entirely by allosteric activation of phospholipid synthesis by PlsB, lipopolysaccharide transport by the Lpt complex, and the activities of peptidoglycan hydrolases. We further hypothesize that many signals that have been proposed to regulate envelope biogenesis pathways act indirectly via known negative feedback loops.

3.1. Introduction

Gram negative bacteria are difficult to eradicate because of their multilayered cell envelope. The inner membrane is a typical phospholipid bilayer, while the outer membrane is asymmetric: phospholipids comprise the periplasmic leaflet, while the outer leaflet presents a barrier of impermeable lipopolysaccharides (LPS). In the periplasm between the membranes is a peptidoglycan mesh. Each layer is assembled from precursors synthesized in the cytoplasm. As envelope assembly and precursor synthesis pathways are well-described in model organisms, current research focusses upon understanding how these pathways are coordinated with each other and with cell growth (*1*).

The questions “how is envelope biogenesis coordinated with cell growth?” and ”how is LPS synthesis coordinated with phospholipid synthesis?” are examples of a general question that has motivated the field of metabolic regulation for decades: how do living cells regulate metabolic pathways? Here, we integrate published proteome and metabolome data sets obtained from *Escherichia coli* (*2–4*) to propose that envelope biogenesis pathways are coordinated not by transcription or metabolism-based mechanisms, but instead by allosteric signals arising from cell growth itself. We further argue that many signals proposed to directly control envelope biogenesis do so only indirectly by triggering negative feedback loops.

3.2. How do cells control metabolic pathways?

The mechanisms that cells use to adjust flux through a metabolic pathway can be inferred by comparing the concentrations of pathway substrates, intermediates, products, enzymes, and regulators across a range of steady-state growth rates(*5*, *6*). When the concentration of a specific enzyme or substrate varies in parallel with pathway flux, it suggests (but does not prove) that the reaction rate is tuned by that changing concentration. For instance, protein translation is tuned primarily by varying ribosome abundance via transcription (*7*), whereas the rates of fatty acid elongation reactions

scale with the concentration of the substrate malonyl-ACP (*2*). Such concentration data are however more powerful for ruling out possible control mechanisms: if synthesis rates change while enzyme or substrate concentrations remain constant (i.e., if concentrations are insensitive to growth rate), then flux control likely arises from another mechanism, such as allosteric regulation. So what does not control envelope biogenesis?

3.3. Transcription does not control envelope biogenesis.

Transcriptional control is an intuitively attractive option for metabolic regulation. Increasing the concentration of an enzyme in an *in vitro* experiment typically accelerates the reaction. Therefore, when growth accelerates, cells might respond by increasing the concentrations of envelope biogenesis enzymes to accelerate envelope precursor and assembly in parallel. However, concentrations of envelope biosynthesis enzymes do not change with growth rate **(Fig. 3.1 and Supplemental Fig. 3.1-3.3)** (*2*, *4*). Thus, envelope biogenesis is not coordinated by transcription. Instead, transcription maintains a fixed envelope synthesis capacity regardless of growth rate, a proteome allocation strategy that is inefficient during slow growth but advantageous in changing environments. Aside from modification pathways activated by specific stresses (*8*), envelope biogenesis is coordinated primarily – perhaps exclusively – via post-translational mechanisms.

3.4. Metabolite and precursor supply do not control envelope biogenesis.

An alternative strategy for controlling the rate of envelope synthesis is to vary concentrations of envelope precursors such as fatty acid thioesters, glycerol-3-phosphate, and UDP-N-acetyl glucosamine. This strategy is also intuitively attractive because envelope precursor synthesis pathways might increase in proportion with other cellular metabolites such as acetyl-CoA. Furthermore, precursor synthesis pathways are connected, so producing more fatty acids for phospholipids might automatically increase production of lipid precursors for LPS. However, available measurements indicate that precursor concentrations are either stable or increase only slightly in parallel with growth rate **(Fig. 3.1)**. Therefore, envelope biogenesis is not controlled by precursor concentrations. Strikingly, precursor concentrations are generally far more stable than upstream metabolite concentrations such as acetyl-CoA, thus eliminating metabolites as potential coordination signals.

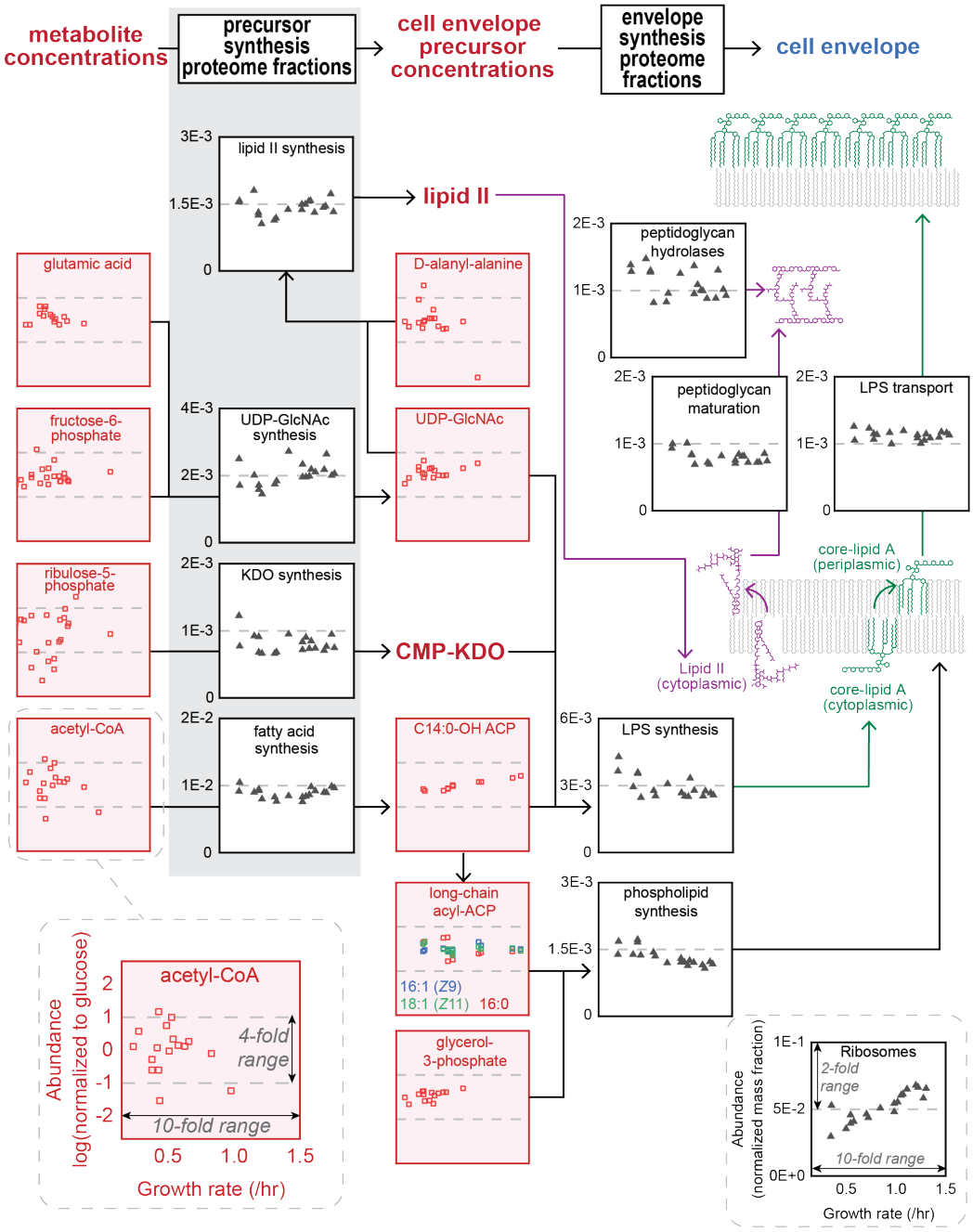
metabolite concentrations
precursor synthesis proteome fractions
cell envelope precursor concentrations
envelope synthesis proteome fractions
cell envelope
lipid II synthesis
lipid II
glutamic acid
D-alanyl-alanine
fructose-6-phosphate
UDP-GlcNAc synthesis
UDP-GlcNAc
ribulose-5-phosphate
KDO synthesis
CMP-KDO
acetyl-CoA
fatty acid synthesis
C14:0-OH ACP
long-chain acyl-ACP
16:1 (Z9)
18:1 (Z11) 16:0
glycerol-3-phosphate
peptidoglycan hydrolases
peptidoglycan maturation
LPS transport
LPS synthesis
phospholipid synthesis
core-lipid A (periplasmic)
Lipid II (cytoplasmic)
core-lipid A (cytoplasmic)
Abundance log(normalized to glucose)
acetyl-CoA
4-fold range
10-fold range
Growth rate (/hr)
Abundance (normalized mass fraction)
Ribosomes
2-fold range
10-fold range
Growth rate (/hr)

Figure 3.1: Cell envelope synthesis pathways and metabolic precursors do not correlate with envelope biosynthesis rates. Steady-state concentrations of metabolites, envelope precursors, and fractions of total cellular proteome dedicated to cell envelope biogenesis across steady-state growth conditions. Metabolite and precursor concentrations are log(2) normalized to the average concentration. Proteome fractions are summed from individual proteins as described in the **Supplemental Text**. For comparison of proteome fractions to a transcriptionally regulated system, concentrations of ribosomal proteins across various growth rates are depicted. All proteomic and metabolomic data was acquired by LCMS, specific protocols are outlined in the respective publications. Proteome fractions were predominantly collected from *E. coli* NCM3722 (a K-12 strain) and derivates predominantly grown on MOPS minimal media, for more details we refer to the original publication (*4*). Metabolite concentrations were collected from *E. coli* BW2511 strain grown on M9 minimal media (Kochanowski et al. 2017 and Radoš et al. 2022), or *E. coli* NCM3722 strain grown on MOPS minimal media (Noga et al. 2020). Measurements of UDP-GlcNAc, glutamate, acetyl-CoA, D-alanyl-alanine, and G3P from (*3*); fructose-6-phosphate and ribulose-5-phosphate from(*9*); acyl-ACP from (*2*) CMP-KDO and lipid II concentrations across growth rates have not been measured to the authors' knowledge. Outliers in G3P plot corresponding to growth in glycerol medium are removed to clarify trend across growth rates in other conditions.

3.5. Envelope assembly controls envelope precursor synthesis through post-translational negative feedback.

If not precursors, metabolites, or transcription, what controls envelope synthesis? The answer can be found by first understanding why precursor concentrations are so stable. The pathways that supply envelope precursors such as fatty acid thioesters, glycerol-3-phosphate, and UDP-N-acetyl glucosamine are feedback-inhibited by their own products, usually via allosteric inhibition **(Supplemental Text)**. Negative feedback stabilizes precursor levels by preventing both precursor excess and precursor depletion. This insulates the process of envelope assembly from disturbances such as transcriptional noise and the variability of upstream metabolite concentrations such as acetyl-CoA. Most importantly, negative feedback also enables the enzymes that assemble the envelope to control the synthesis rates of envelope precursors. This is because pathways under strong negative feedback cannot control product synthesis (*10*). Instead, product synthesis rates respond passively to concentrations of the product, which is also a product synthesis inhibitor. In other words, the "rate-limiting step" of an envelope precursor synthesis pathway under strong negative feedback control is the reaction that consumes the precursor.

To give a concrete example: the fatty acid synthesis pathway is inhibited by its product, long-chain acyl-ACP. Because this inhibitor is primarily consumed by the phospholipid synthesis enzyme PlsB, it is the activity of PlsB that determines the rate of fatty acid biosynthesis. Negative feedback couples acyl-ACP synthesis with phospholipid synthesis: when phospholipid synthesis slows, acyl-ACP accumulation inhibits acyl-ACP synthesis; when phospholipid synthesis accelerates, acyl-ACP depletion increases acyl-ACP synthesis. But what controls PlsB, or the reactions that consume LPS and peptidoglycan precursors? We argue below that negative feedback (acting on the Lpt complex and PlsB) also coordinates LPS and phospholipid synthesis with cell growth.

3.6. Regulatory interactions are often negative feedback loops in disguise.

Many molecules have been proposed to regulate or coordinate envelope biogenesis by directly interacting with pathway enzymes. However, later experiments often reveal that the molecule (or the stress that triggers its production) in fact inhibits the reaction that consumes the pathway product. When product consumption is slowed, the product accumulates, increasing the degree of pathway inhibition through negative feedback. Thus, a more parsimonious explanation for this phenomenon is that the molecule indirectly inhibits the pathway by increasing negative feedback instead of through a novel direct interaction. This principle is well-illustrated by two cases in which proposed inhibitors of the fatty acid synthesis pathway were later shown to act indirectly through negative feedback. Fatty acid synthesis begins with the acetyl-CoA carboxylase complex (ACC), which is feedback-inhibited by the pathway product acyl-ACP (*2*, *11*, *12*). The observation that high concentrations of the alarmone guanosine tetraphosphate (ppGpp) inhibit fatty acid synthesis led to the proposal that ppGpp inhibits ACC (*13*). However, ppGpp also suppresses phospholipid synthesis, leading to acyl-ACP accumulation. Eliminating long-chain acyl-ACP with a thioesterase relieved inhibition despite abundant ppGpp, demonstrating that ppGpp only indirectly inhibits ACC by increasing acyl-ACP levels (*11*). Likewise, the fatty acid catabolism intermediate acyl-CoA was proposed to slow fatty acid synthesis by inhibiting the enoyl-ACP reductase FabI (*14*). However, our measurements of acyl-ACP pools demonstrated that acyl-CoA does not inhibit FabI but instead promotes acyl-ACP accumulation by competing for phospholipid synthesis enzymes PlsB and PlsC (*15*). Thus, neither ppGpp nor acyl-CoA directly inhibit fatty acid synthesis but instead act through feedback inhibition by acyl-ACP.

3.7. Hypothesis: two negative feedback loops acting in series are sufficient to coordinate LPS synthesis with growth.

LPS is synthesized in the cytoplasm and flipped to the periplasmic leaflet of the inner membrane, where it awaits transport to the outer membrane by the Lpt complex **(Supplemental Text)**. LPS synthesis must be tightly regulated because insufficient LPS permeabilizes the outer membrane while excess periplasmic LPS disrupts the inner membrane. In *E. coli*, the amount of LPS produced is highly sensitive to the activity of LpxC, the second enzyme in the LPS synthesis pathway. LpxC is constitutively degraded by the YejM-YciM-FtsH system, which monitors periplasmic LPS levels **(Fig. 3.2A)**. Recent evidence also suggests LpxC may be reversibly inhibited by this system, a mechanism that may be more responsive and economical than proteolysis (*16*). If this is true, LpxC abundance may not necessarily reflect LpxC activity. Regardless of the roles of reversible binding and proteolysis, the system controlling LpxC activity establishes a negative feedback loop that responds to periplasmic LPS accumulation **(Fig. 3.2B)**.

Since the outer membrane is ultimately where LPS ends up, how does periplasmic LPS respond to the demand for outer membrane LPS? *In vitro* experiments with reconstituted Lpt complexes suggest that LPS transport may be feedback-inhibited by the abundance of LPS on the outer membrane (*17*). If this inhibition is also present *in vivo*, it would establish a second negative feedback loop that communicates LPS demand from the outer membrane to the periplasmic LPS pool. In such a scheme, the YejM-YciM-FtsH system does not coordinate LPS synthesis with growth but instead maintains a stable supply of periplasmic LPS for transport while also preventing toxic LPS accumulation **(Fig. 3.2B)**. The role of the YejM-YciM-FtsH system is therefore analogous to the role of cytoplasmic precursor pathways that maintain a supply of precursors rather than controlling the rate of envelope synthesis.

Few pathways have been lavished with as many proposals for regulatory interactions as the LPS synthesis pathway (see (*18*) for an excellent review). We suggest that each proposed regulatory interaction should be experimentally re-evaluated considering the negative feedback loops established by the YejM-YciM and Lpt systems. Just as proposed regulators of fatty acid synthesis were later found to act indirectly by increasing acyl-ACP-mediated negative feedback, we anticipate that many proposed regulators of LPS synthesis will be found to act indirectly via periplasmic LPS. For instance, acyl-CoA generated from phospholipid degradation decreases LpxC proteolysis via an unknown mechanism (*19*). We found that acyl-CoA generated from exogenous fatty acids depletes the LPS precursor C14:0-OH ACP by 50% due to decreased fatty acid synthesis (*15*). We argue that C14:0-OH ACP depletion may in turn deplete periplasmic LPS and therefore stabilize (or activate) LpxC via the YejM-YciM system instead of via direct interactions of any pathway protein with acyl-CoA. Tools for accurately quantifying periplasmic LPS will be essential for testing this hypothesis.

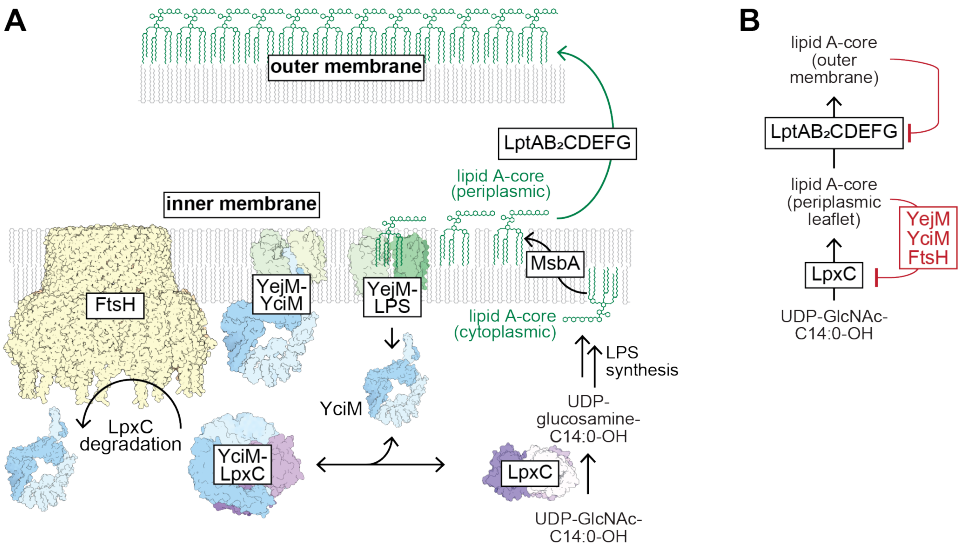

Figure 3.2: Negative feedback loops in the LPS synthesis pathway. **A.** The abundance of periplasmic LPS is monitored by YejM, which sequesters the adaptor protein YciM. When released from YejM, YciM binds to LpxC, which recruits LpxC for degradation by the protease FtsH. Excess periplasmic LPS displaces YciM from YejM, increasing binding of LpxC by YciM, thus increasing LpxC proteolysis and slowing LPS synthesis. Conversely, depleting periplasmic LPS decreases LpxC recruitment, slowing LpxC proteolysis and accelerating LPS synthesis. As LpxC is inhibited when bound with YciM, reversible association of LpxC with YciM may also contribute to controlling LpxC activity and thus LPS synthesis. **B.** A simplified diagram depicting the series of negative feedback loops acting on the LPS synthesis and transport pathways. Inhibition of the Lpt complex by outer membrane LPS coordinates LPS transport with outer membrane expansion, while inhibition of LpxC activity by the YejM-YciM-FtsH system maintains periplasmic LPS at non-toxic concentrations.

3.8. Hypothesis: phospholipid synthesis is regulated by negative feedback.

Phospholipid synthesis is initiated by PlsB, which transfers an acyl chain from acyl-ACP or acyl-CoA to glycerol-3-phosphate to produce lysophosphatidic acid (LPA) **(Supplemental Text)**. As the first enzyme of phospholipid synthesis, PlsB is the most likely target for allosteric regulation (*2*). But what coordinates PlsB activity and membrane synthesis with growth?

Overexpressed PlsB assembles into filaments that wrap helically around a phospholipid core (*20*). While PlsB filaments are enzymatically inactive, dissolution into free monomers restores activity (*21*). While filaments have not been observed in wild-type cells, the low abundance of PlsB (1000/cell) would complicate detection (a filament of 500 PlsB monomers would be 180 nm (*20*)). How might PlsB filamentation establish a negative feedback loop and regulate phospholipid synthesis? Many metabolic enzymes reversibly assemble into inactive filaments in response to accumulation of products of the enzyme or its metabolic pathway (*22*). Thus, enzyme filamentation is often the structural basis of negative feedback. By analogy, PlsB filamentation may be triggered by excess phospholipids accumulating along the inner membrane. This negative feedback mechanism would couple phospholipid synthesis with membrane expansion: growth stretches the membrane, dissolving inactive PlsB filaments into active PlsB monomers and thereby increasing phospholipid synthesis to match the demands of the cell.

Our live-cell fluorescence imaging experiments support this filamentation hypothesis **(Chapter 2)**. GFP-tagged PlsB localizes as discrete foci at wild-type levels, consistent with filament formation. Inhibiting phospholipid synthesis by depleting fatty acid substrates delocalized PlsB, resulting in an even fluorescent distribution within the cytoplasm. Restoring phospholipid synthesis by supplying fatty acids (either by removing the fatty acid synthesis inhibitor or by providing exogenous fatty acids) caused foci to reform after a brief period of cell growth. Thus, the PlsB foci behave in a manner expected of inactive filaments assembling and disassembling in response to phospholipid abundance. Further experiments that disable PlsB filamentation are required to test whether filamentation establishes a negative feedback loop that ensures phospholipid homeostasis. We note that the headgroup composition of *E. coli* phospholipids has long been known to be maintained by a negative feedback loop that responds to membrane charge **(Supplemental Text)**.

3.9. Peptidoglycan synthesis regulation is not controlled by transcription or peptidoglycan precursor supply.

Decades of research into the regulation of peptidoglycan metabolism is converging in support of the ”break-before-make” model, which predicts that the enzymatic step controlled by growth is not insertion of monomers into peptidoglycan strands but rather the hydrolysis reactions that create gaps in existing strands (*23*, *24*). One consequence of this model is that concentrations of the peptidoglycan precursor lipid II do not affect the rate of peptidoglycan mesh expansion, just as lipid precursors do not regulate phospholipid and LPS synthesis. To our knowledge, there are no measurements of lipid II concentrations across growth rates. However, depletion of cell wall precursors does not slow growth in the short-term and overexpression of a cell wall hydrolase transiently increases cell expansion (*25*). This indicates that the rate of peptidoglycan mesh expansion is not sensitive to lipid II abundance.

Since hydrolysis weakens the peptidoglycan mesh, peptidoglycan hydrolases must be tightly controlled. In a striking parallel with LPS synthesis, three endopeptidases (MepS, MepM, and MepH) are degraded by a periplasmic protease, Prc. Proteolysis is mediated by an outer membrane lipoprotein, NlpI. While MepS proteolysis may strictly determine MepS activity, a reversible MepS-NlpI association may also control MepS independently of proteolysis, just as YciM may reversibly inactivate LpxC. Thus, a conformational switch involving NlpI might inhibit (or activate) MepS activity in a reversible manner. How periplasmic lipoproteins regulate peptidoglycan hydrolase activity (either through reversible inhibition alone or in combination with proteolysis) will likely reveal how growth controls peptidoglycan expansion (*24*).

3.10. A GENERAL HYPOTHESIS: ENVELOPE STRETCHING ALLOSTERICALLY ACTIVATES ENVELOPE BIOGENESIS.

We propose that the physical consequences of cell volume expansion allosterically activate specific enzymes and transporters: specifically, PlsB, the Lpt transporter, and the peptidoglycan hydrolases. As both envelope precursor supply and enzyme levels are stable across steady-state growth rates, we predict that these three allosteric control points will prove sufficient to coordinate envelope assembly. Determining the allosteric signals that control these enzymes will likely require structural and biophysical approaches.

We acknowledge several limitations to the data set compiled here: all concentrations have been obtained from steady-state planktonic cultures of *E. coli* K12. Cells in biofilms, colonies, and other nutrient-depleted conditions may use different strategies, and not every Gram-negative species may follow these principles (*1*, *18*). While the notion that growth itself activates envelope biogenesis is not novel, we hope to have demonstrated how tools from the metabolic regulation field can clarify the search for regulatory mechanisms. We also hope to provoke experiments that test whether many proposed signals act via negative feedback. After all, simplifying our understanding by eliminating proposed regulatory interactions is just as important as searching for new interactions. Biology often appears complex because we overlook simplicity.

Bibliography

(*1*) Fivenson, E. M., Dubois, L. and Bernhardt, T. G. (2024). Co-ordinated assembly of the multilayered cell envelope of Gram-negative bacteria. *Current Opinion in Microbiology 79*, 102479.

(*2*) Noga, M. J., Büke, F., van den Broek, N. J. F., Imholz, N. C. E., Scherer, N., Yang, F. and Bokinsky, G. (2020). Posttranslational Control of PlsB Is Sufficient To Coordinate Membrane Synthesis with Growth in *Escherichia coli*. *mBio 11*, e02703–19.

(*3*) Radoš, D., Donati, S., Lempp, M., Rapp, J. and Link, H. (2022). Homeostasis of the biosynthetic *E. coli* metabolome. *iScience 25*, e104503.

(*4*) Mori, M., Zhang, Z., Banaei-Esfahani, A., Lalanne, J.-B., Okano, H., Collins, B. C., Schmidt, A., Schubert, O. T., Lee, D.-S., Li, G.-W., Aebersold, R., Hwa, T. and Ludwig, C. (2021). From coarse to fine: the absolute *Escherichia coli* proteome under diverse growth conditions. *Molecular Systems Biology 17*, MSB20209536.

(*5*) Chubukov, V., Uhr, M., Chat, L. L., Kleijn, R. J., Jules, M., Link, H., Aymerich, S., Stelling, J. and Sauer, U. (2013). Transcriptional regulation is insufficient to explain substrate-induced flux changes in *Bacillus subtilis*. *Molecular Systems Biology 9*, 709.

(*6*) Hackett, S. R., Zanotelli, V. R., Xu, W., Goya, J., Park, J. O., Perlman, D. H., Gibney, P. A., Botstein, D., Storey, J. D. and Rabinowitz, J. D. (2016). Systems-level analysis of mechanisms regulating yeast metabolic flux. *Science 354*, aaf2786.

(*7*) Scott, M., Gunderson, C. W., Mateescu, E. M., Zhang, Z. and Hwa, T. (2010). Interdependence of cell growth and gene expression: Origins and consequences. *Science 330*, 1099–1102.

(*8*) Simpson, B. W. and Trent, M. S. (2019). Pushing the envelope: LPS modifications and their consequences. *Nature Reviews Microbiology 17*, 403–416.

(*9*) Kochanowski, K., Gerosa, L., Brunner, S. F., Christodoulou, D., Nikolaev, Y. V. and Sauer, U. (2017). Few regulatory metabolites coordinate expression of central metabolic genes in *Escherichia coli*. *Molecular Systems Biology 13*, DOI: 10.15252/msb.20167402.

(*10*) Sauro, H. M. (2017). Control and regulation of pathways via negative feedback. *Journal of the Royal Society Interface 14*, 20160848.

(*11*) Davis, M. S., Solbiati, J. and Cronan, J. E. (2000). Overproduction of acetyl-CoA carboxylase activity increases the rate of fatty acid biosynthesis in *Escherichia coli*. *Journal of Biological Chemistry 275*, 28593–28598.

(*12*) Davis, M. S. and Cronan, J. E. (2001). Inhibition of *Escherichia coli* acetyl coenzyme A carboxylase by acyl-acyl carrier protein. *Journal of Bacteriology 183*, 1499–1503.

(*13*) Polakis, S. E., Guchhait, R. B. and Lane, M. D. (1973). Stringent Control of Fatty Acid Synthesis in *Escherichia coli*. *Journal of Biological Chemistry 248*, 7957–7966.

(*14*) Bergler, H., Fuchsbichler, S., Högenauer, G. and Turnowsky, F. (1996). The enoyl-[acyl-carrier-protein] reductase (FabI) of *Escherichia coli*, which catalyzes a key regulatory step in fatty acid biosynthesis, accepts NADH and NADPH as cofactors and is inhibited by palmitoyl-CoA. *European Journal of Biochemistry 242*, 689–694.

(*15*) van den Berg, S. P. H., Zoumaro-Djayoon, A., Yang, F. and Bokinsky, G. (2024). Exogenous fatty acids inhibit fatty acid synthesis by competing with endogenously generated substrates for phospholipid synthesis in *Escherichia coli*. *FEBS Letters 599*, 667–681.

(*16*) Shu, S., Tsutsui, Y., Nathawat, R. and Mi, W. (2024). Dual function of LapB (YciM) in regulating *Escherichia coli* lipopolysaccharide synthesis. *Proceedings of the National Academy of Sciences of the United States of America 121*, e2321510121.

(*17*) Xie, R., Taylor, R. J. and Kahne, D. (2018). Outer Membrane Translocon Communicates with Inner Membrane ATPase to Stop Lipopolysaccharide Transport. *Journal of the American Chemical Society 140*, 12691–12694.

(*18*) Hummels, K. R. (2025). The Regulation of Lipid A Biosynthesis. *Journal of Biological Chemistry 301*, 110556.

(*19*) May, K. L. and Silhavy, T. J. (2018). The *Escherichia coli* Phospholipase PldA Regulates Outer Membrane Homeostasis via Lipid Signaling. *mBio*, e10–1128.

(*20*) Wilkison, W. O., Walsh, J. P., Corless, J. M. and Bell, R. M. (1986). Crystalline Arrays of the *Escherichia coli* sn-Glycerol-3-phosphate Acyltransferase, an Integral Membrane Protein. *The Journal of Biological Chemistry 261*, 9951–9958.

(*21*) Wilkison, W. O., Bell, R. M., Taylor, K. A. and Costello, J. M. (1992). Structural Characterization of Ordered Arrays of sn-Glycerol-3-Phosphate Acyltransferase from *Escherichia coli*. *Journal of Bacteriology 174*, 6608–6616.

(*22*) Park, C. K. and Horton, N. C. (2019). Structures, functions, and mechanisms of filament forming enzymes: a renaissance of enzyme filamentation. *Biophysical Reviews 11*, 927–994.

(*23*) Garde, S., Chodisetti, P. K. and Reddy, M. (2021). Peptidoglycan: Structure, Synthesis, and Regulation. *EcoSal Plus 9*, DOI: 10.1128/ecosalplus.esp-0010-2020.

(*24*) Weidel, W., Frank, H. and Martin, H. H. (1960). The rigid layer of the cell wall of *Escherichia coli* strain B. *Microbiology 22*, 158–166.

(*25*) Oldewurtel, E. R., Kitahara, Y., Cordier, B., Wheeler, R., Özbaykal, G., Brambilla, E., Boneca, I. G., Renner, L. D. and van Teeffelen, S. (2023). Cell envelope growth of Gram-negative bacteria proceeds independently of cell wall synthesis. *The EMBO Journal 42*, e112168.

3.11. SUPPLEMENTAL TEXT

The components of the cell envelope are assembled from precursors synthesized within the cytoplasm. Evidence for product inhibition has been obtained for many precursor pathways. Here we review published work on the mechanisms regulating these pathways.

3.12. FATTY ACID SYNTHESIS

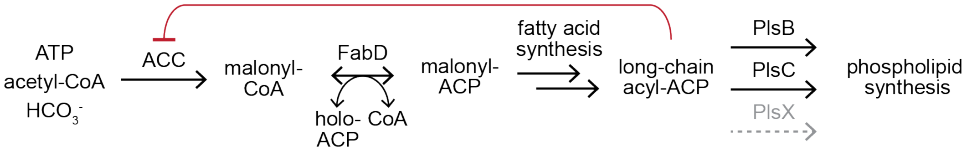

The first step of fatty acid synthesis is catalyzed by the acetyl-CoA carboxylase complex (ACC), which converts acetyl-CoA to malonyl-CoA in a biotin-dependent series of reactions that consumes ATP and bicarbonate (*1*, *2*). Next, the malonyl group is transferred from CoA to the phosphopantethiene thiol of acyl carrier protein (holo-ACP) by malonyl thiotransferase (FabD) (*3*, *4*). Malonyl-ACP provides the carbon required for both fatty acid initiation and elongation reactions. Early studies found that fatty acid synthesis is tightly coupled to phospholipid synthesis. A mutant deficient in G3P (required for long-chain acyl-ACP consumption by the phospholipid synthesis pathway) accumulates abnormally long acyl-ACP and fatty acid synthesis is inhibited by 90% when G3P is withheld (*5*). Cytoplasmic expression of the thioesterase TesA, which depletes acyl-ACP by hydrolyzing the thioester bond, relieves this inhibition. Furthermore, balanced expression of all four ACC subunits increased concentrations of malonyl-CoA by more than 100-fold but did not increase abundance of total phospholipids (*6*). Co-expression of TesA with ACC resulted in a 6-fold increase in free fatty acids and only a mild decrease in total phospholipid abundance. These results are consistent with acyl-ACP acting as a negative feedback inhibitor of ACC activity (*7*). TesA expression short-circuits the acyl-ACP negative feedback loop and is widely exploited in metabolic engineering to generate free fatty acids (*8*, *9*).

Later biochemical experiments found acyl-ACP species with a variety of chain lengths are equally capable of inhibiting ACC. In cell extracts, 40 μM acyl-ACP of all chain lengths tested (C4, C8, C12, C16, C16:1, C18:1, and C20:1) reduces ACC activity by roughly 65%, while holo-ACP did not inhibit ACC (*10*). However, further studies suggest that ACC regulation may not be so simple. Characterization found both competitive and non-competitive inhibition by acyl-ACP (*10*). ACC inhibition exhibits hysteresis (the dependence of a state of a system on its history): varying the length of incubation of the purified ACC complex prior to the addition of palmitoyl-ACP affects the degree of inhibition observed. More recent work suggests that palmitoyl-ACP disrupts binding between the carboxyltransferase and the biotin carboxylase complexes (*11*).

A recent report described how the ACC complex assembles into filamentous structures, a phenomenon long known to exist for eukaryotic ACC (*12*, *13*). In the presence of substrates, ACC assembles into well-ordered hollow tubes (*14*). While the substrate requirement for ordered assembly into filaments hints at a possible importance for activity, the physiological relevance of these filaments is yet to be determined. Nevertheless, the fact that *E. coli* ACC forms filaments is likely an essential feature to account for in models of ACC regulation. Structural studies of *E. coli* ACC filaments will likely be needed to understand how acyl-ACP inhibits ACC.

When PlsB activity was artificially varied to mimic variations in phospholipid synthesis flux in our simple model featuring only ACC inhibition by acyl-ACP, simulated concentrations of both fatty acid and phospholipid synthesis intermediates closely followed our experimental data (*15*). This is strongly consistent with long-chain acyl-ACP inhibiting ACC during steady-state growth. We also found no indication that other proposed targets of acyl-ACP inhibition (specifically FabH and FabI) play any role in controlling the total amount of fatty acids produced, despite earlier *in vitro* evidence suggesting such interactions (*16*, *17*).

3.13. Glycerol-3-phosphate synthesis

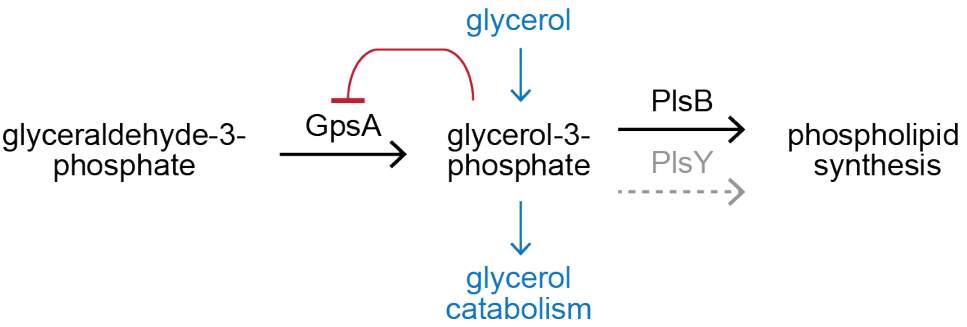

sn-glycerol-3-phosphate (G3P) provides the backbone of all phospholipids in *E. coli* as well as a headgroup for phosphatidylglycerol. G3P is synthesized from glycerone-3-phosphate by the glycerol-3-phosphate dehydrogenase enzyme GpsA. GpsA is product-inhibited by G3P (*18*). Cells expressing feedback-insensitive GpsA exhibit G3P concentration 12-fold higher than wild-type, consistent with negative feedback (*19*). Later *in vitro* measurements obtained a K_I value of 4.4 μM (*20*). G3P concentrations are stable across most growth conditions but slightly increase with growth rate (*15*, *21*). However, G3P is an intermediate of glycerol catabolism and is at least 20-fold more abundant in glycerol cultures (*15*). As glycerol cultures of *E. coli* do not exhibit any increase in phospholipid abundance, physiological concentrations of G3P do not influence membrane synthesis. Instead, GpsA maintains G3P at concentrations well above those required to sustain phospholipid synthesis by PlsB.

3.14. PHOSPHOLIPID HEADGROUP COMPOSITION IS MAINTAINED BY NEGATIVE FEEDBACK

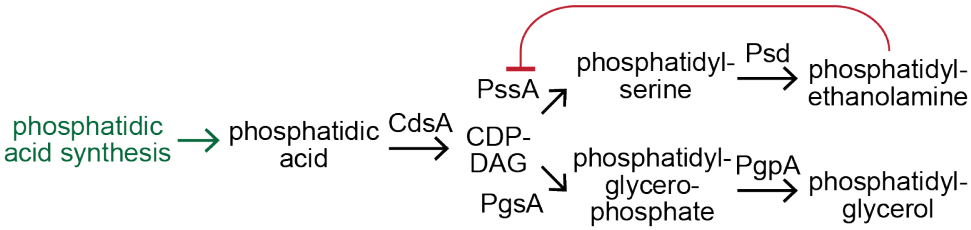

E. coli phospholipids come in three major species: phosphatidylethanolamine (PE) phosphatidylglycerol (PG), and cardiolipin (CL). PG comprises 15-20% of membrane phospholipids, while PE comprises 70-75% of membrane phospholipids. PG synthesis is initiated by CDP-diacylglycerol-glycerol-3-phosphate 3-phosphatidyltransferase PgsA, which displaces CMP with G3P (*22*) to produce phosphatidylglycerolphosphate (PGP). The terminal phosphate of PGP is removed by phosphatase PgpA to form PG (*23*), although the phosphatases PgpB and PgpC also contribute to PG synthesis (*24*, *25*). PE synthesis is initiated by the transfer of serine to CDP-DAG by the phosphatidylserine synthase PssA to produce phosphatidylserine (PS) (*26*), which in turn is decarboxylated by phosphatidylserine decarboxylase Psd to produce PE (*27*).

The PE/PG ratio determines the electrostatic charge of the phospholipid membrane and influences lipid packing and membrane shape (*28*). The PE/PG ratio is determined by the relative activities of PssA and PgsA. Overexpression of either PssA or PgsA has very little effect on membrane composition (*29*, *30*), suggesting the PE/PG ratio is maintained via a post-translational mechanism (*31*). The nature of the mechanism was first hinted at when PssA was found to associate with ribosomes (*32*), suggesting PssA might preferentially associate with anionic phospholipids such as PG. Saha et al. confirmed that PssA activity is impacted by anionic phospholipids (*33*). Further studies demonstrated that anionic phospholipids increase PssA association with the membrane (*34*, *35*). Since headgroup modification reactions require membrane association, increased association increases PE synthesis (*33*, *34*). Dimerization of PssA may also contribute to regulation (*36*). Thus, membrane charge homeostasis is achieved via negative feedback: deficient PE activates PssA, while excess PE inhibits PssA.

3.15. UDP-N-ACETYL GLUCOSAMINE SYNTHESIS

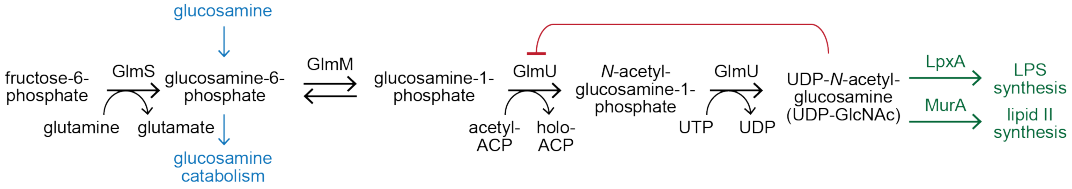

Both LPS and peptidoglycan synthesis rely upon UDP-N-acetyl glucosamine: it provides the anchoring headgroup for multiple lipids for lipid A and the core of peptidoglycan building block Lipid II. Glucosamine and N-acetyl glucosamine can be scavenged from the environment via a dedicated PTS system. In the absence of exogenous glucosamine, glucosamine-1-phosphate is produced from fructose-6-phosphate and glutamine by GlmS and GlmM. Next, the bifunctional enzyme GlmU transfers an acetyl group from acetyl-CoA (or acetyl-ACP, see below) and UDP to produce UDP-N-acetyl glucosamine (*37*–*40*). Remarkably, GlmU is inhibited by N-acetyl glucosamine but only weakly by UDP-N-acetyl glucosamine even at high concentrations (1 mM). As a consequence, UDP-N-acetyl glucosamine is very abundant in growing *E. coli* (2-9 mM) (*41*). This concentration likely drives the initial reaction of LPS biosynthesis, which is thermodynamically unfavorable (*42*).

Recently, an intriguing link between fatty acid synthesis and UDP-N-acetyl glucosamine synthesis was discovered. GlmU has long been thought to use acetyl-CoA as a substrate, although its KM is rather high (600 µM) (*43*). Malonyl-ACP decarboxylase (MadA, also known as FabY and formerly as YiiD), has been recently discovered to generate acetyl-ACP from malonyl-ACP. This study found that the KM of GlmU for acetyl-ACP is far lower (20 µM) (*44*), a strong indication that acetyl-ACP is the true physiological substrate for GlmU rather than acetyl-CoA. This may be important because acetyl-CoA concentrations are highly sensitive to the carbon source but are wholly uncorrelated with growth rate. Our measurements indicate that acetyl-ACP concentrations are far more stable than acetyl-CoA (*15*).

3.16. LPS SYNTHESIS

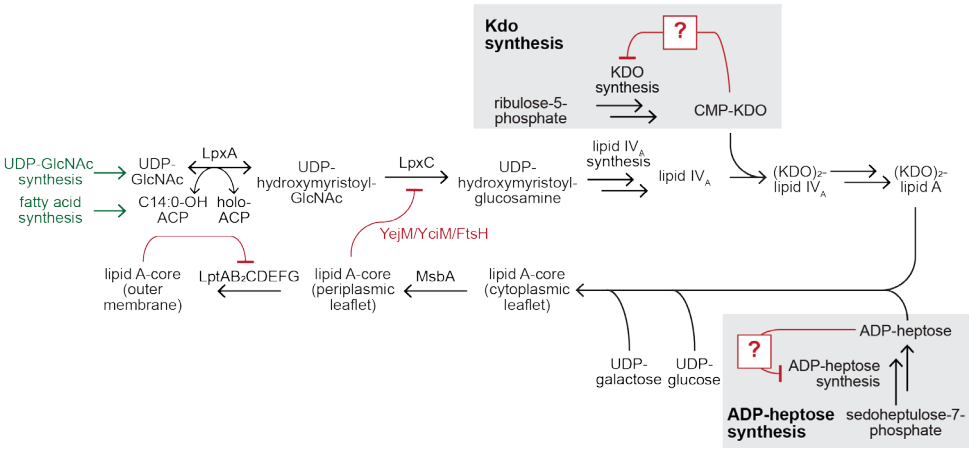

LPS are anchored by the glycolipid moiety Lipid A (a disaccharide functionalized with multiple fatty acids) bearing a core oligosaccharide. Phosphate groups attached to the disaccharide allow divalent ions to electrostatically bridge adjacent LPS. During synthesis within the cytoplasm and prior to transport to the outer membrane, LPS and its synthesis intermediates intercalate into the phospholipid inner membrane. LPS synthesis begins with the synthesis of Lipid A from intermediates of the fatty acid synthesis pathway. The first acylation of the N-acetyl glucosamine headgroup is catalyzed by acyl-ACP-UDP-N-acetylglucosamine O-acyltransferase LpxA, which transfers a C14:0-OH fatty acid from ACP to UDP-N-acetylglucosamine. Deacetylation of this intermediate by UDP-3-O-acyl-N-acetylglucosamine deacetylase (LpxC) commits the intermediate to the LPS biosynthesis pathway. Subsequent steps, which include several additional transfers of acyl groups, yield Lipid IVA. Lipid IVA is glycosylated using CMP-KDO and acylated to generate lipid A, which is further glycosylated with core saccharides to yield mature LPS. LPS is flipped from the cytoplasmic face of the inner membrane to the periplasmic face by MsbA. Periplasmic LPS modulates LpxC proteolysis via the YejM-YciM-FtsH system as described in the main text (*45–54*). Finally, periplasmic LPS is extracted from the inner membrane and transported to the outer membrane by the Lpt system ($LptAB_2CDEFG$). As described in the main text, *in vitro* evidence suggests that LPS transport to the outer membrane is feedback-inhibited by outer membrane LPS.

CMP-3-DEOXY-D-MANNO-OCTULOSONATE (KDO) SYNTHESIS

KDO is attached to the glucosamine headgroup of lipid A and contributes the anchor point for the remaining moieties of the core oligosaccharide. KDO is synthesized via

a 5-step pathway (*55*). KdsD isomerizes D-ribulose-5-phosphate to D-arabinose-5-phosphate. This is a reversible reaction (Keq = 0.5) (*56*); thus the committed step of the pathway is likely catalyzed by KdsA, which condenses D-arabinose-5-phosphate with phosphoenolpyruvate to produce KDO-8-phosphate. KdsA is inhibited by its own product (KI = 590 uM) but whether the final product of the pathway (CMP-KDO) inhibits KdsA is not known. KDO-8-phosphate is dephosphorylated by KdsC to produce KDO (*57*). Finally, KdsB activates KDO by transferring CMP from CTP. CMP-KDO is the substrate of WaaA, which transfers KDO to the LPS synthesis intermediate lipid IVA to produce KDO-lipid A. To our knowledge, CMP-KDO concentrations have not been quantified in growing *E. coli*.

LPS core sugar synthesis

The core sugars of LPS, glycero-β-D-manno-heptose, glucose, and galactose, are added as monomers in a specific order to $(KDO)_2$-lipid A by dedicated enzymes that use nucleotide diphosphate-activated monosaccharides UDP-glucose and UDP-galactose, which both share a 2-step synthesis starting from glucose-6-phosphate. UDP-glucose and UDP-galactose are also precursors for other cell components such as trehalose, and UDP-galactose is an intermediate in galactose catabolism. While the enzymes that produce both sugar nucleotides have been identified and characterized, no regulatory mechanisms have been shown. ADP-L-glycero-β-D-manno-heptose is exclusively used for LPS core saccharide synthesis and features a longer synthesis pathway that begins with isomerization of the central carbon metabolite seduheptulose 7-phosphate by the enzyme GmhA, followed by ATP-driven phosphorylation of the product by HldE. Subsequent steps are dephosphorylation by GmhB, addition of the ADP moiety by HldE, and a final isomerization step by RfaD. As far as we are aware, no regulatory mechanisms for this pathway have been discovered nor have concentrations of ADP-L-glycero-β-D-manno-heptose in growing *E. coli* been reported.

3.17. Peptidoglycan synthesis

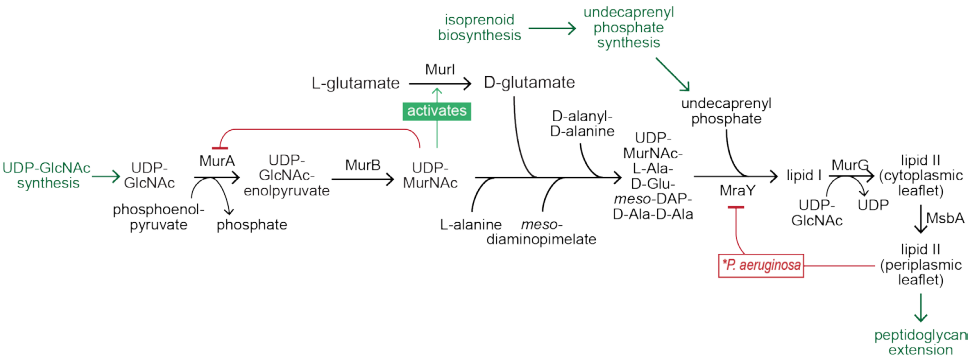

MurA is inhibited by UDP-MurNAc

After the synthesis of UDP-GlcNAc follows the two-step synthesis of UDP-N-acetyl-α-D-muramate (UDP-MurNAc). The first step, the transfer of enolpyruvyl from phosphoenolpyruvate to UDP-GlcNAc, is catalyzed by MurA (*58*). The MurA reaction is followed by a reduction step catalyzed by MurB, forming the intermediate UDP-MurNAc (*59*). This reaction is regulated to control the influx into peptidoglycan synthesis. UDP-MurNAc strongly inhibits MurA, suggesting that the irreversible step is controlled by subsequent steps that consume UDP-MurNAc. Inhibition of MurA by UDP-MurNAc is competitive with regard to phosphoenolpyruvate while inhibition towards UDP-GlcNAc appears to be mixed (*60*).

Glutamate racemase MurI is activated by UDP-MurNAc-L-Ala

The next step in the pathway is the addition of amino acids to the sugar moiety. The first step, addition of L-alanine to UDP-MurNAc to make UDP-N-acetylmuramoyl-L-alanine (UDP-MurNAc-L-Ala), is catalyzed by MurC (*61*). The next step is the addition of D-glutamate, catalyzed by MurD (*62*). Isomerization of L-glutamate to the D form requires the racemase MurI (*63*). Interestingly, MurI is activated by the other substrate of MurD, UDP-MurNAc-L-Ala (*64*). In this way the racemization of glutamate is tightly linked to the available UDP-MurNAc-L-Ala. This regulation likely serves to prevent accumulation of D-glutamate in excess of pathway requirements rather than a mechanism for controlling the rate of lipid II synthesis.

Lipid II synthesis is feedback-inhibited across the inner membrane by periplasmic lipid II in *Pseudomonas aeruginosa*

Recently MraY from *Pseudomonas aeruginosa* was found to be allosterically inhibited by Lipid II (*65*). While *E. coli* and *P. aeruginosa* MraY have only a 67% identity match, the residue implicated in lipid II binding is conserved and it therefore seems worthwhile to investigate if *E. coli* MraY is also inhibited by Lipid II. Such a mechanism would enable the enzymes of peptidoglycan synthesis that are located in the periplasm to control the cytoplasmic biosynthesis of lipid II and its precursors.

3.18. Supplemental Figures

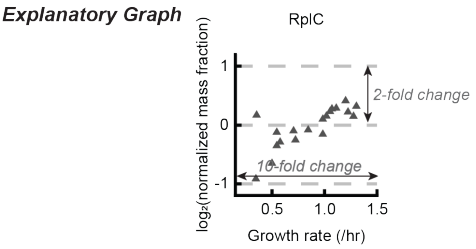

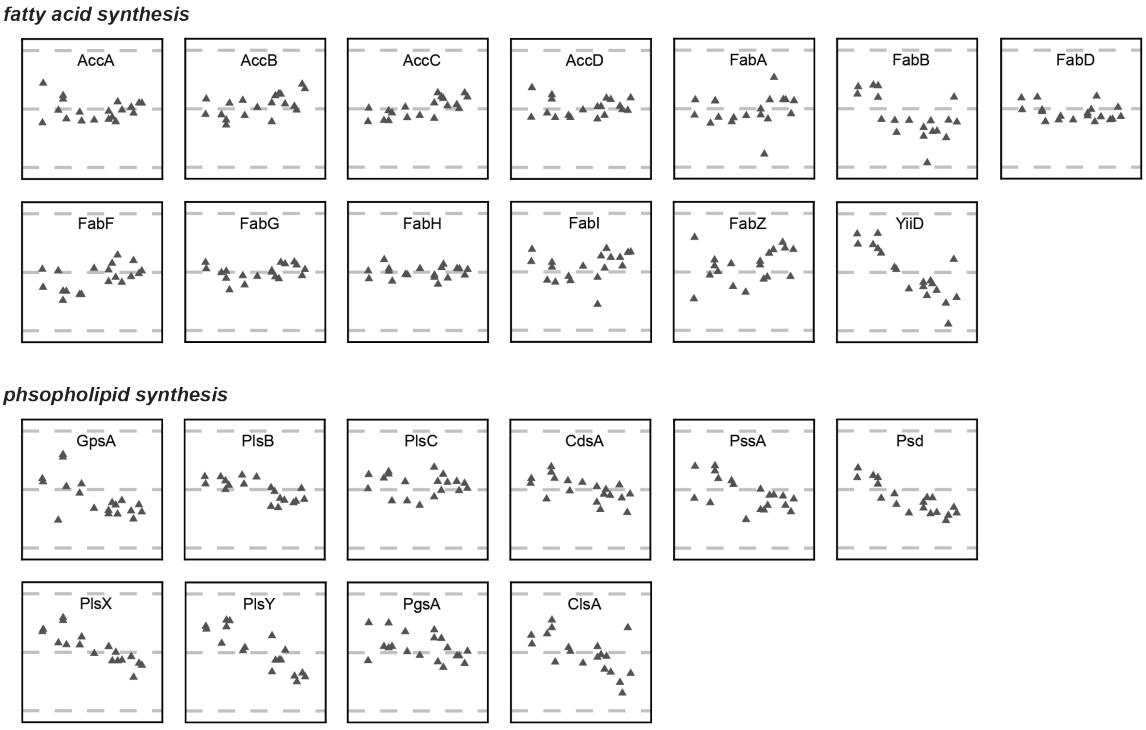

Supp. Fig. 3.1: Proteome mass fractions of enzymes of fatty acid and phospholipid synthesis pathways as growth is varied by nutrient type. Mass fractions are normalized to average value and log2-transformed to depict trends.

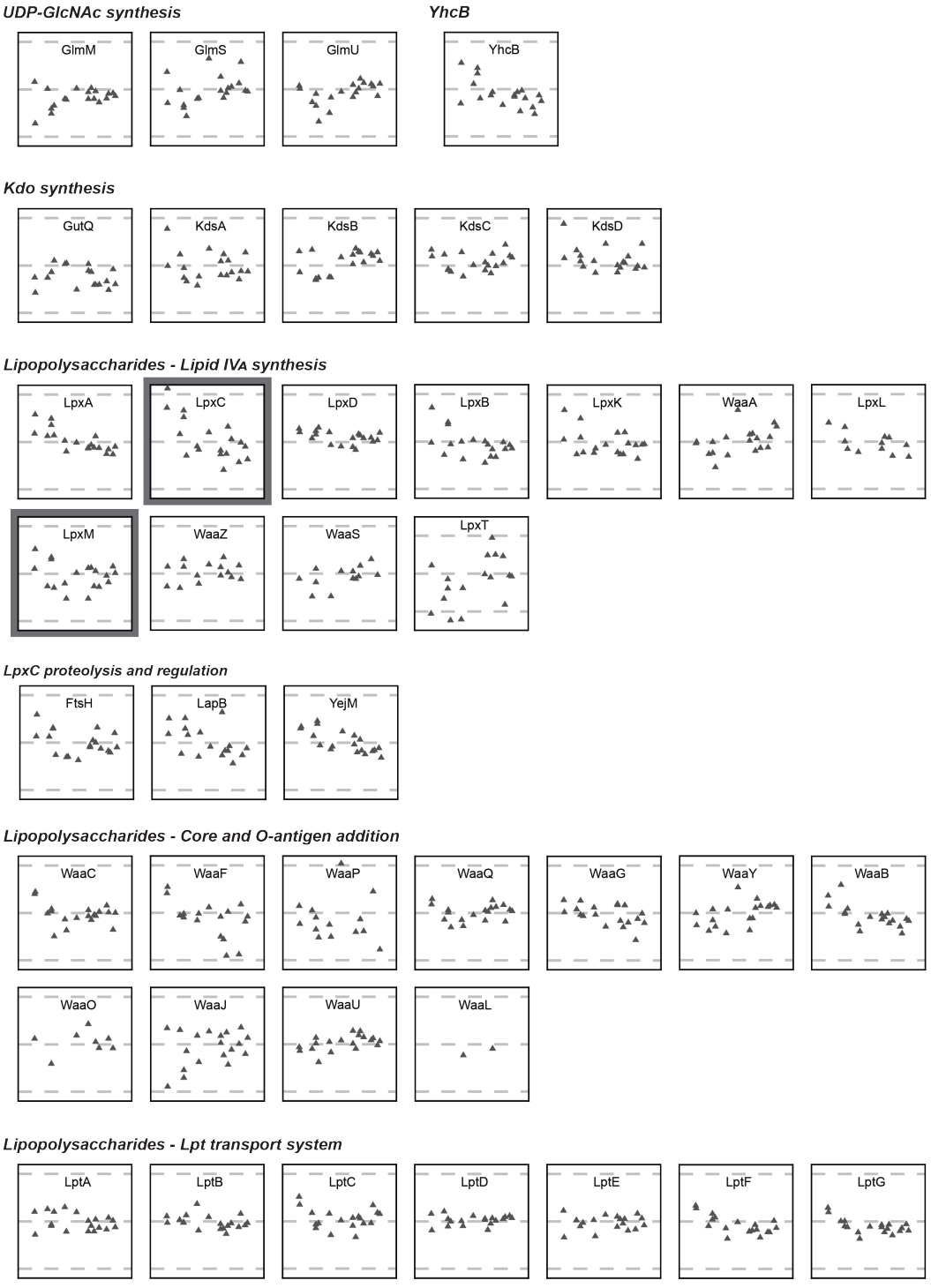
UDP-GlcNAc synthesis
GlmM
GlmS
GlmU
YhcB
YhcB
Kdo synthesis
GutQ
KdsA
KdsB
KdsC
KdsD
Lipopolysaccharides - Lipid IVA synthesis
LpxA
LpxC
LpxD
LpxB
LpxK
WaaA
LpxL
LpxM
WaaZ
WaaS
LpxT
LpxC proteolysis and regulation
FtsH
LapB
YejM
Lipopolysaccharides - Core and O-antigen addition
WaaC
WaaF
WaaP
WaaQ
WaaG
WaaY
WaaB
WaaO
WaaJ
WaaU
WaaL
Lipopolysaccharides - Lpt transport system
LptA
LptB
LptC
LptD
LptE
LptF
LptG

Supp. Fig. 3.2

Supp. Fig. 3.2: Proteome mass fractions of enzymes of LPS precursor synthesis, LPS synthesis, and LPS transport pathways as growth is varied by nutrient type. Mass fractions are normalized as described in **Supplemental Figure 1**. Proteins known to be degraded are highlighted with thick grey box. As samples for this data set were not obtained using a fast quenching method, concentrations of proteins targeted for proteolysis may not reflect physiological values.

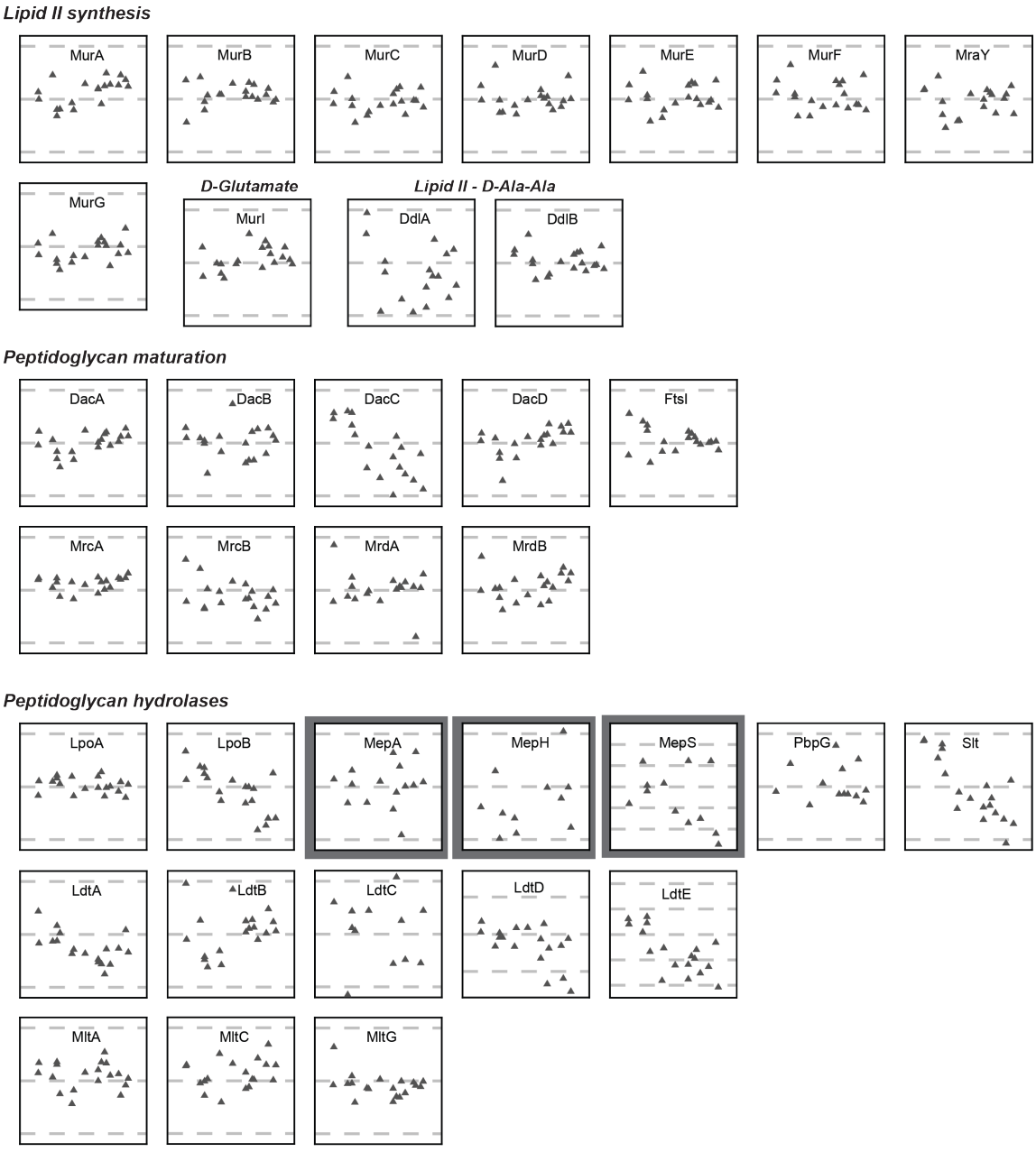

Supp. Fig. 3.3: Proteome mass fractions of enzymes of lipid II synthesis, lipid II transport, peptidoglycan maturase and peptidoglycan hydrolases as growth is varied by nutrient type. Mass fractions are normalized as described in **Supplemental Figure 1**. Proteins known to be degraded are highlighted with thick grey box. As samples for this data set were not obtained using a fast quenching method, concentrations of proteins targeted for proteolysis may not reflect physiological values.

Bibliography

(*1*) Guchhait, R. B., Polakis, S. E., Dimroth, P., Stoll, E., Moss, J. and Lane, M. D. (1974). Acetyl Coenzyme A Carboxylase System of *Escherichia coli*. purification and properties of the biotin carboxylase, carboxyltransferase, and carboxyl carrier protein components. *The Journal of Biological Chemistry 249*, 6645–6653.

(*2*) Li, S.-J. and Cronan, J. E. (1992). The Genes Encoding the Two Carboxyltransferase Subunits of *Escherichia coli* Acetyl-CoA Carboxylase. *The Journal of Biological Chemistry 267*, 16841–16847.

(*3*) Williamson, I. P. and Wakil, S. J. (1966). Studies on the Mechanism of Fatty Acid Synthesis. Preparation and general properties of acetyl coenzyme A and malonyl coenzyme A-acyl carrier protein transacylases. *The Journal of Biological Chemistry 241*, 2326–2332.

(*4*) Oefner, C., Schulz, H., D'Arcy, A. and Dale, G. E. (2006). Mapping the active site of *Escherichia coli* malonyl-CoA-acyl carrier protein transacylase (FabD) by protein crystallography. *Acta Crystallographica Section D: Biological Crystallography 62*, 613–618.

(*5*) Jiang, P. and Cronan, J. E. (1994). Inhibition of Fatty Acid Synthesis in *Escherichia coli* in the Absence of Phospholipid Synthesis and Release of Inhibition by Thioesterase Action. *Journal of Bacteriology 176*, 2814–2821.

(*6*) Davis, M. S., Solbiati, J. and Cronan, J. E. (2000). Overproduction of acetyl-CoA carboxylase activity increases the rate of fatty acid biosynthesis in *Escherichia coli*. *Journal of Biological Chemistry 275*, 28593–28598.

(*7*) Cho, H. and Cronan, J. E. (1995). Defective export of a periplasmic enzyme disrupts regulation of fatty acid synthesis. *Journal of Biological Chemistry 270*, 4216–4219.

(*8*) Park, W. S., Shin, K. S., Jung, H. W., Lee, Y., Sathesh-Prabu, C. and Lee, S. K. (2022). Combinatorial Metabolic Engineering Strategies for the Enhanced Production of Free Fatty Acids in *Escherichia coli*. *Journal of Agricultural and Food Chemistry 70*, 13913–13921.

(*9*) Lennen, R. M. and Pfleger, B. F. (2012). Engineering *Escherichia coli* to synthesize free fatty acids. *Trends in Biotechnology 30*, 659–667.

(*10*) Davis, M. S. and Cronan, J. E. (2001). Inhibition of *Escherichia coli* acetyl coenzyme A carboxylase by acyl-acyl carrier protein. *Journal of Bacteriology 183*, 1499–1503.

(*11*) Evans, A., Ribble, W., Schexnaydre, E. and Waldrop, G. L. (2017). Acetyl-CoA carboxylase from *Escherichia coli* exhibits a pronounced hysteresis when inhibited by palmitoyl-acyl carrier protein. *Archives of Biochemistry and Biophysics 636*, 100–109.

(*12*) Park, C. K. and Horton, N. C. (2019). Structures, functions, and mechanisms of filament forming enzymes: a renaissance of enzyme filamentation. *Biophysical Reviews 11*, 927–994.

(*13*) Meredith, M. J. and Lane, M. D. (1978). Acetyl-CoA carboxylase. Evidence for polymeric filament to protomer transition in the intact avian liver cell. *Journal of Biological Chemistry 253*, 3381–3383.

(*14*) Xu, X., de Sousa, A. S., Boram, T. J., Jiang, W. and Lohman, J. R. (2024). Active *E. coli* heteromeric acetyl-CoA carboxylase forms polymorphic helical tubular filaments. *Preprint, bioRxiv*, DOI: 10.1101/2024.05.28.596234.

(*15*) Noga, M. J., Büke, F., van den Broek, N. J. F., Imholz, N. C. E., Scherer, N., Yang, F. and Bokinsky, G. (2020). Posttranslational Control of PlsB Is Sufficient To Coordinate Membrane Synthesis with Growth in *Escherichia coli*. *mBio 11*, e02703–19.

(*16*) Heath, R. J. and Rock, C. O. (1996). Inhibition of beta-Ketoacyl-Acyl Carrier Protein Synthase III (FabH) by Acyl-Acyl Carrier Protein in *Escherichia coli*. *Journal of Biological Chemistry 271*, 10996–11000.

(*17*) Heath, R. J. and Rock, C. O. (1996). Regulation of fatty acid elongation and initiation by acyl-acyl carrier protein in *Escherichia coli*. *Journal of Biological Chemistry 271*, 1833–1836.

(*18*) Cronan, J. E. and Rock, C. O. (2008). Biosynthesis of Membrane Lipids. *EcoSal Plus 3*, DOI: 10.1128/ecosalplus.3.6.4.

(*19*) Bell, R. M. and Cronan, J. E. (1975). Mutants of *Escherichia coli* Defective in Membrane Phospholipid Synthesis. Phenotypic suppression of sn-glycerol-3-phosphate acyltransferase Km mutants by loss of feedback inhibition of the biosynthetic sn-glycerol-3-phosphate dehydrogenase. *The Journal of Biological Chemistry 250*, 7153–7158.

(*20*) Edgar, J. R. and Bell, R. M. (1979). Biosynthesis in *Escherichia coli* of sn-glycerol 3-phosphate, a precursor of phospholipid. Palmitoyl-CoA inhibition of the biosynthetic sn-glycerol-3-phosphate dehydrogenase. *The Journal of Biological Chemistry 254*, 1016–1021.

(*21*) Radoš, D., Donati, S., Lempp, M., Rapp, J. and Link, H. (2022). Homeostasis of the biosynthetic *E. coli* metabolome. *iScience 25*, e104503.

(*22*) Hirabayashi, T., Larson, T. J. and Dowhan, W. (1976). Membrane-Associated Phosphatidylglycerophosphate Synthetase from *Escherichia coli*: Purification by Substrate Affinity Chromatography on Cytidine 5'-Diphospho-1,2-diacyl-sn-glycerol Sepharose. *Biochemistry 15*, 5205–5211.

(*23*) Icho, T. and Raetz, C. R. H. (1983). Multiple Genes for Membrane-Bound Phosphatases in *Escherichia coli* and Their Action on Phospholipid Precursors. *Journal of Bacteriology 153*, 722–730.

(*24*) Funk, C. R., Zimniak, L. and Dowhan, W. (1992). The pgpA and pgpB Genes of *Escherichia coli* Are Not Essential: Evidence for a Third Phosphatidylglycerophosphate Phosphatase. *Journal of bacteriology 174*, 205–213.

(*25*) Dillon, D. A., Wu, W.-I., Riedel, B., Wissing, J. B., Dowhan, W. and Carman, G. M. (1996). The *Escherichia coli* pgpB Gene Encodes for a Diacylglycerol Pyrophosphate Phosphatase Activity. *Journal of Biological Chemistry 271*, 30548–30553.

(*26*) Raetz, C. R. (1976). Phosphatidylserine synthetase mutants of *Escherichia coli*. Genetic mapping and membrane phospholipid composition. *Journal of Biological Chemistry 251*, 3242–3249.

(*27*) Hawrot, E. and Kennedy, E. P. (1975). Biogenesis of Membrane Lipids: Mutants of *Escherichia coli* with Temperature-Sensitive Phosphatidylserine Decarboxylase. *Proc. Natl. Acad. Sci. USA 72*, 1112–1116.

(*28*) Rowlett, V. W., Mallampalli, V. K. P. S., Karlstaedt, A., Dowhan, W., Taegtmeyer, H., Margolin, W. and Vitrac, H. (2017). Impact of Membrane Phospholipid Alterations in *Escherichia coli* on Cellular Function and Bacterial Stress Adaptation. *Journal of bacteriology 199*, 1110–1128.

(*29*) Tan, Z., Khakbaz, P., Chen, Y., Lombardo, J., Yoon, J. M., Shanks, J. V., Klauda, J. B. and Jarboe, L. R. (2017). Engineering *Escherichia coli* membrane phospholipid head distribution improves tolerance and production of biorenewables. *Metabolic Engineering 44*, 1–12.

(*30*) Ohta, A., Waggoner, K., Louie, K. and Dowhan, W. (1981). Cloning of genes involved in membrane lipid synthesis. Effects of amplification of phosphatidylserine synthase in *Escherichia coli*. *Journal of Biological Chemistry 256*, 2219–2225.

(*31*) Zhang, Y. M. and Rock, C. O. (2008). Membrane lipid homeostasis in bacteria. *Nature Reviews Microbiology 6*, 222–233.

(*32*) Raetz, C. R. and Kennedy, E. P. (1972). The association of phosphatidylserine synthetase with ribosomes in extracts of *Escherichia coli*. *The Journal of Biological Chemistry 247*, 2008–2014.

(*33*) Saha, S. K., Nishijima, S., Matsuzaki, H., Shibuya, I. and Matsumoto, K. (1996). A Regulatory Mechanism for the Balanced Synthesis of Membrane Phospholipid Species in *Escherichia coli*. *Bioscience, biotechnology, and biochemistry 60*, 111–116.

(*34*) Linde, K., Gröbner, G. and Rilfors, L. (2004). Lipid dependence and activity control of phosphatidylserine synthase from *Escherichia coli*. *FEBS Letters 575*, 77–80.

(*35*) Salamon, Z., Lindblom, G., Rilfors, L., Linde, K. and Tollin, G. (2000). Interaction of Phosphatidylserine Synthase from *E. coli* with Lipid Bilayers: Coupled Plasmon-Waveguide Resonance Spectroscopy Studies. *Biophysical Journal 78*, 1400–1412.

(*36*) Lee, E., Cho, G. and Kim, J. (2024). Structural basis for membrane association and catalysis by phosphatidylserine synthase in *Escherichia coli*. *Science Advances 10*, eadq4624.

(*37*) Mengin-Lecreulx, D. and van Heijenoort, J. (1996). Characterization of the essential gene glmM encoding phosphoglucosamine mutase in *Escherichia coli*. *Journal of Biological Chemistry 271*, 32–39.

(*38*) Chmara, H. (1985). Inhibition of Glucosamine Synthase by Bacilysin and Anticapsin. *Journal of General Microbiology 131*, 265–271.

(*39*) Mengin-Lecreulx, D. and van Heijenoort, J. (1993). Identification of the glmU Gene Encoding N-Acetylglucosamine-1-Phosphate Uridyltransferase in *Escherichia coli*. *Journal of Bacteriology 175*, 6150–6157.

(*40*) Wu, H. C. and Wu, T. C. (1971). Isolation and Characterization of a Glucosamine-Requiring Mutant of *Escherichia coli* K-12 Defective in Glucosamine-6-Phosphate Synthetase. *Journal of Bacteriology 105*, 455–466.

(*41*) Bennett, B. D., Kimball, E. H., Gao, M., Osterhout, R., van Dien, S. J. and Rabinowitz, J. D. (2009). Absolute metabolite concentrations and implied enzyme active site occupancy in *Escherichia coli*. *Nature Chemical Biology 5*, 593–599.

(*42*) Anderson, M. S., Bull, H. G., Galloway, S. M., Kelly, T. M., Mohan, S., Radika, K. and Raetz, C. R. H. (1993). UDP-N-acetylglucosamine Acyltransferase of *Escherichia coli* - The first step of endotoxin biosynthesis is thermodynamically unfavourable. *The Journal of Biological Chemistry 268*, 19858–19865.

(*43*) Mengin-Lecreulx, D. and van Heijenoort, J. (1994). Copurification of Glucosamine-1-Phosphate Acetyltransferase and N-Acetylglucosamine-1-Phosphate Uridyltransferase Activities of *Escherichia coli*: Characterization of the glmU Gene Product as a Bifunctional Enzyme Catalyzing Two Subsequent Steps in the Pathway for UDP-N-Acetylglucosamine Synthesis. *Journal of Bacteriology 176*, 5788–5795.

(*44*) Whaley, S. G., Radka, C. D., Subramanian, C., Frank, M. W. and Rock, C. O. (2021). Malonyl-acyl carrier protein decarboxylase activity promotes fatty acid and cell envelope biosynthesis in Proteobacteria. *Journal of Biological Chemistry 297*, e101434.

(*45*) Shu, S., Tsutsui, Y., Nathawat, R. and Mi, W. (2024). Dual function of LapB (YciM) in regulating *Escherichia coli* lipopolysaccharide synthesis. *Proceedings of the National Academy of Sciences of the United States of America 121*, e2321510121.

(*46*) Hummels, K. R. (2025). The Regulation of Lipid A Biosynthesis. *Journal of Biological Chemistry 301*, 110556.

(*47*) May, K. L. and Silhavy, T. J. (2018). The *Escherichia coli* Phospholipase PldA Regulates Outer Membrane Homeostasis via Lipid Signaling. *mBio*, e10–1128.

(*48*) Fivenson, E. M. and Bernhardt, T. G. (2020). An essential membrane protein modulates the proteolysis of LpxC to control lipopolysaccharide synthesis in *Escherichia coli*. *mBio 11*, e00939–20.

(*49*) Nguyen, D., Kelly, K., Qiu, N. and Misra, R. (2020). YejM controls LpxC levels by regulating protease activity of the FtsH/YciM complex of *Escherichia coli*. *Journal of Bacteriology 202*, 1110–1128.

(*50*) Guest, R. L., Guerra, D. S., Wissler, M., Grimm, J. and Silhavy, T. J. (2020). YejM modulates activity of the YciM/FtsH protease complex to prevent lethal accumulation of lipopolysaccharide. *mBio 11*, e00598–20.

(*51*) Shu, S. and Mi, W. (2022). Regulatory mechanisms of lipopolysaccharide synthesis in *Escherichia coli*. *Nature Communications 13*, 4576.

(*52*) Clairfeuille, T., Buchholz, K. R., Li, Q., Verschueren, E., Liu, P., Sangaraju, D., Park, S., Noland, C. L., Storek, K. M., Nickerson, N. N., Martin, L., Vega, T. D., Miu, A., Reeder, J., Ruiz-Gonzalez, M., Swem, D., Han, G., DePonte, D. P., Hunter, M. S., Gati, C., Shahidi-Latham, S., Xu, M., Skelton, N., Sellers, B. D., Skippington, E., Sandoval, W., Hanan, E. J., Payandeh, J. and Rutherford, S. T. (2020). Structure of the essential inner membrane lipopolysaccharide–PbgA complex. *Nature 584*, 479–483.

(*53*) Klein, G., Kobylak, N., Lindner, B., Stupak, A. and Raina, S. (2014). Assembly of lipopolysaccharide in *Escherichia coli* requires the essential LapB heat shock protein. *Journal of Biological Chemistry 289*, 14829–14853.

(*54*) Mahalakshmi, S., Sunayana, M. R., Saisree, L. and Reddy, M. (2014). YciM is an essential gene required for regulation of lipopolysaccharide synthesis in *Escherichia coli*. *Molecular Microbiology 91*, 145–157.

(*55*) Smyth, K. M. and Marchant, A. (2013). Conservation of the 2-keto-3-deoxymanno-octulosonic acid (Kdo) biosynthesis pathway between plants and bacteria. *Carbohydrate Research 380*, 70–75.

(*56*) Meredith, T. C. and Woodard, R. W. (2003). *Escherichia coli* YrbH is a D-arabinose 5-phosphate isomerase. *Journal of Biological Chemistry 278*, 32771–32777.

(*57*) Wu, J. and Woodard, R. W. (2003). *Escherichia coli* YrbI is 3-deoxy-D-manno-octulosonate 8-phosphate phosphatase. *Journal of Biological Chemistry 278*, 18117–18123.

(*58*) Marquardt, J. L., Siegele, D. A., Kolter, R. and Walsh, C. T. (1992). Cloning and Sequencing of *Escherichia coli* murZ and Purification of Its Product, a UDP-N-Acetylglucosamine Enolpyruvyl Transferase. *Journal of Bacteriology 174*, 5748–5752.

(*59*) Anwar, R. A. and Vlaovic, M. (1978). Purification of UDP-N-acetylenopyruvoylglucosamine reductase from *Escherichia coli* by affinity chromatography, its subunit structure and the absence of flavin as the prosthetic group. *Canadian Journal of Biochemistry 57*, 188–196.

(*60*) Mizyed, S., Oddone, A., Byczynski, B., Hughes, D. W. and Berti, P. J. (2005). UDP-N-acetylmuramic acid (UDP-MurNAc) is a potent inhibitor of MurA (enolpyruvyl-UDP-GlcNAc synthase). *Biochemistry 44*, 4011–4017.

(*61*) Liger, D., Masson, A., Blanot, D., van Heijenoort, J. and Parquet, C. (1995). Overproduction, Purification and Properties of the Uridine-diphosphate N-Acetylmuramate: l-alanine Ligase from *Escherichia coli*. *European Journal of Biochemistry 230*, 80–87.

(*62*) Pratviel-Sosa, F., Mengin-Lecreulx, D. and van Heijenoort, J. (1991). Overproduction, purification and properties of the uridine diphosphate N-acetylmuramoyl-l-alanine d-glutamate ligase from *Escherichia coli*. *European Journal of Biochemistry 202*, 1169–1176.

(*63*) Doublet, P., van Heijenoort, J. and Mengin-Lecreulx, D. (1992). Identification of the *Escherichia coli* murI Gene, Which Is Required for the Biosynthesis of D-Glutamic Acid, a Specific Component of Bacterial Peptidoglycan. *Journal of Bacteriology 174*, 5772–5779.

(*64*) Doublet, P., van Heijenoort, J. and Mengin-Lecreulx, D. (1994). The glutamate racemase activity from *Escherichia coli* is regulated by peptidoglycan precursor UDP-N-acetylmuramoyl-L-alanine. *Biochemistry 33*, 5285–5290.

(*65*) Marmont, L. S., Orta, A. K., Baileeves, B. W., Sychantha, D., Fernández-Galliano, A., Li, Y. E., Greene, N. G., Corey, R. A., Stansfeld, P. J., Clemons, W. M. and Bernhardt, T. G. (2024). Synthesis of lipid-linked precursors of the bacterial cell wall is governed by a feedback control mechanism in *Pseudomonas aeruginosa*. *Nature Microbiology 9*, 763–775.

4

Chapter 4

Working toward establishing the link between foci, filaments, and membrane abundance in *E. coli*

J. M. Beije, C. Taisne, L. Lutze, H. Martens, S. Sharma, F. van den Brink, and G. E. Bokinsky

Expression of msGFP2 labeled PlsB resulted in punctuate foci that, while behaving in accordance with our expectations of a filament, presented a markedly different phenotype than the elongated filament we expected. We applied a range of approaches to investigate this discrepancy and to characterize the punctate foci, however, these experiment did not generate satisfactory results. Several electron microscopy methods (negative staining of microtome sections, tomography electron microscopy on minicells, and negative staining of purified PlsB) were attempted. None showed a readily identifiable filamentous structure, most likely due to low abundance of PlsB filaments. Similarly, attempts to determine the mobility of PlsB in foci using FRAP failed to yield clear results due to low fluorescence signal and extensive bleaching. To further probe the behavior of PlsB foci a number of experimental avenues were explored, such as osmotic shocks in vesicles and spheroplasts, and creation of a G3P depletion strain. Unfortunately, persistent difficulties with sample preparation and strain construction frustrated these efforts. Despite these failures, we do believe these attempts pave the way for future experiments and the eventual answering of these important questions.

4.1. Introduction

The development and proliferation of cloning tools has, over the past few decades, made it relatively straightforward to tag any protein of interest with a fluorescent tag such as GFP. This has enabled a lot of research into the localization, co-localization and dynamics of many proteins. However, when applying this technique one must always remain wary of the lurking danger of artifacts. While in most cases the fluorescent signal observed is an accurate reporter for the native behavior of the studied protein, there are unfortunate instances where this has turned out to not be the case. An infamous and unfortunate example is MreB, whose filaments were once lauded as the first example of a bacterial cytoskeleton (*1*). Unfortunately, later research showed that the beautiful helical filaments were but an artifact introduced by the GFP tag (*2*). Keeping such examples in mind, it is always important when using a fluorescent tag to verify the veracity of what you see. While certainly not foolproof, one indication that what you are observing is not an artifact is if its behavior in response to stimuli matches expectations.

While the results discussed in **Chapter 2** point towards the observed punctuate PlsB foci being functional higher order structures, this is neither definitive proof nor does it preclude foci from being something other than a filament. For while elongated foci can be confidently attributed to filaments, this is not so straightforward for punctuate foci. Possible explanations for the punctuate phenotype could be that in the presence of msGFP2, PlsB forms a collection of small filaments or a heavily branched filament. While different, such structures could be understood within the same framework as the elongated filaments shown by Wilkinson et al. (*3*). However, punctuate foci might also be caused by alternative explanations such as co-localization (possibly with lipid rafts or membrane domains), curvature sensing, and liquid condensates (a phenomenon where otherwise (partially) soluble proteins phase separate to form a microdomain of liquid protein). While such alternative explanations might not necessarily be at odds with the core of our hypothesis, it is nevertheless important to determine the nature of the observed foci.

This problem can be approached from multiple angles, the most direct undoubtedly being electron microscopy. If successful, such an approach could not only reveal the nature of the foci, but also provide additional structural information. Most tantalizing is the possibility of uncovering the interactions between monomers that stabilize the filament. Rational design of non-filamenting PlsB mutants can be based on for example successful attempts in literature (*4*–*6*), conservation of amino acids in bacteria, and structural predictions. However, such approaches are far from guaranteed to produce results as they are based on extrapolation, assumptions, and predictions. Therefore, structural information on the filaments would therefore be invaluable for the design of non-filamenting PlsB mutants. However, electron microscopy is a technically challenging method, further complicated by the small size of filaments relative to the cytoplasm. The bacterial cytoplasm is a large and crowded space where spotting small, not readily identifiable, structures is likely to require extensive scanning, akin to looking for the proverbial needle. Therefore, we must also consider alternative avenues that, while perhaps less direct, might nevertheless shed light on the nature of the foci.

One such method exploits one of the key differences between filaments and other supramolecular organizations. Compared to co-localization or liquid-condensates, filaments are more rigid and structured and this has implications for the exchange rate of monomers between filaments and the bulk solution. This exchange rate is generally low, as filaments tend to be stable and exchange only at the growing end(s), though this can of course change should intracellular conditions change in such a way as to promote disassembly of the filament. By utilizing Fluorescent Recovery After Photobleaching (FRAP), a single foci/pole can be selectively photobleached. Afterwards, the cell can be imaged over a small timeframe to measure the degree of recovery. Such information can inform about the exchange rate of the foci and, ideally, give clues as to its nature.

Here, we describe our efforts to apply these, and other, methods to determine whether the punctuate foci are indeed filaments. This is not the only open question we sought to address, as we sought to also further probe the response of the foci to additional environmental conditions. To facilitate all these approaches we attempted to create a strain with an elongated filament phenotype at native PlsB expression level, as overexpression can also be a source of artifacts. Finally, we will discuss avenues of future research we deem most pressing and most likely to yield interesting results.

4.2. Showing dispersion of foci is not unique to fatty acid depletion

Controlling glycerol-3-phosphate abundance using a GpsA knockout

Our results with the fatty acid synthesis inhibitor triclosan have shown that PlsB foci formation and dispersion is strongly correlated with the relative abundance of the membrane **(Chapter 2)**. Under conditions of membrane shortage caused by

depletion of acyl-ACP, foci rapidly disperse. This dispersion is then reversed if the relative abundance is increased, either by alleviating substrate depletion or by rapidly decreasing the intracellular volume through a hyperosmotic shock. Especially the latter shows that foci formation, albeit with morphological differences compared to foci under regular growth conditions, is independent of substrate availability. Nevertheless, we do want to investigate to what degree the observed dispersion and reformation is independent of acyl-ACP depletion.

We therefore sought to deplete the second substrate of PlsB, glycerol-3-phosphate. Unfortunately, there are no known inhibitors that prevent the synthesis of glycerol-3-phosphate. Instead, we sought to create a strain that is auxotrophic for glycerol-3-phosphate under certain growth conditions. *E. coli* has two pathways for synthesizing glycerol-3-phosphate, the first an offshoot from glycolysis and the second a two-step import and conversion of environmental glycerol **(Fig. 4.2A)**. In the first pathway, the enzyme GpsA converts the glycolytic intermediate dihydroxyacetone-phosphate (DHAP) to glycerol-3-phosphate (*7*, *8*). During growth on most carbon sources this is the primary pathway for synthesizing glycerol-3-phosphate. The second pathway starts with GlpF, which imports glycerol from the environment into the cytoplasm (*9*, *10*), followed by GlpK which catalyzes the conversion to glycerol-3-phosphate (*11*). However, in the presence of glucose this secondary pathway is strongly repressed by the transcriptional repressor GlpR (*12*).

This dual pathway creates an opportunity to construct a strain that grows on glucose but is only able to synthesize glycerol-3-phosphate from glycerol. This allows for control of intracellular glycerol-3-phosphate pools by controlling the availability of glycerol in the growth medium. This construct requires two genetic interventions. The first step is to allow import and utilization of both carbon sources (glucose and glycerol) at the same time, which requires deletion of the transcriptional repressor GlpR. Next, deletion of GpsA ensures that only glycerol can be used to synthesize glycerol-3-phosphate. The resulting strain is able to grow on glucose, while at the same time importing and converting glycerol to synthesize glycerol-3-phosphate through the GlpF/GlpK pathway. By controlling the presence of glycerol in the growth medium, we can deplete glycerol-3-phosphate pools without triggering general starvation stress responses.

Unfortunately, the creation of this strain proved more difficult than originally anticipated. While deletion of GlpR was achieved (confirmed by Sanger sequencing), the deletion of GpsA proved more troublesome. Despite several attempts to replace the gene with a null cassette featuring an antibiotic resistance gene, no colonies were ever observed. While there is always the possibility of a faulty construct and experimental/human error, this risk was minimized as much as possible. Another possibility is that in the absence of GpsA, transformants were unable to synthesize sufficient amounts of glycerol-3-phosphate. Glycerol supports a slower growth rate compared to glucose (approximately 45 min doubling time versus 25 min, respectively) and it is therefore possible that deletion of GpsA would create a mismatch between growth and glycerol-3-phosphate synthesis rates. However, we consider this unlikely as it has been observed that intracellular glycerol-3-phosphate concentrations spike during growth on glycerol, indicating GlpF/GlpK are capable of high synthesis rates

(*13*). Furthermore, an insufficient but non-zero supply of glycerol-3-phosphate is not fatal and should merely result in a low growth rate. Nevertheless, we were unable to determine the cause for the failure to generate transformants and therefore opted to pursue alternative avenues of strain construction.

Alternative construct utilizing inducible degradation of GpsA using a pdt3 tag

Since deletion of GpsA did not result in colonies, we hypothesized that deletion (possibly in combination with deletion of GlpR) impacts cell viability and/or growth rate in an unexpected way. To circumvent this, we sought to create a genetically modified version of GpsA which can be selectively degraded upon induction of an exogenous protease. This approach allows for fully functional GpsA at native expression under most conditions, while at the same time allowing for inducible depletion. To achieve specific degradation, we aimed to attach a N-terminal peptide tag called protein-degradation tag 3 (pdt3). This pdt3 tag is recognized by the exogenous protease Mf-Lon, but not by any of the endogenous *E. coli* proteases. Additionally, Mf-Lon only targets proteins with this peptide tag, allowing for a high degree of specificity (*14*).

The final construct would allow us to grow the cells in MOPS glucose medium. In this medium, the cell requires GpsA activity to synthesize glycerol-3-phosphate. Induction and expression of Mf-Lon would lead to depletion of GpsA and therefore result in depletion of glycerol-3-phosphate. This is therefore an alternative means of testing if glycerol-3-phosphate depletion also results in dispersion of the PlsB foci, similar to depletion of acyl-ACP. Unfortunately, this approach also suffered from setbacks. While, based on gel analysis of the PCR product, we successfully constructed the GpsA-pdt3 cassette on a plasmid, insertion into the genome once again proved unsuccessful in our hands. With no realistic avenues to limit glycerol-3-phosphate left to us, and no clear indication of where our cloning efforts were stalling, we investigated other methods to untangle the relationship between foci dispersion, a decrease in membrane abundance, and depletion of acyl-ACP.

4.3. Recovery in the absence of substrate – Can PlsB foci reformation be triggered by osmotic shock?

In previous experiments, we successfully showed that after dispersal, foci reassembly can be triggered by either removing triclosan or supplying acyl-CoA **(Chapter 2)**. However, in these cases there is both an increase in substrate availability and in membrane abundance. To determine which signal causes foci reformation, we sought to test whether we could trigger foci reformation without any phospholipid synthesis. To achieve this, we used a high molarity sucrose solution (1 M) to trigger a hyperosmotic

shock. A hyperosmotic shock causes an immediate decrease in cytoplasmic volume, and as a result an increase in the ratio of phospholipids over surface area. If an increase in membrane abundance is sufficient for foci reformation, we should expect the shrinkage of the cytoplasm to coincide with the appearance of foci.

Indeed, when cells incubated with triclosan and a dispersed fluorescent signal were exposed to a hyperosmotic shock, we observed both a shrinkage of the cytoplasm as well as the formation of small foci in many cells (53%) **(Fig. 4.1A)**. There are marked differences between these foci and those normally observed. The foci observed after hyperosmotic shock appear to have a random localization, rather than being located at the cell poles. Furthermore, their size and number are more diverse **(Fig. 4.1C)**. However, the most puzzling result is that foci reformation also occurred after a hypoosmotic shock (0M sucrose). A hypoosmotic shock should cause an expansion of the cytoplasm (insofar as this is possible due to the cell envelope), if anything causing a decrease in the relative membrane abundance. Despite this, most cells (95%) had at least one foci, markedly more than observed during hyperosmotic shock (53%) and on par with observations during regular growth (>90%) **(Fig. 4.1B)**.

These results are difficult to explain. While it is exciting that foci reappear upon osmotic shocks, showing this is apparently independent of substrate availability. However, the fact that this behavior is observed after both hypo- and hyperosmotic shocks is quite unexpected and counterintuitive. One possibility is that PlsB filaments form in response to membrane perturbations in general, and not just increases in membrane abundance. However, this explanation seems difficult to reconcile with the observed inactivity of filamentous PlsB. Another possibility is that the osmotic pressure itself is responsible for the observed foci formation. There is some evidence that, in an *in vitro* system, actin filament formation can be induced by osmotic pressure, which might perhaps even be a cellular adaptation (*15*). Regardless, while the reassembly of foci in response to osmotic pressure is further evidence of the dynamic nature of foci, it brings us no closer to fully understanding these dynamics.

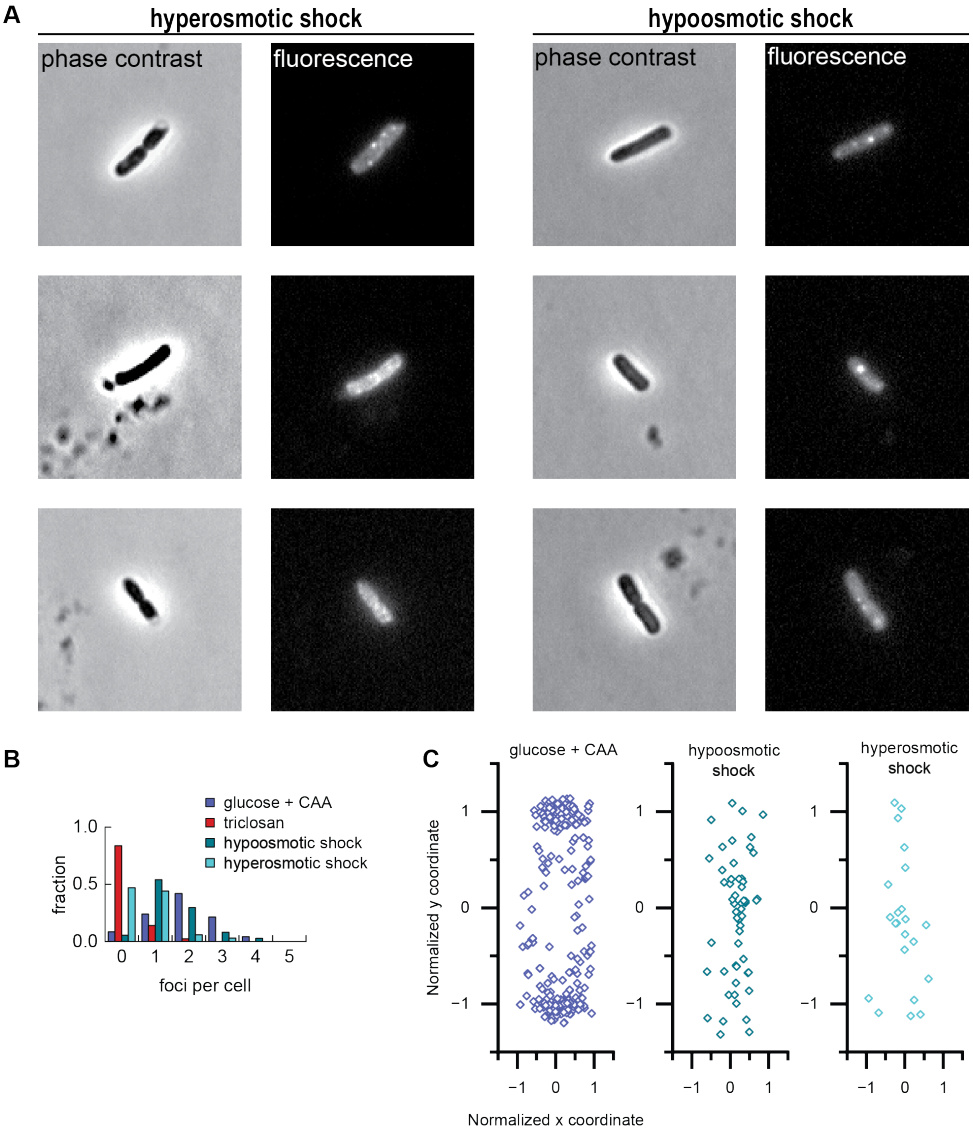

Figure 4.1: Reformation of PlsB foci is triggered upon osmotic shock. **A.** Cells exposed to fatty acid inhibitor triclosan show a dispersed fluorescent signal, rather than the foci observed during growth. However, these foci recover after both a hyperosmotic shock (1M sucrose, left) and a hypoosmotic shock (0M sucrose, right). **B.** Histogram showing both osmotic shocks cause a significant shift in the number of foci per cell, compared to cells exposed to triclosan. **C.** However, while foci observed during growth are predominantly found in the cell poles, foci appearing after osmotic shocks are spread almost homogeneously around the cell

Unshackling the cell – understanding the relationship between foci and osmotic shocks *in vivo* in spheroplasts

While we had successfully utilized hyperosmotic shocks *in vivo* to show reformation of foci after acyl-ACP depletion, the unexpected result of hypoosmotic shocks also triggering reformation complicated our understanding of the system. However, probing this relationship further was problematic, as *E. coli* cells are relatively resistant to osmotic shocks due to the rigidity of the cell wall and osmoregulators that transport solutes in and out of the cell (*16*, *17*). While this still allows for hyperosmotic shocks, as the inner membrane is relatively free to retract, the physical barrier of the cell wall does pose a problem for hypoosmotic shocks. We therefore wanted a system where we could expose cells to both hyper- and hypoosmotic shocks and be able to see the full effect **(Fig. 4.2C)**. To achieve this, we investigated the possibility of using spheroplasts which, owing to their lack of cell wall, are considerably more susceptible to osmotic shocks.

Spheroplasts, and the related protoplasts, have long been described in literature. While the methods of their production might vary, the basic principle is that of bacterial cells from which the cell wall has been (almost) completely stripped away, for example through lysozyme activity. We reviewed a number of existing protocols to generate spheroplasts, found in both older and more recent literature (*18*–*23*). Based on these protocols for our first attempts we started by exposing cells to the antibiotic cephalexin (*18*, *19*, *21*). This β-lactam interferes with the synthesis of the cell wall and in Gram-negative bacteria causes the formation of elongated cells (up to 150 µm) (18). This elongation step is included as it results in larger spheroplasts which are easier to image. After incubation with cephalexin, the outer membrane is first permeabilized by the addition of EDTA. This increased permeability allows the lysozyme to bypass the outer membrane so that it can start digesting the cell wall (*24*).

Unfortunately, in our hands this procedure had a very low yield. Per attempt there would often be only a handful or, more commonly, no spheroplasts at all to be found on the microscope slide. Instead we would observe cells that retained their rod shape, indicating an intact cell wall, cells that had only partial removal of cell wall, or cells that had lysed either partially or fully **(Fig. 4.2B)**. Furthermore, the cell density observed was always low in comparison to previous microscopy experiments. Based on these results we hypothesized that the produced spheroplasts might be unstable and prone to lysis, thereby severely limiting our yield. We investigated this with the addition of a fixation step (using formaldehyde and glutaraldehyde), which did result in an increased number of spheroplasts. However, while this did confirm the instability of the spheroplasts, it did nothing to solve the problem as we were interested in using the spheroplasts for dynamic experiments for which fixed cells are not suitable.

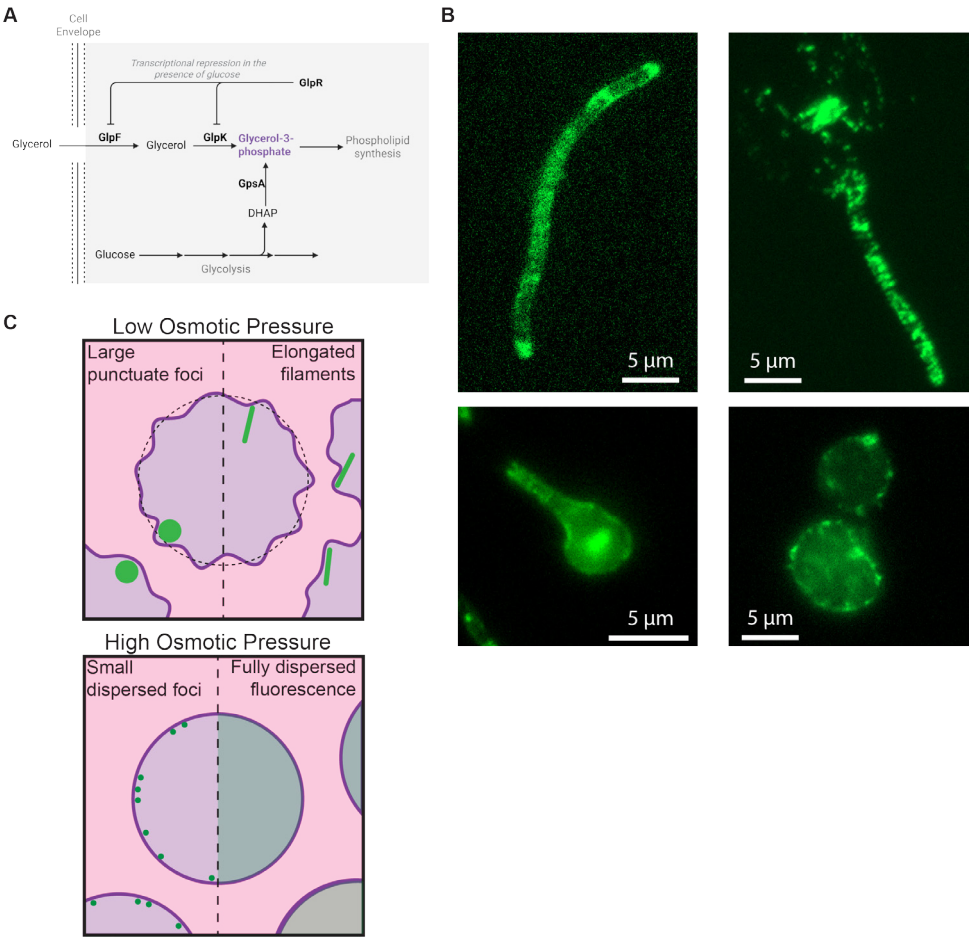

Figure 4.2: **A.** A schematic overview of the two glycerol-3-phosphate synthesis pathways. **B.** Fluorescent microscopy images of cells at various states of spheroplast formation, green fluorescent signal is a result of PlsB-msGFP2 fusion. Top left, an elongated cell as a result of cephalexin treatment. Bottom left, an elongated cell showing partial degradation of the cell wall resulting in partial loss of the rod shape. Top right, an elongated cell that has undergone partial lysis, likely due to degradation of the cell wall at one pole. Bottom right, a fully formed spheroplast stabilized by cell fixation. **C.** A schematic showing our expected results from a osmotic shock experiment on spheroplasts. At the top, a low ambient osmotic pressure should result in a shrunken volume and thus relative excess abundance of membrane. Depending on the proportion of labelled and unlabeled we expect this to cause PlsB to form either punctuate or elongated filaments. At the bottom, a high ambient osmotic pressure should cause swelling and a stretched membrane. We expect this to cause either a fully dispersed fluorescence signal or possibly very small foci throughout the cell if PlsB mono- and dimers co-localize at for example cardiolipin lipid rafts.

We made several attempts to improve our protocol in hopes of raising our spheroplast yield. As we believe lysis after spheroplast formation to be the main culprit, we sought to minimize shear stress by gently pipetting and cutting the ends of pipette tips. Furthermore, to minimize osmotic stress we ensured the osmotic value of the spheroplast formation solution was very close to the osmotic value of regular growing media such as LB. Finally, we also investigated the role of cephalexin by omitting it in several spheroplast preparations as we believe the resulting smaller spheroplasts should be more resistant to physical stressors. However, despite these attempts we did not manage to meaningfully increase our spheroplast yield and eventually moved on to other approaches.

4.4. Determining the structure of PlsB filaments

While earlier work has shown that PlsB can assemble into filaments and is able to do so *in vivo*, this has to date only been observed after significant overexpression of PlsB (*3*). Therefore, while it is plausible, there is no confirmation that PlsB also forms filaments at native concentrations. Furthermore, no structure of either *E. coli* PlsB monomer, dimer, or filament has thus far been successfully resolved. This lack of experimentally verified structural information made our search for a non-filamenting mutant significantly harder **(Chapter 2)**. Finally, while earlier observations indicated the PlsB filaments might be hollow with lipids coating the inside, nothing is known about how the filament interacts with the membrane at its base. To address these questions, we sought to image PlsB filaments using electron microscopy.

Another part of our motivation was our ongoing puzzlement at the punctuate foci phenotype of labeled PlsB. Contrary to our initial expectations, at native expression levels we observed PlsB forming punctuate foci rather than elongated filaments. As further described in **Chapter 2**, we believe this phenotype might in large part be attributed to the GFP tag. Determining if this is indeed the case, or what alternative structure is adopted by the punctuate foci, is another motivation for attempting to obtain high resolution electron microscopy images of the PlsB foci.

In situ electron microscopy imaging of PlsB foci using sectioning

To achieve these goals, we tried several different approaches. The first is imaging negatively stained, microtome sectioned bacteria, a technique which allows for imaging of the filaments in situ. The original plan was to use the fluorescent signal of the msGFP2 to guide our electron microscopy imaging, using correlative light electron microscopy (CLEM) (*25*). However, due to technical issues the alignment between these two imaging modalities was not sufficiently accurate, and we therefore had to look for filamentous structures manually.

The eventual goal of this approach was to find and image labeled PlsB foci at native concentration in order to determine the structure of these structures. However, at native concentration the abundance of PlsB is quite low and the foci therefore quite small; this meant it would likely be too difficult to find these structures. Therefore, we initially opted to try with cells overexpressing PlsB-msGFP2. At this stage we did not try with mixed expression (combining labeled and unlabeled PlsB, described in more detail in Chapter 2, section 2.4) even though the resulting elongated filaments are likely to be more easily recognizable because this technique was still being developed at the time. While we are now able to find elongated filaments in half of the cells (29 out of 51, or 56%, based on manual counting), during initial pilot experiments only a small number of cells containing elongated filaments could be identified. This was likely due to minor deviations in protocol and too short induction times. Regardless, given this low incidence of elongated filaments we chose to try first with cells overexpressing PlsB-msGFP2.

In the initial trial run we therefore used *E. coli* cells containing the inducible pBbE5K-PlsB-msGFP2 plasmid. These we induced to overexpress PlsB during exponential growth. This culture was then concentrated to ensure high cell density. This high-density culture was first fixed with a formaldehyde/glutaraldehyde mixture and subsequently stained with osmium tetroxide. Next, the sample is dehydrated and embedded in epoxy resin (Epon 812). Finally, a diamond microtome was used to make 100 nm slices which were contrasted with lead and uranyl acetate and mounted on an electron microscopy grid.

When imaged (120kV JEOL 1400) the individual cells could be readily identified. The dense culture showed a multitude of cells in the field of view, the various random orientations of cells giving a large variety of slices. Despite this, nothing filamentous or otherwise notable could be readily identified in the cells (Fig. 4.2A). Given that even with higher concentrations of PlsB no filament or similar structure could be found, it seemed rather unlikely that any would be found at native expression levels using this method. The low abundance of filaments, combined with the fact that in many of the cell slices the filament would not be present or sliced in such a way as to be unrecognizable, ultimately makes it very unlikely to spot any filament.

Transmission electron microscopy imaging of foci using minicells

A way to solve this issue is to forgo sectioning and instead image the full volume of the cell. While in principle this can be done with transmission electron microscopy (TEM), this is only possible for thin samples, typically 200-500 nm for biological samples (*26*). The average *E. coli* cell is much thicker (average thickness of 0.5-1 µm) and therefore unsuitable for this method. However, there are multiple methods that can be used to produce thinner cells, such as antibiotics or lysozyme to flatten cells, or by producing minicells. Minicells, a term first coined in 1966 (*27*), are small spherical buds from the poles of cells. They can be produced in a variety of ways, such as overexpressing division machinery like the division protein FtsZ (*28*). After overexpression, the resultant

minicells are centrifuged to filter out only those of the smallest size, around 200 nm in diameter. Because the entire volume of these minicells can be imaged, any filament that is present should be visible and recognizable (*29*).

However, while we were successful in producing minicells, none of the cells we imaged contained large scale structures resembling filaments **(Fig. 4.2B)**. Once again, the problem is likely the low abundance of PlsB filaments in the cells. Even if overexpressed, PlsB still localizes to only 2 foci at most, one in each pole. Since the formation of minicells is a largely random process, many minicells will simply not contain a PlsB foci. Likely, only a fraction of minicells contain a filament, and only a fraction of those is small enough to be imaged. Furthermore, limitations in throughput mean we cannot quickly scan many hundreds (or even thousands) of minicells, limiting our ability to find a filament. Fundamentally it remains the same issue as we faced with sectioning: There are a great many cells, but only a handful of them contain an identifiable structure. With sufficient time the proverbial needle might be found, but this is likely an inefficient use of time and resources. As such, this avenue was shelved for the time being.

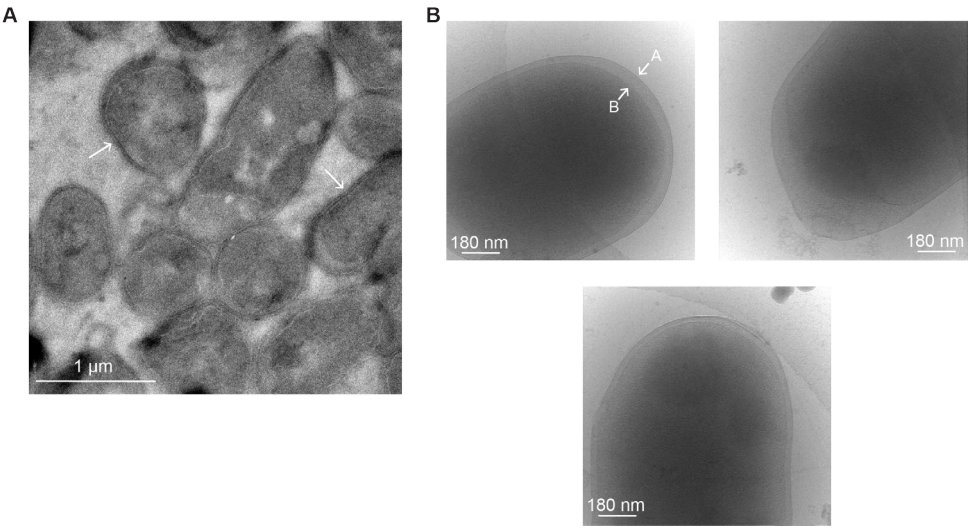

Figure 4.3: Electron microscopy images. **A.** Resin embedded cells sectioned into 100 nm thin slices. The cell envelope is clearly visible (white arrows) but there are no identifiable filaments structures visible in the cytoplasm. **B.** Tomography images of minicells. Again the outer membrane (arrow A) and inner membrane (arrow B), cytoplasm and periplasm are clearly identifiable, but no structures can be seen inside the cytoplasm.

4.5. Determining if punctuate foci are analogous to elongated filaments

Using FRAP to determine the mobility and diffusion rate of PlsB in foci

Unfortunately, we did not manage to determine the nature nor the structure of the observed foci using electron microscopy and we were thus unable to decisively prove that foci are filaments. We therefore sought alternative methods to gather evidence to support this assumption. The main alternative to filamentation is that PlsB localizes at the pole in an unstructured manner. If this is the case, the monomers and dimers should be highly mobile and equilibrate between the two poles. If, on the other hand, the majority of PlsB is organized into filaments (or other, analogous structures), this exchange rate should be much lower.

One method to determine this exchange rate is Fluorescence Recovery After Photobleaching, or FRAP (*30*, *31*). Using this method a part of the cell can be exposed to a high intensity light source, intentionally causing photobleaching of any fluorophores present there. The resulting dark spot can then recover through one of two methods: very slowly through the synthesis of new protein, or much faster through exchange with other, non-bleached areas of the cell. By measuring the degree and speed of recovery the dynamics of a protein (sub)population can be determined. Most solutes and macromolecules such as proteins have been shown to be highly mobile in the cytoplasm, facilitating fast recovery (*32*). In contrast, the exchange rate between soluble proteins and filaments tends to be much slower, which can be seen in a slower recovery rate (*33*). While the exact exchange rate is of course specific to any given filament, the recovery rate can be used as evidence of the state of a protein. In our case, a fast recovery would indicate PlsB is mobile and thus likely predominantly in a mono- or dimeric state, whereas slow recovery would indicate the majority is in an immobile filamentous (or analogous) state.

Since we wanted to determine what the native state of PlsB is without artificially increasing its abundance we imaged cells with a chromosomal copy PlsB-msGFP2 at native expression levels using a confocal microscope. A 480 nm laser was used to photobleach a small area centered on one of the poles. Unfortunately, given the small size of an *E. coli* cell the smallest possible bleach area achievable by our equipment still encompassed roughly half the cell. After the initial light pulse clear photobleaching could be observed, with one pole losing all fluorescent signal **(Fig. 4.3B)**. We then imaged over a short period of 10 minutes to observe if there was any recovery of fluorescent signal in the photo bleached pole. Given a doubling time of roughly 25 minutes under these conditions, recovery in this time interval can be attributed predominantly to protein exchange between the poles, rather than de novo protein synthesis.

Only very limited recovery of fluorescent signal in the bleached pole was observed, but we cannot with full confidence attribute this solely to the filamentous nature of PlsB. This is because we also observed further gradual photobleaching of the rest of the

cell due to the imaging. Confocal microscopy uses a powerful laser to image which can cause photobleaching during regular imaging. Even at minimal settings, the low abundance of our protein means we have to use a relatively high laser power to achieve a significant signal-to-noise ratio. An unfortunate side effect of this laser power is that we observe bleaching during imaging, even after only a single image. In these experiments we could clearly observe bleaching occurring in other cells in the field of view that had not been targeted by the FRAP laser. However, when we repeated this experiment with cells exposed to triclosan under which PlsB shows a dispersed fluorescence and is expected to be predominantly in a fast exchanging mono- and dimeric state. Under these conditions PlsB should diffuse faster and we therefore expect a faster recovery rate. While there does seem to be a slightly more pronounced recovery **(Fig. 4.3C)**, this recovery is still much lower and slower than expected. These results could perhaps in part be explained again by bleaching during imaging, but cannot be the full explanation. Soluble proteins freely diffusing through the cell should equilibrate on much faster timescales as seen in this experiment. Therefore, while the results are promising we cannot with full confidence draw a conclusion. A small amount of recovery might have taken place in cells with foci, but have been masked by the gradual bleaching from the imaging. Furthermore, the lack of equilibration of, supposedly, soluble and freely diffusing PlsB further complicates interpretation.

Further technical and experimental issues exacerbated these problems. The size of the area affected by the laser had a radius roughly equal to that of the average *E. coli* cell, meaning care had to be taken when designating the center point. However, this itself was further complicated by calibration problems that introduced a variable difference between the designated spot and the actual center of the area targeted by the FRAP laser. Coupled with the general difficulty of imaging this strain using confocal microscopy due to bleaching, it resulted in many cells being unusable for analysis. While many of these issues are certainly solvable, the signal-to-noise ratio is harder to improve. So even with more data points, the central issue of accidental bleaching of any recovery remains a problem. We therefore decided instead to devote time to other approaches.

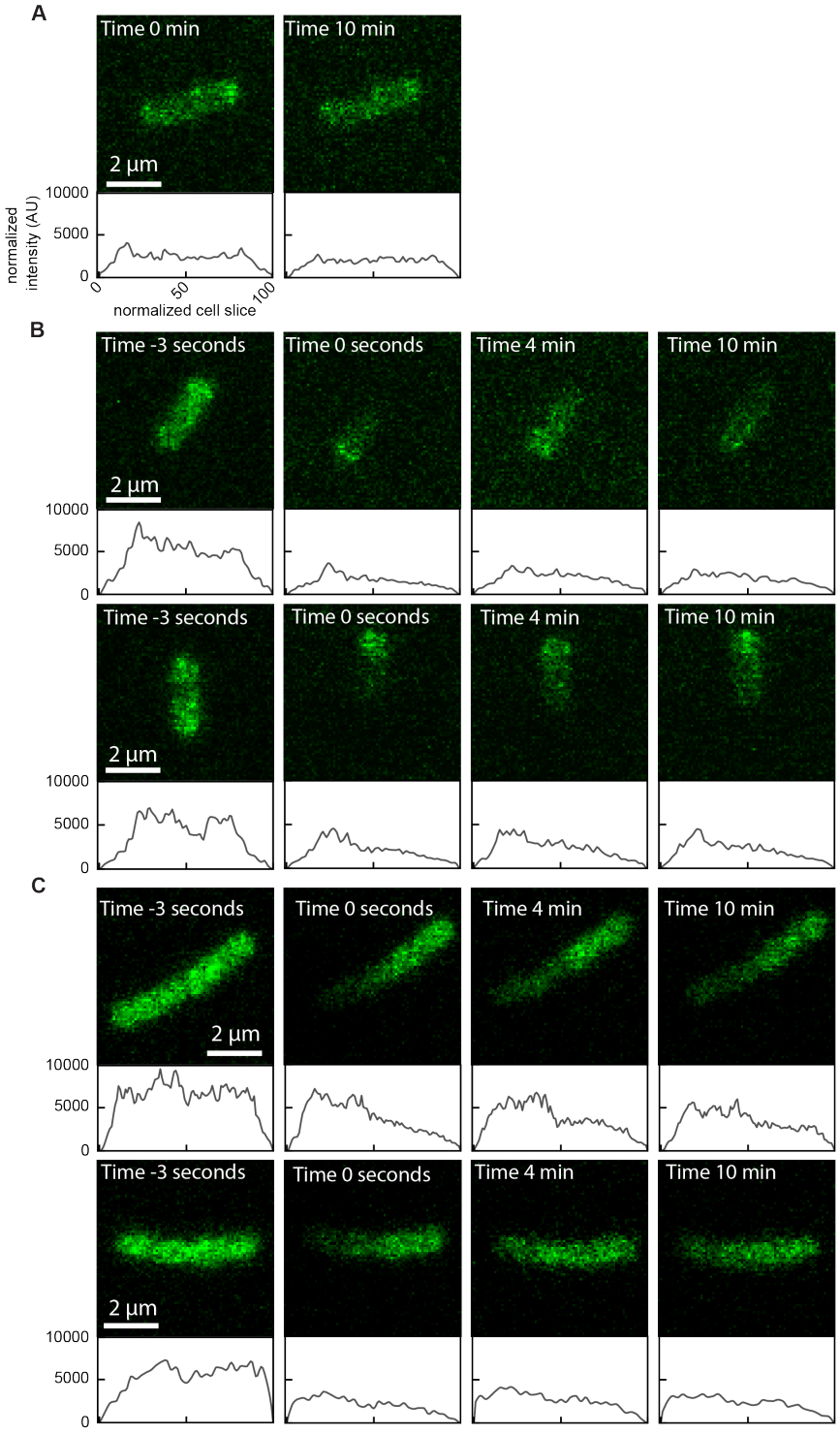
A
Time 0 min
Time 10 min
2 µm
10000
5000
0
normalized intensity (AU)
0
50
100
normalized cell slice
B
Time -3 seconds
Time 0 seconds
Time 4 min
Time 10 min
2 µm
10000
5000
0
C

Figure 4.4

Figure 4.4: Confocal fluorescent microscopy images of NCM 3722 *plsB-msGFP2* exposed to FRAP. **A.** Cells not within the FRAP area still experience bleaching due to imaging. This can be see especially in the dimming of the foci. **B.** One of the cell poles was targeted and bleached with the FRAP laser. While some degree of recovery can be observed there does not appear to be any recovery of the foci itself. Both images and intensity profiles continue to show a lopsided fluorescence **C.** Cells first exposed to triclosan show fully dispersed fluorescent signal prior to bleaching. After 10 min some recovery can be observed, with the fluorescent intensity equalizing across the cell. Note the top image is two cells, hence the stepwise intensity profile

4.6. Generating an elongated filament phenotype at native expression level using stop-codon readthrough

While eventually the mixed expression system proved to be relatively robust and able to produce elongated filaments in most cells, it is not without issue. The largest drawback is the required overexpression of PlsB, whereas we would prefer to study its behavior at native concentrations. For this reason most experiments were done with native expression of PlsB-msGFP2, even though this results in punctuate foci. To resolve this tension we sought to develop a method to achieve mixed expression at native PlsB concentrations by utilizing stop-codon readthrough.

It has long been observed that stop-codons are not absolute and that there is the occasional readthrough event (*34*). Such readthrough events results in misincorporation of an additional amino acid and transcription/translation of the downstream genetic code (*35*). While readthrough events are generally rare, their frequency does depend on both the stop-codon as well as the base pair immediately following the stop-codon (*36*). Varying the upstream codon can have a large effect on readthrough frequency, resulting in an up to 30-fold difference in readthrough (*37*). Finally, environmental conditions can also affect readthrough, under certain stress conditions readthrough has been reported to occur in up to 80% of transcription/translation events (*38*).

We sought to utilize stop-codon readthrough by designing a construct with a stop codon between the PlsB gene and the following linker-msGFP2 fusion cassette **(Fig. 4.5A)**. This way, the majority of transcription/translation events should result in unlabeled PlsB, while a readthrough event would instead result in a fluorescent PlsB-msGFP2. The aim was to maximize the number of readthrough events by carefully selecting the stop codon and following base pair, allowing us to strike a balance between ensuring we have sufficient fluorescent signal for imaging while still allowing for elongated foci. Because we aimed to study PlsB under growth conditions we were not able to utilize environmental conditions to increase the rate of readthrough, as these conditions are invariably stress conditions.

Based on previous studies we selected those stop codons and following base pairs reported to have the highest incidence of readthrough: UGA A and UGA C (*36*, *39*, *40*). Quick-change mutagenesis was used to insert the stop codon into existing PlsB-msGFP2 constructs and to alter the immediate upstream base pair. These constructs were then inserted into a plasmid, which in turn was transformed into a wild-type (NCM 3722) strain. The cells carrying these constructs were imaged at both leaky expression and after induction to achieve overexpression of PlsB **(Fig. 4.5B)**. While leaky expression produced no meaningful increase in fluorescent signal above the base autofluorescence of *E. coli* cells, a faint increase in signal could be observed when overexpressed. Of the two constructs, UGA C produced a higher fluorescent signal, indicating higher incidence of readthrough. However, in no case was any foci, elongated or punctuate, visible. Furthermore, a faint fluorescent signal could only be achieved after overexpression while the goal was to have mixed expression at native concentrations. Together, we must conclude that the frequency of readthrough events is too low to produce a sufficient number of labeled proteins for imaging. As we had already selected the stop codons with the highest readthrough rate there was little avenue for improvement and this line of experimentation was not pursued further.

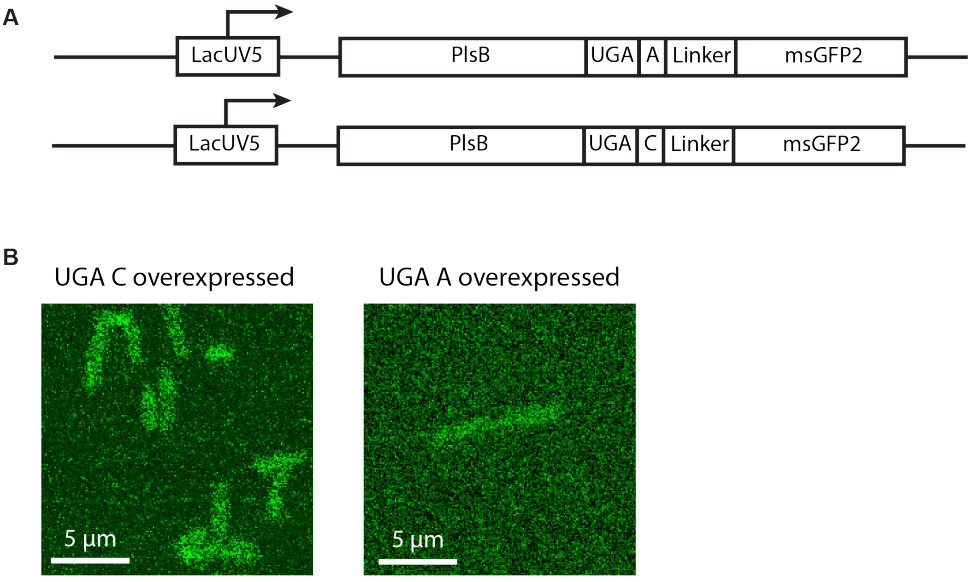

Figure 4.5: **A.** A schematic showing the construct with wither UGA A or UGA C stop codon in between PlsB and msGFP2. **B.** Confocal fluorescent microscopy images of both constructs after overexpression. Left, while the UGA C construct has sufficient readthrough to have clearly visible cells, there are no foci or filaments visible. Right, the fluorescence of the UGA A construct is only slightly above the background noise, a level of fluorescence likely attributable to unspecific autofluorescence of the cell.

4.7. Unable to find a non-filamenting mutant through semi-rational design

Our previous results have shown a strong link between phospholipid synthesis and foci formation. However, these results all approach the problem from the cellular side, we perturb the cell and the foci respond. We aimed to also approach this from the other perspective, perturbing the foci and observing the cellular response. To achieve this, we set out to design and make a non-filamenting mutant of PlsB. The first obstacle is a lack of information on PlsB filamentation. Unfortunately, there is no known crystal structure of PlsB nor is there any detailed information on the structure of the filaments. Instead, we turned to computational tools and literature to inform our decisions. From previous reports of successful attempts at generating non filamenting mutants we learned that for example exposed hydrophobic residues can be involved in filamentation (*4–6*, *41*, *42*). We then applied this knowledge to a predicted PlsB structure generated by AlphaFold **(Fig. 4.6A)** (*43*, *44*). The prediction of this PlsB model has a very high confidence (average pLDDT 90.12, with low and very low confidence regions (4.7% and 1.6%, respectively) primarily located in small unstructured loops (for predicted aligned error (PAE) see **Supp. Fig. 4.2B**). Furthermore, the model shows a clearly defined hydrophobic domain, which aligns with PlsB being a peripheral membrane protein **(Supp. Fig. 4.2A)**. Finally, the active site residues appear to cluster together to form in an accessible active site **(Supp. Fig. 4.2A)**. Structural information gleaned from this model was used to inform our initial library of mutants.

We expected that any mutation that affected the activity of PlsB or its ability to filament would have a measurable effect on growth rate, foci formation, or both. To determine the effect of each mutation we placed the PlsB-msGFP2-mut on plasmids with wild-type copy of PlsB in the chromosome. We then measured the growth rates of these strains, both with background expression and induction. For most strains no significant effect could be discerned. Furthermore, each strain was imaged to determine if it showed no or aberrant foci formation. In all cases except one, no change in phenotype could be observed **(Fig. 4.6D)**. The one exception is F92S, which in some cases showed a more distributed phenotype **(Fig. 4.6D, apparent membrane bound PlsB)**. That said, this phenotype was only observed in a small subset of cells and only on some occasions.

Next, we took a different approach and instead focused on disrupting the dimer interface, hoping this would also prevent filament formation. To design these mutants we were able to study and cross reference a recent experimental dimer structure of PlsB from *Thermomonas haemolytica* reported by Li et al. and an *E. coli* dimer structure predicted by AlphaFold (*45*) **(Fig. 4.6A & B)**. We did a comparative study of the residues involved in dimerization as identified by Li et al, their conservation in *E. coli* and the residues identified in the predicted dimer interface **(Supp. Fig. 4.2C)**. As a result, we identified several residues which we deemed likely to be important for dimerization **(Fig. 4.6C)**. We prepared single mutations and measured their growth rate and whether they formed foci (**Supp. Table 4.1** gives an overview). We detected no significant changes in either growth rate or phenotype **(Fig. 4.6D)**.

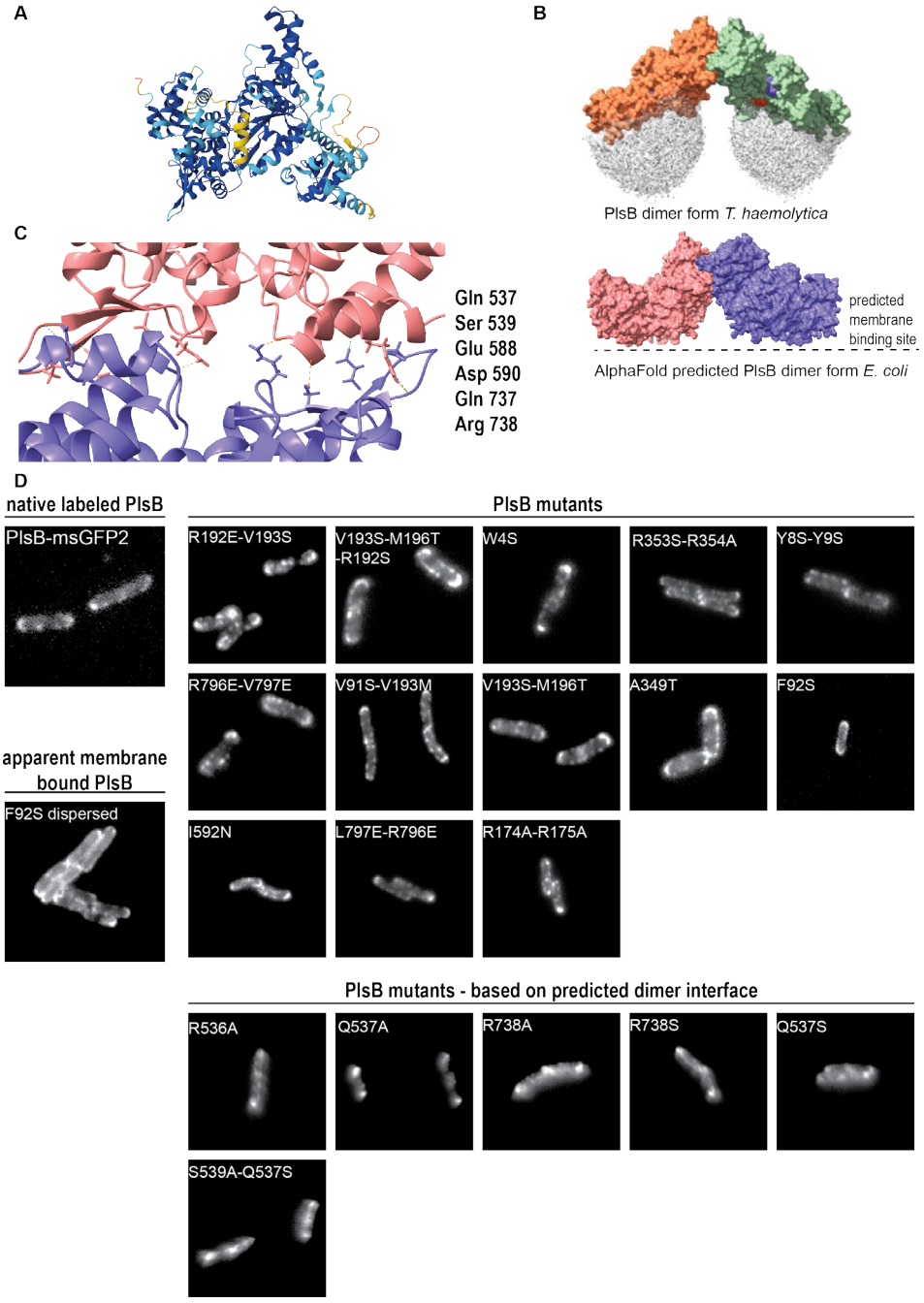
A
B
PlsB dimer form T. haemolytica
predicted
membrane
binding site
AlphaFold predicted PlsB dimer form E. coli
C
Gln 537
Ser 539
Glu 588
Asp 590
Gln 737
Arg 738
D
native labeled PlsB
PlsB-msGFP2
apparent membrane
bound PlsB
F92S dispersed
PlsB mutants
R192E-V193S
V193S-M196T
-R192S
W4S
R353S-R354A
Y8S-Y9S
R796E-V797E
V91S-V193M
V193S-M196T
A349T
F92S
I592N
L797E-R796E
R174A-R175A
PlsB mutants - based on predicted dimer interface
R536A
Q537A
R738A
R738S
Q537S
S539A-Q537S

Figure 4.6

Figure 4.6: **A.** Ribbon protein structure of PlsB based on an AlphaFold prediction (*43*, *44*). The color indicates the certainty of the prediction: Orange = very low, yellow = low, light blue = high, dark blue = very high. **B.** Top is a published structure of a PlsB dimer from *Thermomonas haemolytica* adapted from Li et al 2023 (*45*) in white are phospholipid residues. On the bottom is an AlphaFold predicted dimer of *E. coli* PlsB, a dashed line indicates the likely membrane binding domain based on hydrophobicity of the surface. **C.** The AlphaFold predicted *E. coli* PlsB dimer interface with on the right the amino acids involved in stabilizing interactions. **D.** An overview of PlsB mutants. Top left a unmodified PlsB-msGFP2 as control. All mutants show a phenotype roughly equivalent to the control. Only exception is F92S, which on occasion showed a more dispersed phenotype (bottom left).

Unfortunately, while we prepared many different mutants, we found none where filamentation was clearly disrupted. The lack of structural information makes it hard to pinpoint why, it could be that multiple mutations are required, or it could be that the residues we targeted are not involved in filamentation. For this reason we were forced to conclude that in the absence of a solved structure of the *E. coli* PlsB filament we would not be able to find a non-filamenting mutant.

4.8. Attempts at probing the characteristics of purified PlsB using *in vitro* approaches

Purification of PlsB - possible but problematic

In vitro techniques can be great tools to probe the function and behavior of proteins in a low complexity environment, away from the complicating factors introduced by cells. However, before one can utilize such systems it is imperative to first obtain the protein in questions in suitable purity and concentration. The first step we took to facilitate the purification process was to construct a modified PlsB gene tagged with msGFP2 and an additional histamine peptide tag (for a final PlsB-msGFP2-His construct). This construct was inserted into a high copy number inducible plasmid to allow for high expression of PlsB-msGFP2-His. The cells were lysed and the extract purified by affinity chromatography using a HisTrap column using 250 mM imidazole for elution. The final concentration was assessed using a Bradford assay and the final purity using SDS gels **(Supp. Fig. 4.1)**. While we were able to achieve high purity, the resulting concentrations were low and insufficient for further use. In an attempt to increase the concentration spin concentrators were used (*46*). Furthermore, dialysis was done to remove the imidazole as the high concentration needed for elution significantly increases the osmotic value of the solution.

It was these final two steps that proved problematic. Despite concentrating the samples, we continued to have a low overall yield of PlsB. Given these low yields each purification would only generate sufficient purified PlsB for at most a single experiment. While possible, such a process would be rather inefficient and time-intensive. Furthermore, there was a larger problem: the solubility of PlsB. During a purification run that achieved a higher concentration, both initially and after concentrating, the dialysis proved problematic. During the dialysis there was precipitation and we lost all the PlsB. This indicates that PlsB might have solubility issues at high concentrations. These problems proved difficult to overcome, in part likely because the membrane-associated nature of PlsB makes purification more difficult. While these issues are likely solvable, the simple fact is we lacked both the expertise and time to bring this to a good conclusion within the timeframe of the current project. We therefore chose to devote our time and resources to other avenues of research.

Nevertheless, these forays into *in vitro* work with purified PlsB did yield preliminary results we will now discuss. Our efforts first focused on probing the response of PlsB to osmotic shocks using vesicles as a simplified alternative to spheroplasts. Next, we sought to determine the structure and nature of PlsB foci using both direct EM imaging of purified PlsB as well as native gels.

Vesicles as an alternative *in vitro* system for osmotic shock experiments

Given our continued difficulties in working with spheroplasts we sought alternative systems where we could test the response of PlsB to membrane changes due to osmotic shocks. One alternative for spheroplasts is using *in vitro* systems such as large unilamellar vesicles, which function as a highly simplified model of the cell envelope. The production of such vesicles is well described and, importantly, done on a routine basis within our department. Furthermore, inherently lacking a cell wall or analogous structure, these vesicles are highly susceptible to osmotic shocks, making them an interesting system to work with. The first step was to successfully form vesicles in high quantities. Once accomplished, the next step is to purify PlsB and encapsulate it in these vesicles. This encapsulation could potentially be done in conjunction with one or both substrates, allowing for observation of activity. Finally, vesicles with encapsulated PlsB can be exposed to osmotic shocks to monitor the effect on PlsB localization and foci formation.

Based on work of others using vesicles to study *E. coli* proteins, our initial plan was to prepare vesicles composed of 50% phosphatidylcholine (18:1 Δ9 DOPC), 36% phosphatidylethanolamine (18:1 Δ9 DOPE), 12% phosphatidylglycerol (18:1 Δ9 DOPG), and 2% cardiolipin (18:1 CL). This composition seeks to mimic the *E. coli* membrane by using 50% non-native phosphatidylcholine and 50% native E. coli composition. Phosphatidylcholine is a phospholipid not endogenous to *E. coli* but included in the lipid mixture due to its shape. Unlike phosphatidylethanolamine, which has a conical shape, phosphatidylcholine has a cylindrical shape well suited to, and perhaps even

required for, bilayer formation in *in vitro* systems (*47*). Furthermore, the chemical properties of phosphatidylcholine are somewhat analogous to phosphatidylethanolamine as both are zwitterionic, therefore we hope its inclusion does not cause too large a perturbation for PlsB. This assumption is strengthened by literature examples that show that despite not being endogenous, *E. coli* can tolerate a membrane composition of up to 30% phosphatidylcholine. However, while cells containing such quantities of phosphatidylcholine do not show major growth defects, the structure of their membranes is considerably perturbed (*48*). Nevertheless, concessions must be made when employing *in vitro* systems, and the lipid composition as described seeks to strike a balance between the requirements of vesicle formation while also aiming to stay true to native *E. coli* membranes. Unfortunately, in our hands initial preparations of this composition did not result in vesicle formation and we therefore switched to a more robust composition: 86% phosphatidylcholine, 12% phosphatidylglycerol, and 2% cardiolipin. Finally, a small amount of Cy5 labeled phosphatidylethanolamine (18:1 Cy5 DOPE) was included to fluorescently label the vesicles.

The vesicles were prepared using the emulsion droplet interface crossing encapsulation (eDICE) method (*49*). In this method, the mixture of phospholipids is dissolved in an organic solvent and subsequently emulsified with an aqueous solution. For our pilot experiments, the aqueous solution consisted only of a buffer as well as sucrose for osmotic regulation. After the formation of an emulsion, the aqueous droplet, now surrounded by a single layer of lipids, are pushed through an aqueous-oil interface by centrifugation, creating the final unilamellar vesicles. By incorporating a fluorescent lipid dye into the phospholipid mix the vesicles can be easily visualized and we could verify that a great number of vesicles were produced this way. Our initial attempts produced irregularly shaped vesicles, indicating a mismatch between the osmotic force of the inner and outer aqueous solutions **(Fig. 4.7A)**. By adjusting the osmotic value of the inner aqueous solution to match the outer aqueous phase this issue could be easily resolved, but these initial results do clearly show the susceptibility of vesicles to osmotic pressure. Unfortunately, due to the difficulties of obtaining purified PlsB, we were not able to encapsulate and begin characterizing its response to osmotic shocks.

Structural determination of purified PlsB using EM

Our initial attempts at structural determination of the PlsB filament were focused on *in situ* imaging. We had hoped to visualize PlsB inside the cell, thereby having the greatest chance of preserving its native conformation and organization. However, in these earlier *in vivo* attempts at identifying PlsB in (partial) bacterial cells, the problem was not producing a sufficient number of (mini-)cells, but rather the low number of PlsB filaments within these cells. We attempted to maximize the intracellular PlsB concentration, thereby increasing size and/or number of PlsB filaments, through overexpression. However, despite overexpressing PlsB no filamentous structures were observed, we speculate that might be due to the resulting structures still only occupying a small

percentage of the total cell volume. To alleviate these problems we wanted to increase the density of PlsB filaments as well as removing other structures that might complicate identification. To achieve this, we sought to purify PlsB filaments from cells and image them *in vitro*, a method that has been previously been reported (*3*, *50*, *51*).

Unfortunately, as described above while we were able to achieve a high purity, we were not able to obtain a high yield of PlsB. Nevertheless, despite the relatively low concentration of PlsB we still attempted to image these samples. First, the sample was loaded onto a grid and front blotted for between 5 and 7 seconds after which the grids were plunge frozen in liquid ethane. Grids were then imaged with the EM at 300 kV JEOL 3200. Unsurprisingly given low starting concentrations we found nothing that we could definitively attribute to PlsB filaments. While there were a few interesting structures, these were present in only a subset of samples and even then at low abundance, preventing identification **(Fig. 4.7B)**. Without higher purification yields further attempts seemed unlikely to produce better results. We therefore decided to not not continue pursuing this line of inquiry for the time being.

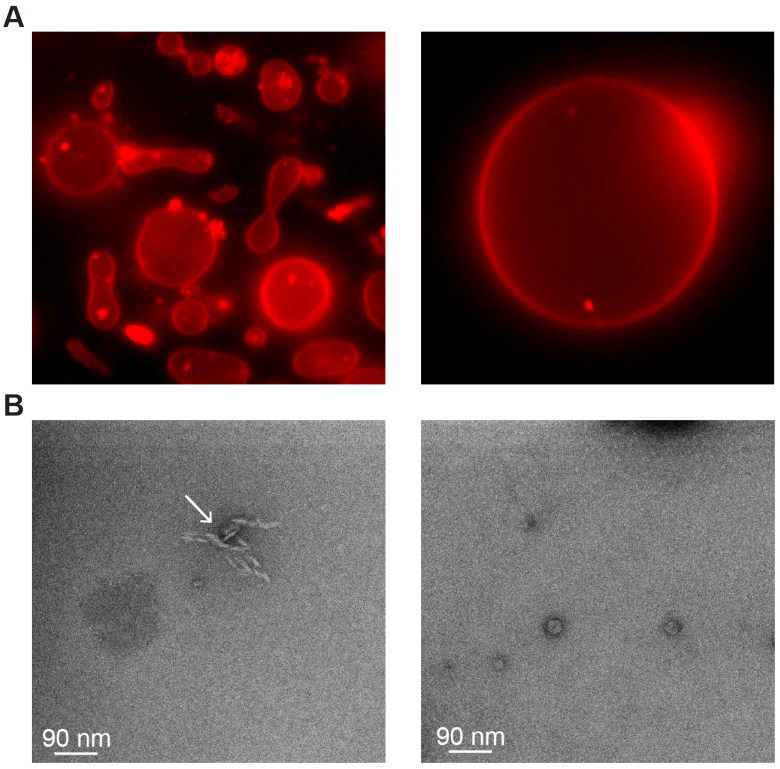

Figure 4.7

Figure 4.7: Electron microscopy images of purified PlsB and confocal microscopy images of lipid vesicles. **A.** Vesicles formed from 86% DOPC, 12% DOPG, 2% CL. Red fluorescent signal is a result of inclusion of Cy5 labeled lipids (Cy5-DOPE). Left, vesicles with mis-match between the osmotic value of the inner and outer aqueous phases, showcasing the susceptibility of these vesicles to osmotic pressure. Right, vesicles not experiencing such a mis-match in osmotic pressure are well formed and spherical. **B.** Cryo-EM images of purified PlsB. Left, while some odd structures (white arrow) could be seen at low abundance in some of the samples, these could not be readily identified. Right, in most field of views no structures of interest could be observed, likely due to low PlsB concentrations.

Using native gel to show PlsB is present as higher order structures

Our final attempt to glean any information as to what degree PlsB is natively organized into high-order structures was to use a native gel. Based on prior published research, purifying PlsB can be done while preserving any high order structures (*3*, *50*, *51*), and since native gels preserve the natural conformation of the protein we hoped it would also not perturb these structures. However, since these high order structures are significantly larger than the average protein, they will likely not be able to enter the gel matrix. Therefore, these higher order structures would instead remain in the well while mono- and dimeric PlsB can enter the gel. This should then be observable as a large concentration of fluorescent signal that remains in the well while a dimmer band should be observable in the gel itself. By comparing different conditions, for example regular growth with punctuate foci and exposure to triclosan with dispersed fluorescence, information can be gleaned on the state of PlsB in these conditions. While this method gives very little to no information about the type, size or number of higher order structures, it can be further evidence of their higher-order structure.

Unfortunately the previously outlined problems surrounding the purification process meant that we only had access to low concentrations of PlsB. As a result, the fluorescent signal inside both the gel and the wells is relatively weak **(Supp Fig. 4.3)**. Furthermore, the isoelectric point of PlsB (estimated at 8.5 and 6.93 for PlsB and PlsB-msGFP2, respectively) necessitated a high pH in both the anode and cathode buffers, resulting in very low current, causing errors and generally complicating the experimental procedure. Without obtaining a higher concentration of PlsB, it seemed unlikely a better signal could have been obtained. Furthermore, there is no guarantee our purification method and subsequent experimental steps preserve any higher order structures that might have existed *in vivo*. As such, this approach was not pursued further.

4.9. Discussion

The nature of PlsB foci remain a mystery

There are many different ways proteins can self-organize and assemble into higher order structures. PlsB has previously been shown to assemble into a filament, but at the time the physiological relevance of these filaments was still unclear. In **Chapter 2** we argue that the formation of these filaments, which have been shown to inhibit enzymatic activity, is the regulatory mechanism of PlsB. By fluorescently labelling PlsB we were able to show that PlsB assembles into foci and that this foci formation is dependent on the relative abundance of the membrane.

However, the exact nature of these foci remained an open question. While PlsB has previously been shown to form filaments, this was under conditions of overexpression, which can sometimes affect protein behavior. And while the behavior of the foci certainly matched our expectations of filament behavior, there are alternative hypotheses such as liquid condensates. In this chapter we sought to further probe the foci through several approaches. These include further testing the behavior of the foci in response to changes in the relative membrane abundance using osmotic shocks, as well as depletion of glycerol-3-phosphate. Furthermore, we sought to determine the structure of the foci using electron microscopy. Finally, we attempted to glean more information about the dynamics of the foci using FRAP.

Lessons borne from failure

Unfortunately, none of these methods were wholly successful, and each faced their own specific experimental and technical problems. This does not, however, mean that they have taught us nothing. For example, even though our initial ventures with spheroplast did not yield results, the attempt set on us the path of doing hyperosmotic shocks on regular cells, an experiment that did yield meaningful results **(Chapter 2)**. Other approaches such as vesicle formation and electron microscopy of purified samples can be regarded as pilot experiments, identifying the pain points in these experiments. With more time and resources, the problem of PlsB purification can surely be resolved, at which point both these techniques can be revisited. At such a time, some of the groundwork in terms of protocols and strain construction will already have been done.

Other experiments, while not definitive, did provide a tantalizing glimpse at an answer. While the problem with gradual bleaching and overall low fluorescent signal impacted our ability to utilize FRAP, the results we did observe are still interesting. Though hard to quantify and with questionable significance, they do seem to suggest that there is indeed a difference between the foci and dispersed fluorescence. While there appears to be a mild degree of recovery of dispersed signal, we never observed a recovery of foci. While it cannot be fully excluded that this is due to experimental factors, this does seem to support our assumption that the foci are indeed a less mobile and more structured configuration of PlsB. This is further supported by the Native gel, which appears to show a fraction of PlsB is in a conformation too large to enter the gel. Of course, experimental factors here also decrease the certainty of such statements.

We also attempted to disrupt filament formation and thereby show filaments are required for regulation of phospholipid synthesis. We made many mutations, targeting exposed hydrophobic residues, double arginine fingers and residues proposed to form the dimer interface. None of these mutations reliably produced a definitive result that we could associate with a disruption of filamentation. The simplest reason for this is that none of the residues we targeted are involved in filament formation, certainly a plausible explanation given the lack of structural data. The lack of a strong response, be that in foci formation, cell morphology or growth rate, made it impossible to determine whether we were on the right track and thus impossible to implement iterative design. Without additional structural information, this line of experimentation is simply unlikely to generate meaningful results.

Finally, some of the results have forced us to reconsider our approach on a broader scale. Our attempts at *in situ* imaging of PlsB filaments, either with minicells or sectioning, have shown us how difficult this approach is when there are only one or two small filaments in a cell. A further complication is that neither of these approaches captures the whole cell volume. Each individual section or minicell represents only a fraction of the original cells, and thus only a certain percentage will actually contain (part of) a PlsB filament. Furthermore, even if a PlsB filament is present, it will not necessarily have the orientation and/or size suitable for identification. Therefore, we expect the most promising way forward is to use methods that capture the whole cell volume, thereby ensuring each cell imaged has at least one PlsB filament. Another example of a result forcing us to reconsider our approach is our work with the stop-codon readthrough. While unsuccessful, these experiments demonstrated that imaging requires a sufficient number of fluorescently labelled PlsB. Thus, if we want the majority of PlsB to be unlabeled to allow for elongated filaments to form, while at the same time requiring a (near-)native abundance of labelled PlsB for imaging, we will be forced to overexpress PlsB. Therefore, while in this thesis we always attempted to stay as close to native conditions as possible by conducting experiments at native concentrations of PlsB, in the future we might have to consider abandoning this standard, at least for certain experiments.

Of course, this in part depends on how important the distinction between elongated filaments and punctuate foci really is. The experiments described in this chapter have, with the possible exception of FRAP, done little in the way of answering this question. However, all previous experiments described in **Chapter 2** show that punctuate foci are dynamic structures that respond to environmental and cellular perturbations. So, while it is still important to understand if and how punctuate foci might differ from elongated filaments, the distinction might not be crucial when describing the regulation of PlsB and phospholipid synthesis in general terms. Unless later experiments show this to not be the case, we assert that our current assumption that punctuate foci are representative of PlsB filaments appears reasonable.

Future steps: towards determination of a structure

We advocate that these experiments be performed, and suggest three follow-up experiments aimed at determining the structure of PlsB foci and filaments.

Our first recommendation is to revisit FRAP, as this technique appears closest to providing meaningful results in a short time span. We would recommend repeating this experiment with cells co-expressing PlsB and PlsB-msGFP2 since the elongated filaments are both a larger, and might therefore be partially bleached, and easier to interpret target. If this is achieved, this would allow easier measurement of the recovery rate. However, we do caution that the relative imprecision of FRAP when targeting small bacterial cells and the overall low fluorescent signal due to the small fluorescently labelled pool are likely to continue to complicate such an experiment. Nevertheless, we believe it is worthwhile to make the attempt.

The second recommendation, while more difficult, is to make further attempts at purifying PlsB. Successful purification of PlsB could open up several promising experimental avenues. Purification of intact PlsB filaments could lead to structure elucidation if imaged with electron microscopy. Alternatively, the existence of stable higher order structures could be shown using native gels. Even if purification results in exclusively mono- or dimeric PlsB, such a sample could still be used for incorporation into vesicles. For such a purpose, optimization of the protocol described in this chapter coupled with larger cultures might even suffice, paying special attention to the solubility of PlsB.

Finally, our third recommendation is a renewed and more thorough imaging of PlsB filaments in situ. While the structure of the PlsB filament could be solved by purifying the filaments and imaging them with electron microscopy, in situ imaging can be an alternative approach. In the attempts described in this chapter, the main problem has been the small size and low abundance of the filament in combination with capturing only a fraction of the total cell volume. The former might be solved by using the mixed expression system, which yields a larger filament. The latter meanwhile could be solved with a recently published method (*52*). In this method cells, ideally spheroplasts, are placed onto an EM grid and flattened through gentle lysis. This makes the cells thin enough for TEM but still allows the full volume to be imaged. This way any filaments present should be identifiable. Furthermore, using mixed labelling this technique could potentially be combined with CLEM to aid in finding and identifying filaments. Solving the structure would not only be valuable to understand how the filaments form, but also to determine which residues are crucial for filament formation. With this information mutants can be created that are unable to filament. This could then be used to determine if filament formation is required for regulation.

4.10. Methods

Culture conditions

Cells were cultured on MOPS (3-(N-morpholino)propanesulfonic acid) minimal media, specifically MOPS 0.2% Glucose 0.1% Cas Amino Acids (CAA). For strains containing additional plasmids with antibiotic resistance markers this media was further complemented with the appropriate antibiotics. Unless otherwise stated cells were cultured in small volumes (5 mL) in glass tubes. Cultures were incubated at 37°C while rotating at 400 rpm.

Plasmids, strains and cloning

Plasmids and strains

For all experiments NCM3722, a K12 *E. coli* strain, was used as a base. Many experiments were performed with modified strain where chromosomal copy of PlsB was tagged with msGFP2, referred to as NCM3722 *plsB-msGFP2*. Both of these strains were used as a base and further modified with plasmids, a full list is found in **Supp. Table 4.1**. For these strains the naming convention is the base strain followed by the plasmid (e.g. NCM3722 *plsB-msGFP2* + pBbE5K-PlsB).

Table 4.1: Strains used in this work

Strains	Antibiotics resistance marker	Inducer
NCM3722 *plsB-msGFP2*	NA	NA
NCM3722 *plsB-msGFP2* + pBbE5K-PlsB-msGFP2	Kanamycin	IPTG
NCM3722 + pBbE5K-PlsB-msGFP2-His	Kanamycin	IPTG
NCM3722 + pBbE5K-PlsB-msGFP2-UGAC	Kanamycin	IPTG
NCM3722 + pBbE5K-PlsB-msGFP2-UGAA	Kanamycin	IPTG
NCM3722 + pBbE5K-PlsB-msGFP2-*mutation*	Kanamycin	IPTG

GpsA-pdt3 strain construction

Starting from plasmid pECT3 containing the pdt3-frt-KanR-frt sequence, 60 bp primers were designed with 12 bp overlap to the pdt3 (forward) or 13 bp overlap to the second frt (reverse) sites. The rest of the primers were homologous to the end of the *E. coli* GpsA gene. A strain of NCM 3722 *plsB-msGFP2* Δ*gplR* was made chemically competent and transformed with the plasmid pKD46, which is a temperature sensitive plasmid containing XX and is inducible by arabinose. A 30 mL culture was grown at 30°C to OD 0.1, at which point 5% arabinose was added. The culture was grown until the OD reached 0.8, at which point the cells were pelleted by centrifugation (10,000 g, 10 min, 4°C). The pellet was resuspended was washed twice with 25 mL cold 10% glycerol, centrifuged and resuspended in 2 mL cold 10% glycerol. This dense cell suspension was transferred to a 2 mL Eppendorf tube, centrifuged (10,000 g, 5 min,

4°C) and resuspended in 200 µL cold 10% glycerol. The optical density of the culture was measured as approximately 110 OD (measured by diluting 1:1000). The culture was divided into 4 aliquots of 50 µL and to each aliquot 250 ng (5 µL) of DNA was added (the pdt3-frt-KanR-frt with GpsA homolog sequence at each end). Each of the aliquots was transferred to an electro cuvette and electroporated at 2500 V. After, 1 mL of LB was added to each of the aliquots and they were first chilled on ice for 5 min before recovering at 37°C for 1 hour. The full volume was plated on LB agar with kan50 and incubated overnight at 37°C.

Stop codon cloning

This work was done based on the QuickChangeTM method. Primers were designed to insert a UGA stop codon in between the sequence of PlsB and the sequence of the linker. The primers had 6 bp homology in both sequences, with an additional 10 – 12 bp binding region in the PlsB or linker region for the reverse and forward primers, respectively. A PCR was run using pBbE5K-PlsB-msGFP2 as template at 44 ng/µL concentration. The reaction mix was composed of 37.5 µL milliQ, 10 µL 5x GC buffer, 1 µL 10 mM dNTP, 0.5 µL template, 0.5 µL primer mix, and 0.5 µL Phusion polymerase. The PCR was run for 25 cycles, with melting temperature set at 66°C and an elongation time of 3.5 minutes. After PCR, a gel purification and dpn1 digestion was performed. Aliquots of chemical competent *E. coli* Dh5α were thawed and transformed with the PCR product. To each aliquot was added 20 µL 5x KCM buffer, 60 µL milliQ, and 20 µL PCR product. For both constructs, 3 colonies were selected and send for sanger sequencing to verify correct insertion of the stop codon and no other mutations had occurred. From these a colony of each construct was chosen and the plasmid was transformed into *E. coli* NCM 3722 strain.

Table 4.2: Primers designed for introducing stop codons. In bold are given the homology regions on either side of the introduced stop codon. In red is the stop codon itself, in blue the base pair immediately downstream of the stop codon. The non bold text denotes the additional binding region.

Name	Primer	Melting temperature
UGA A forward	**GAAGGGTGAAGCGGT**GGCGGTGGCA	67.5 °C
UGA A reverse	**ACCGCTTCACCCTTC**GCCCTGCGTCG	65.7 °C
UGA C forward	**GAAGGGTGACGCGGT**GGCGGTGGCAG	68.2 °C
UGA C reverse	**ACCGCGTCACCCTTC**GCCCTGCGTCGC	68.8 °C

Microscopy

The cultures used for microscopy were prepared at outline in the “culture conditions” section. To ensure the bacteria are able to grow and/or continue to be exposed to antibiotics during the imaging they were placed on agar pads. To make these pads, first a larger batch of agarose was prepared using 1.5 g low gelling point agarose dissolved in 50 mL milli-Q for a final concentration of 3%. This agar was then autoclaved to ensure sterility. Afterwards, the full volume was divided into 0.5 mL aliquots which were stored at -20°C. For each experiment, one of these aliquots was used and remelted at 80°C in a heating block. Once melted, 0.5 mL of a 2x medium (e.g. MOPS 0.2% glucose 0.1% CAA) is added as well as any inducer or antibiotic. The solution is mixed through vortexing and briefly (less than 5 min) placed back in the heating block to ensure it does not gel in the tube. Three 15 x 15 mm glass coverslips are place on a flat piece of parafilm and 0.3 mL of agar is pipetted on each of these. A second coverslip is then gently placed on top of the agar droplet, spreading it out to a (near) uniform shape. These are covered and left to gel, after they have solidified they are placed at 37°C to pre-heat.

The slides for microscopy were prepared in two different ways, depending on the microscope used. For widefield, a prepared and pre-heated agar pad is taken and one of the coverslips peeled off. |Aa small amount of culture (1 – 2 µL) is then placed onto the agar pad, which is then placed agar side down onto a larger 22 x 50 mm coverslip. If used for a timelapse, the sides are sealed to prevent drying of the agar pad during the acquisition. For confocal microscopy there is a slight variation on the above protocol, instead of placing the agar onto a 22 x 50 mm coverslip, they are instead placed onto a microscopy dish with a lid and a small amount of wet tissue paper inside. This is done because the holder on the confocal microscope is not suitable for the coverslip slides and this way still ensures the sample does not dry out.

Widefield microscopy was done initially on an Inverted Olympus IX81 equipped with a Andor Luca R camera (EM-CCD, 104x1002 pixel chip size, 8x8µm pixel size, 14-bit dynamic range, 65% quantum efficiency at 600nm), CoolLED pE-4000 fluorescence excitation source, 100x 1.45 NA oil objective (0.13 mm WB), GFP filter cube (ET-EGFP, 470/40 excitation filter, T515lp dichroic filter cut-off, 525/50 emission filter, reference: C229863), phase ring and heating box. The microscope was heated to 37°C before the start of the experiment, at least 30 minutes in advance to ensure a stable temperature. At the start of acquisition the 10x or 20x objective was used to check alignment of the phase ring and make adjustments if needed. Positions were chosen keeping in mind a sufficient number of cells in the field of view and no or minimal non-cell debris. Images were taken in two channels, one in phase contrast (50 ms exposure) and one for GFP (1000 ms exposure, 490 nm, 40% intensity). Phase contrast imaged were taken through the GFP filter cube to save time switching blocks. Where relevant, Z-stacks were taken using a 0.2 µm interval between slices. For timelapses, multiple positions are marked and imaged at 2.5 minute intervals, generally for at least 4 hours but up to 8 hours.

Confocal microscopy is done on a Nikon Eclipse Ti microscope with a 488 nm laser (confocal-CW, 16 mW), a 100x SR Apo TIRF 1.49 NA oil objective (0.12 mm WB), a 482/35 fluorescence emission filter, a EM-CCD Andor iXon X3 DU897 detection device (512x512 pixel chip size, 16x16 µm pixel size, 14 bit dynamic range, >90% quantum efficiency at 600nm), and Tokai Hit sample incubator chamber. The sample is incubated at 37°C during imaging. Suitable locations are found by looking at the sample using the Resonant scanning. Once a position is found a high resolution image is taken using Galvano scanning.

FRAP

A culture of NCM 3722 *plsB-msGFP2* was grown to exponential phase (OD 0.3 – 0.4) in MOPS 0.2% glucose 0.1% CAA at 37°C. A thin agar pad was prepared (1:1 mixture of 2% agar and 2x (MOPS 0.2% glucose 0.1% CAA)) and 1 µL of culture was transferred onto the pad. This pad was then placed inside an imaging dish which in turn was placed inside a heated sample holder (temperature set to 37°C). Resonant scanning confocal microscopy using a 488 nm laser and 100x objective was used to find cells, care was taken to minimize live imaging in order to prevent bleaching. Once a cell was in the center of the field of view and in focus, one cell pole was marked for FRAP. A 1 second FRAP pulse was used. The experimental design was as follows: 2 image taken before hand with a 60 second interval, a 1 second FRAP pulse, an image immediately after, followed by 10 subsequent images following the recovery at 60 second intervals.

Imaging was done on a Nikon Eclipse Ti microscope with a 488 nm laser (confocal-CW, 16 mW), a 100x SR Apo TIRF 1.49 NA oil objective (0.12 mm WB), a 482/35 fluorescence emission filter, a EM-CCD Andor iXon X3 DU897 detection device (512x512 pixel chip size, 16x16 µm pixel size, 14 bit dynamic range, >90% quantum efficiency at 600nm), and Tokai Hit sample incubator chamber. The sample is incubated at 37°C during imaging. Suitable locations are found by looking at the sample using the Resonant scanning. Once a position is found a high resolution image is taken using Galvano scanning.

Spheroplast preparation

The following protocol is based on the one described in Renner et al. 2011 (*18*). An overnight culture was grown from a single colony in LB at 37°C. The next morning, this culture was diluted 1:100 in fresh LB medium, this culture was incubated at 37°C until OD reaches 0.5-0.7. In the meantime, LB supplemented with 60 µg/mL cephalexin is prewarmed to 37°C. Once the OD reaches 0.5-0.7 dilute 1:10 culture into the pre-warmed LB. This is incubated for 3 – 4 hours at 37°C. Transfer 1 mL aliquots of this culture into 1.5 mL Eppendorf tubes. Centrifuge for 1 min at 3000 g and carefully remove the supernatant. Gently resuspend the cell in 500 µL 800 mM sucrose solution by inverting the Eppendorf tube. Add 50 µL 1 M tris HCl (pH 8.0), 24 µL 0.5 mg/mL lysozyme, 6 µL DNase, and 6.5 µL 115 mM EDTA. Incubate for 15 min at 25°C and then add 100 µL STOP solution (10 mM Tris HCl (pH 8.0), 0.7 M sucrose, 20 mM mgCl2). For imaging, 1.5 µL of this mixture is placed onto a thin agar pad on a microscopy slide.

Optionally, for fixation add 35 µL 37% formaldehyde and incubate for 30 min. If fixating, centrifuge at 3000 g for 10 min and gently remove the supernatant. Carefully wash the pellet with 700 µL PBS (pH 7.2), then wash with 150 µL PBS three times, finally resuspend in 150 µL PBS. For imaging, 1.5 µL of this mixture is placed onto a thin agar pad on a microscopy slide.

Vesicle preparation

The following protocol is based on the one described in Van de Cauter et al. 2021 (*53*). First, the inner and outer aqueous phases were prepared. The outer aqueous phase is composed of 150 mM Glucose. The inner aqueous phase is composed of 20 mM Tris HCl (pH 7.4), 50 mM Sucrose, 6.5% optiprep. The outer buffer is composed of 67 mM Tris HCl (pH 7.4), 6.7 mM MgCl2. The osmolarity of all three solutions should be similar. After measurement it was determined that the outer aqueous solution needed to be supplemented with 3 mL 20% glucose per 100 mL of solution to adjust the osmolarity.

Second, imaging chambers should be prepared through surface passivation with beta-casein. Prepare a passivation solution of 1mg/mL beta-casein and 10 mM Tris, place in chamber to cover the glass surface and incubate for 15 min. Afterwards, wash twice with MilliQ.

A lipid mixture was prepared composed of 168 µL DOPC (10 g/L). 24 µL DOPG (10 g/L), 7.6 µL CL (10 g/L), and 1 µL Cy5-DOPE (1 g/L) was prepared **(see table 2.2)**. First, 50 µL of chloroform was added to a glass vial, after which each lipid volume was transferred to the glass vial using a glass syringe that was first cleaned using chloroform. Compressed air is used to gently evaporate the organic solvent until the dry lipids are deposited on the bottom of the vial. The vial is placed in a desiccator overnight to ensure dryness.

Next, in a glovebox the dry lipids are first resuspended in 50 µL chloroform, after which 370 µL of decane is added. The vial is gently swirled to ensure mixing and that all the lipid is resuspended. In another, empty, glass vial 1.3 mL of mineral oil and 5.2 mL of silicon oil are mixed together. While gently vortexing the lipid mixture, add the oil mixture in a dropwise manner. Remove the glass vial from the glovebox and wrap the lid with parafilm. Fill a large glass beaker with crushed ice and water. Place the glass vial into a smaller glass beaker and add some water so that the bottom half of the glass vial is submerged. Place the large beaker into a sonicator bath, set the small beaker into the large one and use a clamp stand to keep it in place. Sonicate for 15 minutes.

Place a clean eDICE chamber onto the rotor, slowly increase the voltage 14.5 V. First, pipette 1 mL of outer aqueous phase into the chamber. Follow this with 5 mL of your sonicated lipid mixture. In a 1.5 mL Eppendorf tube, place 1 mL of lipid mixture and 50 µL of inner aqueous phase. Scratch the tube vigorously to create a fine emulsion. Add this emulsion to the chamber and leave it to rotate for 4 minutes. Reduce the voltage to zero and let the chamber rotate to a stop. Carefully remove as much of the oil phase as possible, at least until the chamber can be held at a 45° degree angle. Take a

200 mL pipette tip and, using a scissor, cut of the tip (roughly 1 mm). Carefully transfer 50 µL of the aqueous solution into an imaging chamber, taking care to not transfer any of the oil phase.

The resulting vesicles were imaged using a confocal microscope. A cy5 filter and excitation laser was used together with a 60x objective.

Table 4.3: Phospholipids used in preparation vesicles

Lipid	Provider	Code
18:1 Cy5 PE (DOPE-Cy5)	Avanti Polar Lipids (via Sigma)	810335C-1mg
DSPE-PEG(2000) Biotin	Avanti Polar Lipids (via Sigma)	880129C-10mg
18:1 (Δ9-Cis) PC (DOPC); 1,2-dioleoyl-sn-glycero-3-phosphocholine	Avanti Polar Lipids (via Sigma)	850375C-25MG
18:1 (Δ9-Cis) PG (DOPG)	Avanti Polar Lipids (via Sigma)	840475C-25MG
18:1 (d9-cis) PE (DOPE)	Avanti Polar Lipids (via Sigma)	850725C-25mg
18:1 Cardiolipin	Avanti Polar Lipids (via Sigma)	710335C-25mg

Purification of PlsB

The following protocol is based on the one described in Exterkate et al. 2018 (*54*). 250 mL of 2xYT medium (16 g/L peptone, 10 g/L yeast extract, 5 g/L NaCl) was supplemented with 100 µg/mL ampicillin and 5 g/L glucose. This medium was inoculated with 5 mL of overnight culture of NCM 3722 + pBbE5K-PlsB-msGFP2-His. The culture was grown until reaching OD 1.25, at which point it was induced with IPTG (final concentration 100 µM). The culture was incubated for an additional 5 hours, then transferred to a 1 centrifuge bottle and centrifuged for 20 min at 4000 g. The supernatant was discarded and the pellet resuspended in 30 mL L1 buffer (50 mM Na-P, 10% glycerol, 2mM MgCl2). This was transferred to a 50 mL falcon tube and centrifuged for 10 minutes at 4000 g. The supernatant was again discarded and the pellet stored at -80°C.

The next day, the pellet was thawed and resuspended in 40 mL L1 buffer. This resuspension was transferred to another falcon tube using a syringe and needle to further break up the cell pellet. The cells were disrupted using a French press set to 10 kpsi. The resulting cell debris was ultracentrifuged at 40,000 rpm for 30 min.

Ni-NTA bead purification

In a 1.5 mL Eppendorf tube 80 µL of Ni-NTA magnetic beads and 320 µL equilibration buffer (100 mM Na-P, 600 mM NaCl, 30 mM imidazole) were vortexed. The beads were collected to the sides and the supernatant discarded. This was repeated with 800 µL equilibration buffer. After this, 400 µL of crude cell lysate was mixed with 400 µL equilibration buffer and incubated with the Ni-NTA beads for 30 min while shaking at room temperature. After, the beads were collected at the side using a magnetic stand and the supernatant was discarded. The beads were then washed four times with 800

µL wash buffer (100 mM Na-P, 600 mM NaCl, 30 mM imidazole). Finally, the PlsB was eluted off the beads by incubating the beads with 50 µL elution buffer (100 mM Na-P, 600 mM NaCl, 500 mM imidazole) three times each saved separately.

His-Trap column purification using the AKTA

The sample was purified by affinity chromatography, using a HisTrap column. The column was first equilibrated with running buffer (50 mM Tris (pH 8.0), 600 mM NaCl, 40 mM imidazole), after which the crude cell lysate was loaded. After washing with running buffer, the PlsB was eluted using elution buffer (50 mM Tris (pH 8.0), 600 mM NaCl, 500 mM imidazole), the fraction were saved in a deep-well 96-well plate.

Determining concentration and purity

For both purification techniques, a Bradford assay was used to determine the protein concentration. Samples were taken and mixed 1:4 with 4x cracking buffer, samples were not boiled to preserve the relatively robust nature of msGFP2. Samples were loaded onto a gel and run at 200 V for 30 min in SDS running buffer (25 mM Tris base, 194 mM glycine, 3.5 mM SDS). Since the msGFP2 had not been completely denatured, a typhoon imager could be used to image the fluorescent signal of the msGFP2. Spin concentration and dialysis Since the protein concentration in the samples was low they were concentrated using a 10 kDa centrifugal filter. Furthermore, to remove the imidazole and reduce salt content the sample was loaded into a dialysis cassette (Slide-A-LyzerTM dialysis cassette 10K MWCO) and left to equilibrate overnight with a new buffer (50 mM Tris, 150 mM Na-Cl) twice.

Imaging of purified PlsB

Purified sample was loaded onto a EM grid, front blotted for between 5 and 7 seconds and subsequently plunge frozen in liquid ethane. Imaging was performed at 300kV JEOL 3200.

Sectioning of *E. coli* cells and imaging

A culture of NCM 3722 *plsB-msGFP2* + pBbE5K-PlsB-msGFP2 was grown to exponential phase (OD 0.3 – 0.4) and induced with IPTG for 30 minutes. 2 mL of this culture was pelleted in a 1.5 mL Eppendorf tube. Cells were fixed with 2% paraformaldehyde and 0.2% glutaraldehyde with PHEM buffer for 1h and subsequently washed with PHEM buffer. After this point, two methods of further preparation were applied.

Epoxy resin method

Next, cells were infused in a 2% Agarose solution while gently centrifugated, forming a pellet at the bottom. This pellet is then carved into small pieces and stained with osmium tetroxide 4%. The cells are dehydrated with ethanol in step wise fashion, incubation in 10%, 30%, and 50% for 10min followed by incubation in 70%, and 90% for 15min and finally in 100% ethanol for 20min. Afterwards, the cells are embedded in Epoxy resin (Epon 812), first in 50% then 100%. This is left to polymerize over the week-end at 60°C. Using a microtome 100 nm section are shaved from the prepared cells. These 100nm section are contrasted with Lead and Uranyl acetate and acquired with the electron microscope at 120kV JEOL 1400.

Tokuyasu method

Cells are infused in a 12% Gelatine solution while gently centrifugated, forming a pellet at the bottom. This pellet is then carved into small pieces and infiltrated with 80% sucrose solution over night at 4°C. The pellet is then cryofixed in liquid nitrogen and 80nm + 100nm cryo-ribbons were thawed in methylcellulose and washed with PBS buffer. Fluorescent images were acquired using microscope EVOS from Invitrogen, afterwards the cryo-ribbons were contrasted with methylcellulose and uranyl acetate and then acquired with the electron microscope at 120kV JEOL 1400.

Minicell preparation and imaging

A culture of NCM 3722 *plsB-msGFP2* + pBAD24-FtsZ was grown in LB medium at 37°C overnight. The next morning, 1 mL of this overnight was diluted in 200 mL fresh LB medium supplemented with 0.2% arabinose. The cultures were left to grow until the start of stationary phase (OD 1.0). The culture was transferred to falcon tubes and centrifuged for 5 min at 4°C and 3000 g. The pellet was discarded and the supernatant transferred to clean falcon tubes. The supernatant was chilled on ice for 45 min before being transferred to ultracentrifuge tubs. These were centrifuged using a Beckman-Coulter ultracentrifuge using a type 45 Ti rotor at 12,400 rpm for 30 minutes at 4°C. The supernatant was discarded and the small pellet resuspended in 5 mL LB. This resuspension was centrifuged for 5 min at 5000 g. The pellet was discarded and the supernatant transferred to Eppendorf tubes. These were centrifuged for 20 min at 20,000 g and 4°C, after which the supernatant was discarded and the pellet resuspended with 100 µL LB. These were stored overnight at 4°C. Next day, cells were fixed with 2% paraformaldehyde and 0.2% glutaraldehyde with PHEM buffer for 1h and subsequently washed with PHEM buffer. 3.5 µL of the minicell suspension was placed onto an EM grid and front blotted for 6 seconds. The grid were plunge frozen in liquid ethane and images were acquired at 300kV JEOL 3200.

4.11. Acknowledgments

We thank Michal Shemesh for expertise and extensive assistance with microscopy, SaFyre Reese and Federico Ramirez Gomez for expertise and assistance with vesicles, and Ramon van der Valk for expertise and assistance with purification of PlsB. We thank Arjen Jakobi for encouragement and insightful suggestions, especially related to electron microscopy, and the entire Bokinsky Lab for stimulating discussions and support.

4.12. Author Contributions

JB: designed and performed experiments, built image analysis pipeline, evaluated data. CT: designed and conducted electron microscopy experiments. LL: performed osmotic shock experiments. HM & SS: constructed and characterized part of mutant library. FvdB: performed spheroplast experiments. GB: supervised project, constructed part of mutant library and GplR deletion strain, evaluated data. JB and GB wrote the manuscript.

4.13. Supplementary Figures

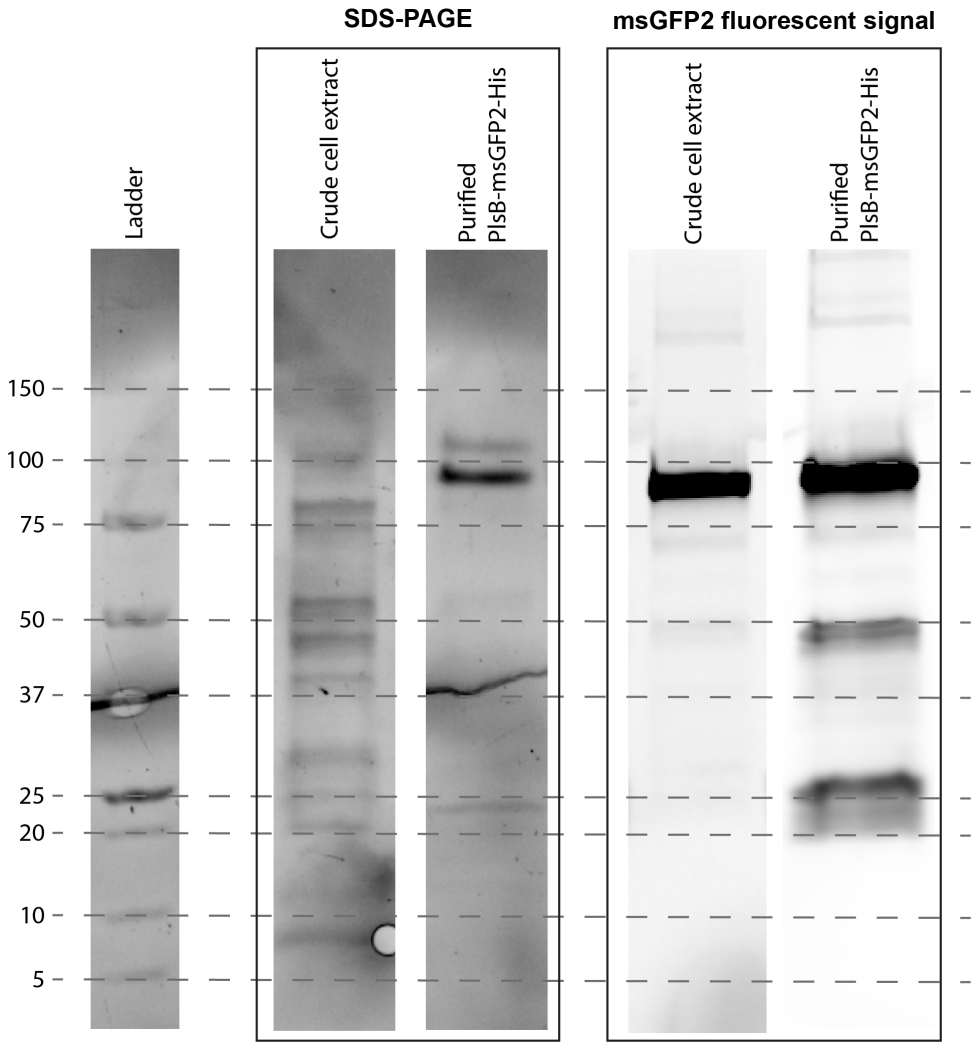

Supp. Fig. 4.1: SDS page gel showing the protein content of both crude cell extract and a purified sample. In the crude extract, dye imaging reveals many protein bands while msGFP2 imaging shows one band with a strong fluorescent signal. Dye imaging of the purified sample shows clear enrichment of PlsB-msGFP2 and exclusion of most other bands. The fluorescent image does reveal two additional, fainter bands suspected of being breakdown products.

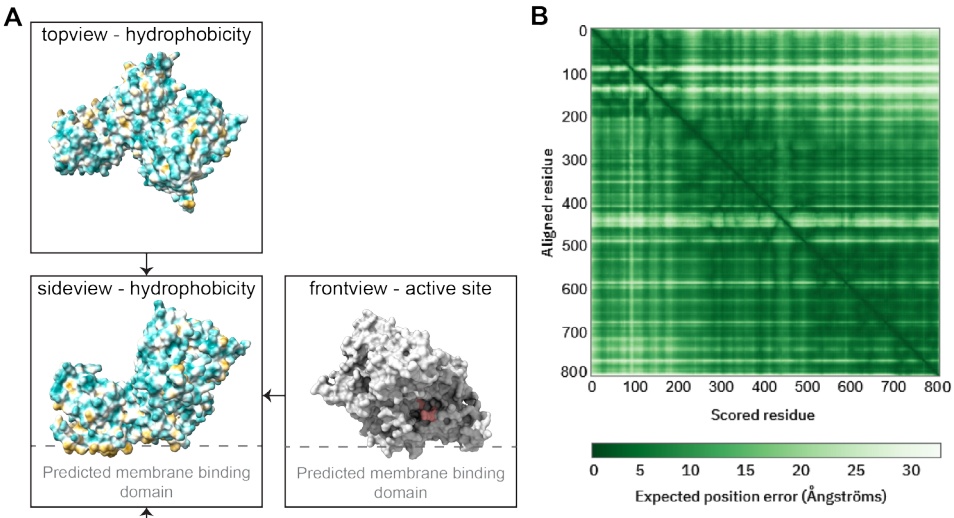

C

T. haemolytica interactions dimer interface	Interactions between atoms	Conservation of amino acids	
		T. Haemolytica	*E.coli*
Arg 808 — Gly 654	NE-O	Lys 598	Gln 537
Arg 808 — Asp 655	NH2-O	Asp 605	Gln 544
Ser 810 — Lys 598	NZ-O	Leu 653	Ile 592
Tyr 813 — Lys 598	O-NZ	Gly 654	Gly 593
Arg 866 — Gln 757	N-OE1	Asp 655	Asp 594
Arg 866 — Asp 605	NH1-OD1 | NH2-OD2 | NH1-OD2	Gln 757	His 692
Arg 866 — Asp 759	NH1-OD1 | NH1-OD1	Asp 759	-
Arg 869 — Gln 757	NH2-O	Arg 808	Arg 738
His 870 — Asp 759	NE2-OD1 | NE2-OD2	Ser 810	Ser 740
Lys 874 — Leu 653	NZ-O	Tyr 813	His 743
		Arg 866	Ser 793
		Arg 869	Arg 796
		His 870	Leu 797
		Lys 874	Ser 801

Supp. Fig. 4.2: An AlphaFold prediction of the *E. coli* PlsB structure (*43*, *44*). **A.** Different views of the PlsB model. On the left is shown the top, side and bottom views of the model with a hydrophobicity overlay, where blue indicates hydrophilic residues and yellow indicates hydrophobic residues. It can be seen that there is enrichement of hydrophobic residues at the bottom, making this the presumed membrane binding domain. On the right is a front view of the model where in red are indicated those residues implicated in the enzymatic function of PlsB (*55–57*). **B.** The predicted aligned error of the PlsB model. Lighter colors indicate a larger expected error. **C.** A table showing the dimer interface interactions in *T. haemolytica* as reported by Li et al 2023 (*45*). Also shown is the conservation of the amino acids implicated in the dimer interface in *E. coli* based on sequence alignment.

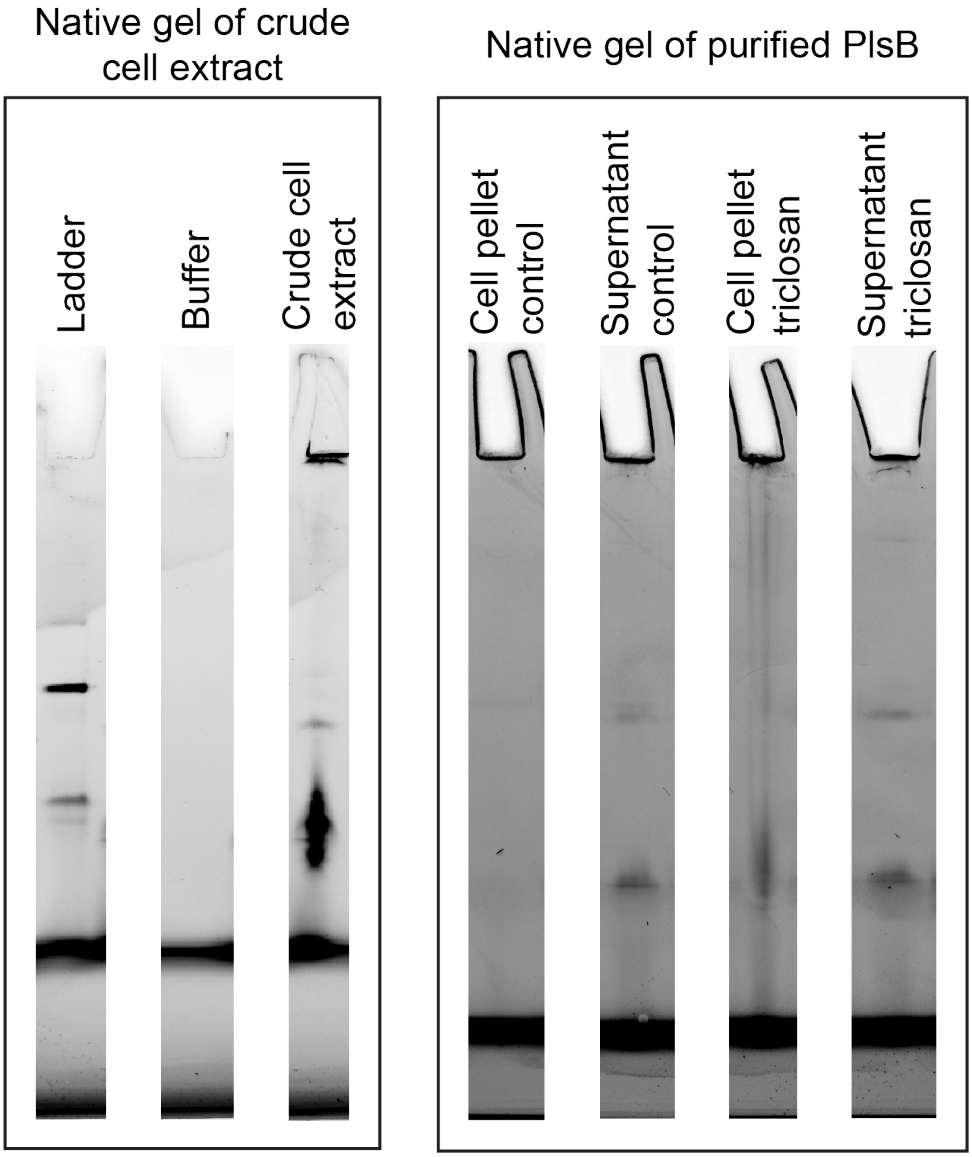

Supp. Fig. 4.3: Native gels of both crude cell extract and purified PlsB. **Left box**, lanes from a native gel imaged using a Typhoon gel imager showing msGFP2 fluorscence signal. Crude cell extract clearly shows bands not seen in neither the ladder nor the buffer, presumed to be PlsB. Apart from signal that has entered the gel, there also appears to be a fraction that has not entered the gel but is instead stuck at the top of the well. **Right box**, another native gel this time showing partially purified PlsB samples obtained either during normal growth conditions (control) or during exposure to triclosan. Notable is the low intensity of the bands, as well as the lack of clear signal at the top of the well

Supp. Table 4.1: Overview of PlsB mutants

Mutant	Growth rate (h^{-1})	Foci	Remarks
Control strains			
WT NCM 3722	0.50 ±0.01	N.A.	
PlsB-msGFP2	0.55 ±0.02	Yes	
Mutants based on common filament features			
R192E-V193S	0.48 ±0.01	Yes	
V193S-M196T-R192S	0.52 ±0.01	Yes	
W4S	0.49 ±0.01	Yes	
R796E-V797E	0.53 ±0.01	Yes	
V91S-V193M	0.49 ±0.01	Yes	
V193S-M196T	0.52 ±0.01	Yes	
A349T	0.48 ±0.01	Yes	
F92S	0.42 ±0.03	Yes	Occasional distributed signal, not reliably reproducible
R174A-R175A	0.51 ±0.01	Yes	
Mutants based on predicted dimer interface			
R536A	0.36 ±0.05	Yes	
Q537A	0.43 ±0.01	Yes	
R738S	0.52 ±0.02	Yes	
Q537S	0.35 ±0.03	Yes	

Results were obtained from strains containing a high-copy plasmid carrying a copy of the plsB gene with the specified mutation. These were cultured on MOPS minimal media complemented with 0.2% glucose and 0.1% Cas amino acids (CAA). Cultures were grown in well plates and OD600 measurements were taken every 5 min using a well plate reader. Each growth rate represents three technical replicates.

Bibliography

(*1*) Shih, Y.-L., Le, T. and Rothfield, L. (2003). Division site selection in *Escherichia coli* involves dynamic redistribution of Min proteins within coiled structures that extend between the two cell poles. *PNAS 100*, 7865–7870.

(*2*) Swulius, M. T. and Jensen, G. J. (2012). The helical MreB cytoskeleton in *Escherichia coli* MC1000/pLE7 is an artifact of the N-terminal yellow fluorescent protein tag. *Journal of Bacteriology 194*, 6382–6386.

(*3*) Wilkison, W. O., Walsh, J. P., Corless, J. M. and Bell, R. M. (1986). Crystalline Arrays of the *Escherichia coli* sn-Glycerol-3-phosphate Acyltransferase, an Integral Membrane Protein. *The Journal of Biological Chemistry 261*, 9951–9958.

(*4*) Stoddard, P. R., Lynch, E. M., Farrell, D. P., Dosey, A. M., Dimaio, F., Williams, T. A., Kollman, J. M., Murray, A. W. and Garner, E. C. (2020). Polymerization in the actin ATPase clan regulates hexokinase activity in yeast. *Science 367*, 1039–1042.

(*5*) Barry, R. M., Bitbol, A. F., Lorestani, A., Charles, E. J., Habrian, C. H., Hansen, J. M., Li, H. J., Baldwin, E. P., Wingreen, N. S., Kollman, J. M. and Gitai, Z. (2014). Large-scale filament formation inhibits the activity of CTP synthetase. *eLife 3*, e03638.

(*6*) Petrovska, I., Nüske, E., Munder, M. C., Kulasegaran, G., Malinovska, L., Kroschwald, S., Richter, D., Fahmy, K., Gibson, K., Verbavatz, J. M. and Alberti, S. (2014). Filament formation by metabolic enzymes is a specific adaptation to an advanced state of cellular starvation. *eLife 3*, e02409.

(*7*) Edgar, J. R. and Bell, R. M. (1979). Biosynthesis in *Escherichia coli* of sn-glycerol 3-phosphate, a precursor of phospholipid. Palmitoyl-CoA inhibition of the biosynthetic sn-glycerol-3-phosphate dehydrogenase. *The Journal of Biological Chemistry 254*, 1016–1021.

(*8*) Hsu, C. C. and Fox, C. F. (1970). Induction of the Lactose Transport System in a Lipid-Synthesis-Defective Mutant of *Escherichia coli*. *Journal of Bacteriology 103*, 410–416.

(*9*) Sweet, G., Gandor, C., Voegele, R., Wittekindt, N., Beuerle, J., Truniger, V., Lin, E. C. C. and Boos, W. (1990). Glycerol Facilitator of *Escherichia coli*: Cloning of glpF and Identification of the glpF Product. *Journal of Bacteriology 172*, 424–430.

(*10*) Braun, T., Philippsen, A., Wirtz, S., Borgnia, M. J., Agre, P., Kühlbrandt, W., Engel, A., Stahlberg, H. and Müller, M. E. (2000). The 3.7 Å projection map of the glycerol facilitator GlpF: a variant of the aquaporin tetramer. *The EMBO Reports 1*, 183–189.

(*11*) Hayashi, S.-I. and Lin, E. C. C. (1967). Purification and Properties of Glycerol Kinase from *Escherichia coli*. *Journal of Biological Chemistry 242*, 1030–1035.

(*12*) Larson, T. J., Ye, S. Z., Weissenborn, D. L., Hoffmann, H. J. and Schweizer, H. (1987). Purification and characterization of the repressor for the sn-glycerol 3-phosphate regulon of *Escherichia coli* K12. *The Journal of Biological Chemistry 262*, 15869–15874.

(*13*) Noga, M. J., Büke, F., van den Broek, N. J. F., Imholz, N. C. E., Scherer, N., Yang, F. and Bokinsky, G. (2020). Posttranslational Control of PlsB Is Sufficient To Coordinate Membrane Synthesis with Growth in *Escherichia coli*. *mBio 11*, e02703–19.

(*14*) Cameron, D. E. and Collins, J. J. (2014). Tunable protein degradation in bacteria. *Nature Biotechnology 32*, 1276–1281.

(*15*) Ito, T. and Yamazaki, M. (2006). The ”Le Chatelier’s principle”-governed response of actin filaments to osmotic stress. *Journal of Physical Chemistry B 110*, 13572–13581.

(*16*) Mueller, E. A. and Levin, P. A. (2020). Bacterial Cell Wall Quality Control during Environmental Stress. *MBio 11*, e10–1128.

(*17*) Auer, G. K. and Weibel, D. B. (2017). Bacterial Cell Mechanics. *Biochemistry 56*, 3710–3724.

(*18*) Renner, L. D. and Weibel, D. B. (2011). Cardiolipin microdomains localize to negatively curved regions of *Escherichia coli* membranes. *Proceedings of the National Academy of Sciences of the United States of America 108*, 6264–6269.

(*19*) Sun, Y., Sun, T. L. and Huang, H. W. (2014). Physical properties of *Escherichia coli* spheroplast membranes. *Biophysical Journal 107*, 2082–2090.

(*20*) Witholt, B., Boekhout, M., Brock, M., Kingma, J., van Heerikhuizen, H. and de Leij, L. (1976). An Efficient and Reproducible Procedure for the Formation of Spheroplasts from Variously Grown *Escherichia coli*. *Analytical Biochemistry 74*, 160–170.

(*21*) Kikuchi, K., Sugiura, M., Nishizawa-Harada, C. and Kimura, T. (2015). The application of the *Escherichia coli* giant spheroplast for drug screening with automated planar patch clamp system. *Biotechnology Reports 7*, 17–23.

(*22*) Cambré, A., Zimmermann, M., Sauer, U., Vivijs, B., Cenens, W., Michiels, C. W., Aertsen, A., Loessner, M. J., Noben, J. P., Ayala, J. A., Lavigne, R. and Briers, Y. (2015). Metabolite profiling and peptidoglycan analysis of transient cell wall-deficient bacteria in a new *Escherichia coli* model system. *Environmental Microbiology 17*, 1586–1599.

(*23*) Lin, Y., Zheng, L. and Bogdanov, M. (2019). Measurement of lysophospholipid transport across the membrane using *Escherichia coli* spheroplasts. *Methods in Molecular Biology 1949*, 165–180.

(*24*) Hardaway, K. L. and Buller, C. S. (1979). Effect of Ethylenediaminetetraacetate on Phospholipids and Outer Membrane Function in *Escherichia coli*. *Journal of Bacteriology 137*, 62–68.

(*25*) de Boer, P., Hoogenboom, J. P. and Giepmans, B. N. (2015). Correlated light and electron microscopy: Ultrastructure lights up! *Nature Methods 12*, 503–513.

(*26*) Tizro, P., Choi, C. and Khanlou, N. (2019). Sample preparation for transmission electron microscopy. *Methods in Molecular Biology 1897*, 417–424.

(*27*) Adler, H. I., Fisher, W. D., Cohen, A. and Hardigree, A. A. (1966). Miniature *Escherichia coli* Cells deficient in DNA. *Proceedings of the National Academy of Sciences 57*, 321–326.

(*28*) Ward, J. E. and Lutkenhaus, J. (1965). Overproduction of FtsZ Induces Minicell Formation in *E. coli*. *Cell 42*, 941–949.

(*29*) Farley, M. M., Hu, B., Margolin, W. and Liu, J. (2016). Minicells, back in fashion. *Journal of Bacteriology 198*, 1186–1195.

(*30*) Koppel, D. E., Axelrod, D., Schlessinger, J., Elson, E. L. and Webb, W. W. (1976). Dynamics of fluorescence marker concentration as a probe of mobility. *Biophysical Journal 16*, 1315–1329.

(*31*) Axelrod, D., Koppel, D. E., Schlessinger, J., Elson, E. and Webb, W. W. (1976). Mobility measurement by analysis of fluorescence photobleaching recovery kinetics. *Biophysical Journal 16*, 1055–1069.

(*32*) Verkman, A. S. (2002). Solute and macromolecule diffusion in cellular aqueous compartments. *Trends in biochemical sciences 27*, 27–33.

(*33*) Esue, O., Rupprecht, L., Sun, S. X. and Wirtz, D. (2010). Dynamics of the bacterial intermediate filament crescentin in vitro and in vivo. *PLoS One 5*, e8855.

(*34*) Kopelowitz, J., Hampe, C., Goldman, R., Reches, M. and Engelberg-Kulkat, H. (1992). Influence of Codon Context on UGA Suppression and Readthrough. *Journal of molecular biology 225*, 261–269.

(*35*) Nilsson, M. and Rydén-Aulin, M. (2003). Glutamine is incorporated at the nonsense codons UAG and UAA in a suppressor-free *Escherichia coli* strain. *Biochimica et Biophysica Acta - Gene Structure and Expression 1627*, 1–6.

(*36*) Poole, E. S., Brown, C. M. and Tate, W. P. (1995). The identity of the base following the stop codon determines the efficiency of in vivo translational termination in *Escherichia coli*. *The EMBO Journal 14*, 151–158.

(*37*) Mottagui-Tabar, S., Bjornsson, A. and Isaksson, L. A. (1994). The second to last amino acid in the nascent peptide as a codon context determinant. *The EMBO Journal 13*, 249–257.

(*38*) Romero, M. L. R., Poehls, J., Kirilenko, A., Richter, D., Jumel, T., Shevchenko, A. and Toth-Petroczy, A. (2024). Environment modulates protein heterogeneity through transcriptional and translational stop codon readthrough. *Nature Communications 15*, 4446.

(*39*) Zhang, H., Lyu, Z., Fan, Y., Evans, C. R., Barber, K. W., Banerjee, K., Igoshin, O. A., Rinehart, J. and Ling, J. (2020). Metabolic stress promotes stop-codon readthrough and phenotypic heterogeneity. *Proceedings of the National Academy of Sciences 117*, 22167–22172.

(*40*) Fan, Y., Evans, C. R., Barber, K. W., Banerjee, K., Weiss, K. J., Margolin, W., Igoshin, O. A., Rinehart, J. and Ling, J. (2017). Heterogeneity of Stop Codon Readthrough in Single Bacterial Cells and Implications for Population Fitness. *Molecular Cell 67*, 826–836.e5.

(*41*) Park, C. K. and Horton, N. C. (2019). Structures, functions, and mechanisms of filament forming enzymes: a renaissance of enzyme filamentation. *Biophysical Reviews 11*, 927–994.

(*42*) Ingerson-Mahar, M., Briegel, A., Werner, J. N., Jensen, G. J. and Gitai, Z. (2010). The metabolic enzyme CTP synthase forms cytoskeletal filaments. *Nature Cell Biology 12*, 739–746.

(*43*) Jumper, J., Evans, R., Pritzel, A., Green, T., Figurnov, M., Tunyasuvunakool, K., Ronneberger, O., Bates, R., Žídek, A., Bridgland, A., Meyer, C., Kohl, S. A. A., Potapenko, A., Ballard, A. J., Cowie, A., Romera-Paredes, B., Nikolov, S., Jain, R., Adler, J., Back, T., Petersen, S., Reiman, D., Steinegger, M., Pacholska, M., Silver, D., Vinyals, O., Senior, A. W., Kavukcuoglu, K., Kohli, P. and Hassabis, D. (2020). Highly accurate protein structure prediction with AlphaFold. *Nature 596*, 583–589.

(*44*) Fleming, J., Magana, P., Nair, S., Tsenkov, M., Bertoni, D., Pidruchna, I., Afonso, M. Q. L., Midlik, A., Paramval, U., Žídek, A., Laydon, A., Kovalevskiy, O., Pan, J., Cheng, J., Avsec, Ž., Bycroft, C., Wong, L. H., Last, M., Mirdita, M., Steinegger, M., Kohli, P., Váradi, M. and Velankar, S. (2025). AlphaFold Protein Structure Database and 3D-Beacons: New Data and Capabilities. *Journal of Molecular Biology 437*, 168967.

(*45*) Li, Y., Li, A. and Liu, Z. (2023). The phospholipid biosynthesis enzyme PlsB contains three distinct domains for membrane association, lysophosphatidic acid synthesis and dimerization. *preprint, bioRxiv*, DOI: 10.1101/2023.04.30.538836.

(*46*) Prabudiansyah, I., van der Valk, R. and Aubin-Tam, M. E. (2021). Reconstitution and functional characterization of the FtsH protease in lipid nanodiscs. *Biochimica et Biophysica Acta (BBA)-Biomembranes 1863*, 183526.

(*47*) Shah, S., Dhawan, V., Holm, R., Nagarsenker, M. S. and Perrie, Y. (2020). Liposomes: Advancements and innovation in the manufacturing process. *Advanced Drug Delivery Reviews 154*, 102–122.

(*48*) Chen, F., Zhao, Q., Cai, X., Lv, L., Lin, W., Yu, X., Li, C., Li, Y., Xiong, M. and Wang, X. G. (2009). Phosphatidylcholine in membrane of *Escherichia coli* changes bacterial antigenicity. *Canadian Journal of Microbiology 55*, 1328–1334.

(*49*) Baldauf, L., Frey, F., Perez, M. A., Idema, T. and Koenderink, G. H. (2023). Branched actin cortices reconstituted in vesicles sense membrane curvature. *Biophysical Journal 122*, 2311–2324.

(*50*) Wilkison, W. O., Bell, R. M., Taylor, K. A. and Costello, J. M. (1992). Structural Characterization of Ordered Arrays of sn-Glycerol-3-Phosphate Acyltransferase from *Escherichia coli*. *Journal of Bacteriology 174*, 6608–6616.

(*51*) Wilkison, W. O. and Bell, R. M. (1997). sn-Glycerol-3-phosphate acyltransferase from *Escherichia coli*. *Biochimica et Biophysica Acta (BBA)-Lipids and Lipid Metabolism 1348*, 3–9.

(*52*) Hugener, J., Xu, J., Wettstein, R., Ioannidi, L., Velikov, D., Wollweber, F., Henggeler, A., Matos, J. and Pilhofer, M. (2024). FilamentID reveals the composition and function of metabolic enzyme polymers during gametogenesis. *Cell 187*, 3303–3318.e18.

(*53*) van de Cauter, L., Fanalista, F., van Buren, L., de Franceschi, N., Godino, E., Bouw, S., Danelon, C., Dekker, C., Koenderink, G. H. and Ganzinger, K. A. (2021). Optimized cDICE for Efficient Reconstitution of Biological Systems in Giant Unilamellar Vesicles. *ACS Synthetic Biology 10*, 1690–1702.

(*54*) Exterkate, M., Caforio, A., Stuart, M. C. and Driessen, A. J. (2018). Growing Membranes in Vitro by Continuous Phospholipid Biosynthesis from Free Fatty Acids. *ACS Synthetic Biology 7*, 153–165.

(*55*) Heath, R. J. and Rock, C. O. (1999). A missense mutation accounts for the defect in the glycerol-3-phosphate acyltransferase expressed in the plsB26 mutant. *Journal of Bacteriology 181*, 1944–1946.

(*56*) Heath, R. J. and Rock, C. O. (1998). A conserved histidine is essential for glycerolipid acyltransferase catalysis. *Journal of Bacteriology 180*, 1425–1430.

(*57*) Lewin, T. M., Wang, P. and Coleman, R. A. (1999). Analysis of amino acid motifs diagnostic for the sn-glycerol-3-phosphate acyltransferase reaction. *Biochemistry 38*, 5764–5771.

5 Conclusion

Bacteria depend on their cell envelope to maintain cell shape, control the in- and outflow of solutes, and to protect them from environmental insults. This crucial role, coupled with the fact that their cell envelopes are fundamentally different from ours, has made cell envelope synthesis a preferred target for antibiotics. Despite the decades of research this has inspired, there are still significant gaps in our understanding of how synthesis of various cell envelope components is regulated. For example, while in the past decades we have learned much about the regulation of the composition of the membrane, how the total phospholipid flux is regulated remains unclear. Previous research has identified PlsB as the primary regulator of the phospholipid and fatty acid synthesis pathways, and therefore of membrane synthesis. The data clearly suggest PlsB is regulated by allosteric control. Furthermore, earlier research on PlsB identified its ability to reversibly form inactive filaments. In this work we investigated whether these filaments might constitute a regulatory mechanism.

Using a fluorescent label (msGFP2) we were able to localize PlsB *in vivo* and observe its dynamics across a range of conditions. These results (**Chapter 2**) show that PlsB forms distinct foci, presumed to be filaments, during exponential growth, regardless of growth rate. Furthermore, we have shown that depletion of acyl-ACP and subsequent stretching of the membrane due to inhibition of fatty acid synthesis causes complete dispersal of these foci. The observation that protein synthesis inhibitors do not cause this effect shows that this is not a side effect of growth arrest but a specific response to a decrease in membrane abundance. Furthermore, we have shown that this process is highly reversible and foci are able to rapidly reform upon reintroduction of substrate, either after the inhibitor is removed or if external acyl-CoA is added. Finally, by co-expressing labeled and unlabeled PlsB we have been able to demonstrate that PlsB forms elongated filaments *in vivo* during exponential growth. Together these data support our hypothesis that PlsB forms filaments in response to relative membrane abundance, though unanswered questions remain.

Of course, PlsB is not an island unto itself, but part of a larger regulatory network governing the entire cell envelope. The vast and ever-increasing body of literature on *E. coli* membrane and cell envelope regulation shows not only the importance of the topic, but also how much there is still left to learn. In **Chapter 3** we take a broader look at cell envelope biosynthesis and argue that, much like phospholipid synthesis, the pathways involved are regulated and coordinated through negative feedback loops. By reviewing our current knowledge on these pathways and combining this with proteomic and metabolomic data, we show that neither enzyme nor metabolite concentrations are likely to regulate these pathways. By highlighting several regulatory mechanisms that have since been shown to be negative feedback loops, for example LpxC regulation, we assert that the remaining pathways are likely to have their own feedback loops. Finally, we pose several hypotheses, based on current understanding and our own research, on what form these unresolved regulatory mechanisms might take.

In **Chapter 4** we set out to resolve the open questions related to PlsB filamentation. Primarily, we set out to capture direct evidence that the foci we observed are indeed filaments, as well as that regulation of phospholipid synthesis depends on the ability of PlsB to form filaments. To resolve the nature of the foci we attempted several methods of electron microscopy: negative staining of microtome slices, tomography of minicells, and negative staining of purified PlsB. Unfortunately, these initial attempts did not yield a readily identifiable filament structure. Furthermore, using FRAP we attempted to determine the diffusiveness of the foci in an attempt to differentiate between (relative) immobile oligomeric states and mobile mono- or dimeric states. However, low abundance of PlsB and the small size of *E. coli* cells complicated imaging, and no conclusive results were obtained. To further probe the relationship between PlsB foci and membrane abundance we sought to apply osmotic changes in different systems, both *in vivo* and *in vitro*. Finally, an attempt was made to discover a non-filamenting mutant of PlsB, but while many mutants were investigated, none showed a sufficiently different phenotype. Nevertheless, we believe the questions we asked with these lines of experiments are vital to fully unraveling the mystery of PlsB regulation and should therefore be the focus for future research.

5.1. Recommendations for further research

While we believe the results described in this thesis support and make plausible our central hypothesis, there are several questions that have not been (satisfactorily) resolved. To address these questions we have several recommendations, based both on literature and our insights described in **Chapter 4**.

Perhaps most pressing is addressing the central assumption underpinning much of our research: that the foci observed with fluorescent microscopy are indeed filaments as previously reported. To address this, a more rigorous attempt at direct imaging of these filaments should be made using electron microscopy. A promising avenue would be to utilize the mixed expression described in **Chapter 2**, which gives elongated structures *in vivo*, and combine this with a method that allows whole-cell imaging. One method, recently described in Hugener et al. 2024, is to use spheroplasts deposited on an EM grid and subsequently lysed to flatten them. This method allows the whole cell volume to be imaged and was shown to successfully find, identify, and resolve the structure of filaments (*1*). Depending on the obtained resolution, the results might range from merely confirming the existence of structured filaments to obtaining a crystal structure of the PlsB filament.

Such a structure would form the basis from which further questions can be addressed. Chief among these is whether filamentation of PlsB is required for the regulation of phospholipid synthesis. We attempted to address this question by finding a non-filamentous mutant of PlsB but were unsuccessful. However, a resolved filament structure, presuming a suitably high resolution, should enable the identification of interacting amino acids, stabilizing the filament. This knowledge would be immensely valuable in a second, more rational and informed attempt at discovering a non-filamenting PlsB mutant.

Finally, a filament structure could help form a mechanistic model of PlsB filamentation to address a number of open questions. First is determining the mechanism by which filamentation inactivates PlsB, whether this occurs through conformational change, occlusion of the active site, or another mechanism. Furthermore, if information can be gleaned on how the filaments interact with phospholipids and the membrane in general, insights might be gained as to the mechanism and triggers of PlsB filamentation. This will likely be crucial in determining how PlsB interacts with membrane abundance to trigger filament formation.

5.2. Open questions of *E. coli* cell envelope biosynthesis

Is phospholipid synthesis regulated by membrane abundance?

While it is clear that PlsB is regulated allosterically, the exact mechanism is still disputed. Our fluorescent microscopy evidence certainly shows filaments (or equivalent structures) are tightly correlated with growth and phospholipid abundance. However, there remain open questions, elaborated upon in the previous section, that will need to be addressed for the matter to be settled. We believe a structural biology approach will be crucial to not only decisively determine if filaments are the regulatory mechanism, but also derive a mechanistic model for filament formation and inhibition.

LPS synthesis: is inhibition of LpxC activity by LapB more relevant to LPS flux than LpxC degradation?

Models of LPS regulation have long placed the active proteolytic degradation of LpxC by FtsH center stage. Discovery of adaptor proteins LapB (YciM) and LapC (YejM) has augmented this model, showing that periplasmic LPS concentrations are the signal determining LpxC degradation. However, it remains puzzling that proteolytic degradation, an inherently energetically expensive form of regulation, should be the primary regulatory mechanism of a pathway that is constitutively expressed during growth. Indeed, recent findings suggest that LapB not only serves to increase proteolytic rates but also has a direct inhibitory effect upon binding LpxC. Such an interaction could serve as a faster, more flexible and less costly form of regulation. Further research will have to determine the physiological relevance of the inhibition and if it is the primary mechanism of LPS regulation during growth, as we suspect might be the case.

LPS synthesis: Is the apparent feedback inhibition of the Lpt system observed *in vitro* relevant *in vivo*?

Another recent and exciting discovery within the LPS pathway has been the feedback inhibition of the Lpt transport complex. This holds the promise of being the missing link between the outer membrane and periplasmic LPS pools, the latter of which ultimately regulates LpxC. However, as far as we can tell the physiological relevance of this feedback inhibition, which has been observed *in vitro*, has yet to be confirmed. Further investigation into the role of Lpt in regulating LPS transfer to the outer membrane and to

what degree this constitutes a regulatory mechanism will be invaluable to increase our understanding of the LPS synthesis pathway. We believe *in vivo* characterization of this feedback loop, as well as structural investigation into the inactive and active forms of the Lpt complex will be vital to answering these questions.

LPS synthesis: is periplasmic LPS truly the feedback signal?

While largely presented as fact, we do have to concede that periplasmic LPS is not the sole contender for the role of feedback signal. Alternative signals have been proposed, for example acyl-CoA generated from mislocalized phospholipids. We believe analysis of wild-type cells will be the surest way to determine if there are indeed alternative feedback signals or if their effects are mediated via periplasmic LPS. While technically challenging, we believe the most direct evidence would be to isolate and analyze the concentrations of periplasmic LPS and the alternative signals across a variety of conditions.

Outer membrane proteins: what role do they play in coordinating cell envelope synthesis?

During this thesis, especially in **Chapter 3**, we have neglected outer membrane protein export and insertion into the outer membrane. This is because proteins are not the immediate product of a metabolic pathway and therefore outside our scope. Nevertheless, we do wish to acknowledge proteins are a major component of the outer membrane surface: rather than the conventional image of isolated proteins floating in a sea of LPS, atomic force microscopy has shown that the outer membrane is more akin to bricks of proteins separated by mortar a few LPS thick. As such it must be that their insertion via the BamA system (after transport across the periplasm by the Lol pathway) influences outer membrane expansion and therefore the cell envelope as a whole. It is however not yet clear whether protein insertion is a driver of cell expansion, or if it takes its cues from the cell envelope biosynthesis pathways. This is something we believe is worth exploring.

Bibliography

(*1*) Hugener, J., Xu, J., Wettstein, R., Ioannidi, L., Velikov, D., Wollweber, F., Henggeler, A., Matos, J. and Pilhofer, M. (2024). FilamentID reveals the composition and function of metabolic enzyme polymers during gametogenesis. *Cell 187*, 3303–3318.e18.

Acknowledgements

In many ways a PhD is your own project, your responsibility, your personal journey. But I have not found it to be a lonely journey. I have been lucky to have been surrounded by a great deal of wonderful people who have all been gracious enough to support me in their own way. Now, at journeys' end, I want to thank each and every one of you, whether I call you by name specifically or not.

First of all, a heartfelt thank you to **Greg** for your advice and supervision all these years. I have learned so much the past years. Your endless enthusiasm for science and the communication of science is both inspiring and infectious. I have lost count how many pages of feedback on presentations I've received in your relentless crusade for better scientific presenting. This has tremendously improved my scientific communication, my ability to tell a captivating and informative story. I also greatly appreciate your advice in career, your honest opinion and your enthusiastic support when I decided to pursue an education direction. I also want to thank my co-promoter, as well as the rest of my supervisory team. **Christophe**, thank you for the fresh perspective and interesting questions and discussions you brought to all our meetings. **Duncan**, thank you for your enthusiasm and for sharing your expertise with membranes. **Arjen**, thank you for your expertise in EM, your support for the experiments, and your knowledge and insights.

I don't think I could have done this without you, **Danielle**. A lot has happened these past years, big moments both happy and not. Throughout it all you have been my immense and endless source of support. Thank you for always being there for me. You hear my doubts, my worries and frustrations and help me carry the load. I'm happy to have experienced all the wonderful moments together with you, knowing I always have you in my corner makes everything better. While this chapter of my life might be finished, I cannot wait to share the rest of it with you.

To my wonderful parents, **Laila and Martin**, I would not have been the man I am today without your love and unconditional support. From my earliest fascination of dinosaurs you have always fostered my spark, encouraged my curiosity and allowed me to flourish. You have inspired me to follow my dreams, shifting though they have been. Of course, the family is not complete without **Niva**, my dear little sister who at first seemed determined to follow in my footsteps but has since found her own path. Your endless curiosity and desire to know the essence of the thing is an inspiration. I am lucky to have a sister like you. I look forward to many more evenings of conversation together with **Jakob**, whom I have come to consider as a brother. Finally, family need

not be limited to blood ties. **Ralph & Lianne**, your friendship and the open, honest joy you bring has been a great support these last few years.

Without the support of colleagues I would not have been able to finish my PhD. **Flora**, thank you for showing me around the lab when I was just getting started. **Adja**, thank you for the conversations and for all your efforts to make the lab a more social place. **Ferhat**, you were a source of inspiration and immense help when I was just getting started. **Milan**, thank you for the fun conversations, the memories and for being an inspiration as I was finishing up this thesis. **Tijn**, thank you for breathing new life into the group and for taking up the torch. **Michal**, thank you for the boundless enthusiasm with which you aided me with everything microscopy. Many hours were spent optimizing, troubleshooting, and bug fixing and the joy and optimism you bring made all the difference. **Wiel**, thank you for always being ready to help me with a variety of tasks, be it managing a microscope, 3D printing my PlsB models or as simple as helping me move a whiteboard to a new office. **Clémence**, thank you for being willing to take on the difficult project of imaging my difficult protein with electron microscopy. I am immensely grateful for all your time and effort, for taking an active interest and thinking along on how we could best approach this problem.

I also want to extend a heartfelt thank you to all the students who were brave enough to join me on this project. **Desi**, thank you for sticking with a thoroughly unprepared and green supervisor, I probably learned as much from you as you did from me. **Amba**, you brought an infectious energy and desire to learn to everything you did, be that in the lab or honing your English with the ”word of the day”. **Finn**, you pioneered a new direction in the research and brought relentless positivity and humor despite the many setbacks and difficulties that come with such pioneering work. **Henrieke**, you laid the groundwork for the work on mutagenesis. Though you were only here for a short time you were fully integrated into the group. **Leander**, you pushed your project forward and were never afraid to ask questions, no matter how difficult the answer. Your thoughtful discussions and the work you put in are greatly appreciated. **Shambhavi**, you brought perseverance, positivity, and an eagerness to learn to everything you did, and the delicious food you introduced me to was always a much-appreciated bonus. **Allegra**, I greatly enjoyed our discussions on puzzling results and trying to determine how they might fit together. I also appreciate your endless patience whenever I attempted to use your MacBook.

Finally, a PhD is not a sprint and you need to take a rest every so often. The social connections I have made have been incredibly important for seeing me through to the end. **Ramon** not only are you one of the punniest people I know, you are also thoughtful, kind, and always ready to lend a hand or ear. **Marieke**, thank you for jokes, the friendly banter and (sometimes) allowing me to peer pressure you into tea breaks. It is humbling to have found someone who is possibly more into boardgames than me. **Nynke**, thank you for the cheery attitude you bring to everything, for showing me opportunities I didn’t know existed, and for always being ready to give me a push when I needed one. **Fede**, thank you for sharing your food, the fast pace of speech and for always bringing an open warmth. **Leander**, you get a second thank you, befitting a shift from student to colleague and friend. You are an incredibly kind person with a quick laugh, the best office mate you can ask for. **SaFyre**, thank you for all the interesting conversations, you’ve changed the

way I look at the world in many ways, not least of all that I now suspect every bunch of small white flowers of being wild carrots. **Esther**, Thank you for all the lovely tea break conversations, including the one where my complete lack of response warranted the construction of a memorial. **Frank**, thank you for keeping me up to date on F1 racing and always taking the initiative for grabbing a cup of tea. **Cecilia**, thank you for your cheery outlook and for being your own wonderful and delightful brand of odd. **Jeffrey**, thank you for the games and for always being a good sport about my awful chess moves whenever we teamed up.

List of Publications

1. **Beije, J.**, Fierlier, D., Guurink, M., Stapert, A., Zoumaro-Djayoon, A., & Bokinsky, G. (2025). Coordination of membrane synthesis with cell growth: localization of the *Escherichia coli* phospholipid synthesis enzyme PlsB responds to membrane abundance in a manner consistent with filamentation-mediated inhibition. *bioRxiv, 2025-11*.

2. Paola De Magistris, Greg Bokinsky, **Jaïrus Beije** & Ben Tilly, Open interactive textbook for Biochemistry, Available at: https://interactivetextbooks.tudelft.nl/biochemistry/. *Copyright Delft University of Technology, CC-BY 4.0.*